Optimization of Ventilation System Design and Operation in Office Environment

Liang Zhou

A Thesis

in

The Department

of

Building, Civil and Environmental Engineering

Presented in Partial Fulfillment of the Requirements
for the Degree of Doctor of Philosophy at
Concordia University
Montréal, Québec, Canada

June, 2007

© Liang Zhou, 2007

Library and Archives Canada

Published Heritage Branch

395 Wellington Street
Ottawa ON K1A 0N4
Canada

Bibliothèque et Archives Canada

Direction du Patrimoine de l'édition

395, rue Wellington
Ottawa ON K1A 0N4
Canada

Your file Votre référence
ISBN: 978-0-494-31135-6
Our file Notre référence
ISBN: 978-0-494-31135-6

NOTICE:
The author has granted a non-exclusive license allowing Library and Archives Canada to reproduce, publish, archive, preserve, conserve, communicate to the public by telecommunication or on the Internet, loan, distribute and sell theses worldwide, for commercial or non-commercial purposes, in microform, paper, electronic and/or any other formats.

The author retains copyright ownership and moral rights in this thesis. Neither the thesis nor substantial extracts from it may be printed or otherwise reproduced without the author's permission.

AVIS:
L'auteur a accordé une licence non exclusive permettant à la Bibliothèque et Archives Canada de reproduire, publier, archiver, sauvegarder, conserver, transmettre au public par télécommunication ou par l'Internet, prêter, distribuer et vendre des thèses partout dans le monde, à des fins commerciales ou autres, sur support microforme, papier, électronique et/ou autres formats.

L'auteur conserve la propriété du droit d'auteur et des droits moraux qui protège cette thèse. Ni la thèse ni des extraits substantiels de celle-ci ne doivent être imprimés ou autrement reproduits sans son autorisation.

In compliance with the Canadian Privacy Act some supporting forms may have been removed from this thesis.

While these forms may be included in the document page count, their removal does not represent any loss of content from the thesis.

Conformément à la loi canadienne sur la protection de la vie privée, quelques formulaires secondaires ont été enlevés de cette thèse.

Bien que ces formulaires aient inclus dans la pagination, il n'y aura aucun contenu manquant.

Canada

ABSTRACT

With growing concern about the impact of indoor environment quality on office workers' well-being and productivity, coupled with the concern over the rising energy costs for space heating and cooling in office building sector, ventilation principles that integrate flexible and responsive elements have grown in popularity in office buildings. Such advanced elements as *Underfloor air distribution* (UFAD), passive swirl diffusers, and demand control on ventilation rate pose challenges to system design and operation.

This thesis is concerned with the development and implementation of a practical and robust optimization scheme, with the goal of aiding the office building designers and operators to enhance the thermal comfort and *indoor air quality* (IAQ) without sacrificing energy costs of ventilation. The path taken is a simulation-based optimization approach by using *computational fluid dynamics* (CFD) techniques in conjunction with *genetic algorithm* (GA), with the integration of an *artificial neural network* (ANN) for *response surface approximation* (RSA) and for speeding up fitness evaluations inside the GA loop. It breaks the problem into three sequential steps.

First, the performance of various ventilation systems was predicted and evaluated by CFD simulations for an assumed set of indoor/outdoor environmental conditions. By varying the external temperature, the internal heat load, the geometric configuration in the office, the supply air states, and the placement of air terminals in the CFD model and examining the consequent effects, the influential parameters significantly affecting the objectives of interest can be identified and examined. Though CFD is often quoted as a method of acquiring detail and accuracy, the excessive computational costs retards the direct conflation of it into the optimization underway. It is then a worthy effort establishing a low fidelity model for RSA, which can be then used in the place of CFD to evaluate fitness during optimization search. In the second step, an ANN model was trained and tested for this purpose by using data obtained from pre-conducted CFD simulations. When created properly, such a model significantly decreases the computing time for optimization objectives and constraints calculation without compromising accuracy. Finally, a GA was applied in the third step to search for the near-optimal

combinations of the controlled variables, using the pre-trained ANN model for fitness evaluations inside searching loops. The objective function is formulated in a way attempting to integrate and weight indicators such as *predicted mean vote* (PMV for thermal comfort assessment), *ventilation effectiveness* (ε_v for IAQ evaluation), and energy usage by space cooling and a supply fan into one performance index.

The CFD simulations in this study are pre-validated using experimental data from baseline cases with both UFAD system and ceiling mounted *mixing system* (MS). Good agreements between the measured and the predicted air velocity/temperature profiles provide the justification for the current choice of turbulence model and the present specification of boundary conditions. It can be observed that the ANN model obtained and used cuts down the execution time from 17 hours per CFD simulation (thus, per fitness evaluation in GA originally) to a time scale of a few minutes for the whole GA search (invoking approximate 5000 fitness evaluations in total). Within a particular office space with a given indoor pollutant emission rate and internal/external thermal conditions, the final optimization solution contains a set of near optimal ventilation system design/operation parameters, including the ventilation system type, diffuser type, number of diffusers, supply air temperature, amount of supply air, as well as the location of diffusers and return grilles, which can substantially enhance the thermal comfort level and IAQ with saving in the energy costs simultaneously. Such optimization results indicate that the present choices of objective function and optimization approach are able to result in great improvements in the design and operation of ventilation systems in office environments.

This thesis also provides a brief discussion regarding the potential advancements of this work, with the hope to provide a practical tool for aiding decision making during building system design and operation process.

ACKNOWLEDGEMENTS

I can hardly express my greatest gratitude to my thesis supervisor Dr. F. Haghighat. Throughout the course of my studies, he has continuously motivated, inspired, and supported me. Without any of these, this work could never be accomplished. He has been a mentor to me in the true sense of work and life.

This work was financially supported by the funding of the Innovations & Solutions Directorate at Public Works and Government Services Canada (PWGSC). I wish to express my gratitude to Dr. E. Morofsky and Dr. S. Rastan from PWGSC for having the vision to support my studies and for the many inspiring suggestions.

I also gratefully acknowledge my supervising committee: Dr. W. Ghaly, Dr. A. Athienitis, and Dr. C. Mulligan for their knowledgeable and stimulating advices. This thesis owes an enormous intellectual debt to Dr. T. Mengistu from the Department of Mechanical Engineering at Concordia University, as most of the ideas in the thesis have been developed from long discussions with him.

My sincere appreciation is given to Dr. C. Y. Chao and Dr. M. P. Wan from the Hong Kong University of Science and Technology for their selfless assistances with conducting the experimental work. Special thanks are due to Dr. A. Melikov and Dr. R. Cermak from Technical University of Demark for providing comprehensive experimental data.

Many thanks go to my colleagues in our research group—Jian Zhang, Brian Coffey, Jérôme Conraud, Kai Qiu, Hongyu Huang, Chang-Seo Lee, and Yashar Farajollahi for their valuable comments and for creating a supportive atmosphere. I would especially thank Sylvain Bélanger, the systems analyst in our department, for helping me solve the many problems related to computer resources.

Finally, and most importantly, I wish to express my warmest appreciation and love for my husband, Zhenyu Li, and for my dear parents, Jianhua Zhou and Guanghua Rao. I could not have accomplished my goal without their unconditional love, support, and encouragement.

TABLE OF CONTENT

LIST OF FIGURES

LIST OF TABLES

LIST OF SYMBOLS

English letters

a	Coefficient in the linear transfer function in ANN output layer	
ACE	Air Change Effectiveness	
ACH	Air Change Rate	(1/hour)
$ADPI$	Air Diffusion Performance Index	(%)
c	CO_2 concentration at the measurement point	(ppm)
c_p	Specific heat of air	(J/kg°C)
c_{br}	CO_2 concentration at breathing level near the occupant	(ppm)
c_{return}	CO_2 concentration in the return air	(ppm)
c_{supply}	CO_2 concentration in the supply air	(ppm)
C_E	Contaminant concentration in the exhaled air	(ppm)
C_I	Contaminant concentration in the inhaled air	(ppm)
$C_{I,O}$	Contaminant concentration in the inhaled air without personal ventilation	(ppm)
C_p	Contaminant concentration at the measurement point	(ppm)
C_{PV}	Contaminant concentration in the personalized air	(ppm)
C_{return}	Contaminant concentration in the return air	(ppm)
C_{supply}	Contaminant concentration in the supply air	(ppm)
C_{ws}	Average contaminant concentration in a workstation	(ppm)
C_μ	Empirical constant used to calculate turbulent viscosity	
$C(-)$	Non-dimensional CO_2 concentration	

COP	Coefficient Of Performance	
COP_{ref}	|Reference value of COP	
d	Humidity ratio of air	(kg water vapor/kg dry air)
d_{out}	Humidity ratio in outdoor air	(kg water vapor/kg dry air)
d_{return}	Humidity ratio in return air	(kg water vapor/kg dry air)
DDO	Distance from diffuser to occupant	(m)
DRS	Distance from return grille to contaminant source	(m)
e_j	Error signal associated with a neuron in the output layer	
E_c	Contaminants removal efficiency	
$E_{cooling}$	Cooling energy requirement (equals the power input to the chiller)	(W)
$E_{coolingmax}$	Maximum value of cooling energy requirement observed from the training data	(W)
E_{fan}	Power input to the central supply fan	(W)
E_{fanmax}	Maximum value of fan power input observed from the training data	(W)
E_P	Personal exposure effectiveness	
E_{RI}	Re-inhaled exposure index	
E_v	Ventilation effectiveness	
$Error$	Error calculated over the entire network using regularization	
$Error'$	Modified error calculation function over the entire network	
ET	Equivalent Temperature	(°C)
f_{cl}	Ratio of the area of clothed body to the surface area of the nude body	
h	Specific enthalpy	(J/kg)
h_c	Convective heat transfer coefficient between the outer surface of clothing	

	and the ambient air or between first node to the nearest wall	($W/m^2°C$)
h_{out}	Specific enthalpy of the outdoor air	(J/kg)
h_{return}	Specific enthalpy of the return air	(J/kg)
i	ith neuron in the previous ANN layer or ith output variable in ANN	
I	Summation of weighted inputs to a neuron	
I_{cl}	Thermal resistance of the clothing	($m^2°C/W$)
$Input(i, j)$	Raw value of ith input variable (to ANN) in the jth data set	
$Input(i, j)_{nor}$	Normalized value of ith input variable (to ANN) in the jth data set	
j	jth output neuron in the ANN or the jth training data pair	
k	Turbulent kinetic energy	(m^2/s^2)
K	Total number of design variables	
l	Length scale used to calculate turbulent viscosity	(m)
L	Thermal load on the human body	(W/m^2)
$\dot{m}_{air,total}$	Total mass flow rate of supply air	(kg/s)
$\dot{m}_{fresh}$	Mass flow rate of outdoor air	(kg/s)
M	Metabolic rate per unit body surface area	(W/m^2)
$MaxInput(i)$	Maximum value of ith input (to ANN) variable over all data sets	
$MaxOutput(i)$	Maximum value of ith output variable (in ANN) over all data sets	
$MinInput(i)$	Minimum value of ith input variable (to ANN) over all data sets	
$MinOutput(i)$	Minimum value of ith output variable (in ANN) over all data sets	
MSW	Mean value of summed squares of the up-to-date network weights	
MTV	Mean Thermal Vote	
n	Iteration n in ANN (corresponding to the nth training data set)	

N	Resolution of the design variable (or number of design points)	
$Output(i, j)$	Raw value of ith output variable (in ANN) in the jth data set	
$Output(i, j)_{nor}$	Normalized value of ith output variable (in ANN) in the jth data set	
P_c	Crossover rate	
$P_{chiller}$	Power input into the chiller	(W)
P_m	Mutation rate	
P_s	Saturated water vapor pressure at local temperature	(Pa)
P_v	Partial water vapor pressure in the local air	(Pa)
Pr_{eff}	Effective Prandtl number	
PD	Percentage of dissatisfied people due to Draft	(%)
PMV	Predicted Mean Vote	
PMV_{max}	Maximum values of PMV observed from the training data	
PPD	Predicted Percentage of people Dissatisfied	(%)
PT	Penalty term in the objective function	
$Q_{cooling}$	Total cooling load	(W)
Q_{space}	Cooling energy used to offset sensible heat load in the indoor space	(W)
Q_t	Local heat loss rate from occupant's skin surface	(W/m^2)
Q_{vent}	Cooling energy used to condition the outdoor air to return air states	(W)
R	Regression correlation coefficient	
RH	Relative humidity in local air	(%)
SSE	Sum of Squared Error in ANN training	
SSW	Sum of Squared Weights	
t_{bl}	Mean age of air at breathing level	(s)

t_{return}	Mean age of air in the return air	(s)
T_{air}	Air temperature at the measurement point	(°C)
$T_{ambient}$	Ambient temperature in the test room	(°C)
T_{cl}	Outer surface temperature of clothing	(°C)
T_{dew}	Dew point temperature at the measurement point	(°C)
T_{indoor}	Local indoor air temperature	(°C)
T_{mrt}	Mean radiant temperature	(°C)
T_{out}	Temperature of outdoor air	(°C)
T_{ref}	Reference temperature when calculating COP	(°C)
T_{return}	Temperature of return air	(°C)
T_s	Occupant's skin temperature	(°C)
T_{supply}	Temperature of supply air	(°C)
T_{surf}	Inner surface temperature of external wall	(°C)
V	Local air velocity	(m/s)
V_{air}	Air velocity at measurement points	(m/s)
$\dot{V}_{air,total}$	Overall volumetric flow rate through the central supply fan	(L/s)
V_{sup}	Supply air flow rate	(L/s)
$w_{cooling}$	Weighting factor associated with cooling energy requirement index	
w_{fan}	Weighting factor associated with fan energy requirement index	
w_{iaq}	Weighting factor associated with indoor air quality index	
w_{tc}	Weighting factor associated with thermal comfort index	
W	Connection weights in ANN, or external work applied to occupant	(W/m^2)

x	Controlled variable in GA	
x_i	Input to a neuron in the first layer or an intermediate layer	
x_j	Input to a neuron in the output layer	
X	Input vector in GA	
y	The output from a neuron	
y_i	Output from a neuron in the input layer or the intermediate layer(s)	
y_j	Output from a neuron in the output layer	
y_{jD}	Desired output from a neuron in the output layer	
$y_{next\text{-}to\text{-}wall\text{-}node}$	Actually distance from the nearest wall to the next-to-wall grid	(m)

Greek symbols

α	A constant representing the influence of the weight change in the previous epoch on the weight correction in current epoch	
β	Performance ratio in the modified error calculation function	
ε_v	CO_2 concentration-based ventilation effectiveness	
ε_{vmax}	Maximum values of ε_v observed from the training data	
ε	Dissipation rate of turbulent kinetic energy	(m^2/s^3)
η	Learning rate adopted in ANN training	
η_{fan}	Fan efficiency	
μ	Molecular viscosity	(Pa·s)
μ_t	Turbulent viscosity	(Pa·s)
μ_{eff}	Effective viscosity	(Pa·s)
ρ	Density of air	(kg/m^3)
ΔP	Pressure rise through the central supply fan	(Pa)

$\Delta T_{HeadToAnkle}$	Head to ankle temperature difference	(°C)
ΔW	Correction term used to adapt connection weights in ANN	

Subscript

max	Maximum value
new	Adapted connection weight after the current epoch
nor	Normalized value of input/output quantities in ANN
old	Connection weight after the previous epoch
out	Outdoor air
return	Return air
supply	Supply air

CHAPTER 1

INTRODUCTION

1.1 Thermal Comfort, IAQ, and Energy Issues in Office Buildings

Whether one considers the issues related to office workers' well-being and productivity, or the issues from an energy and environmental perspective, there is clear evidence in favor of improving the quality of office built environment.

In North America, approximately two-thirds of employees work in offices and they typically spend up to 90% of their working hours indoors (EPA, 2001). Fanger (2000) stated that thermally comfortable micro-environments in office lead to higher employee productivity, greater satisfaction, and lower operating costs. Compounding this, many others claim that better *indoor air quality* (IAQ) in an office could substantially improve the performance of and lower the risk of *sick building syndrome* (SBS) among office workers (e.g., Wargocki et al., 2000). More impressively, Fisk (2002) estimated the benefits from improving the perceived air quality in American offices and reducing respiratory diseases could potentially result in an annual saving in the range of $6 to $14 billion.

On top of this, statistics demonstrate that the operation of office buildings contributes substantially to global energy consumption and raises many energy-related environmental issues. Data from National Resources Canada (2005) show that commercial and institutional buildings contributed to 13.7% of Canada's secondary energy use and 13.4% of the nation's annual *green house gases* (GHG) emissions in 2004, and a large portion is

attributed to the office buildings. These numbers reveal that plenty of room remains for improvement and call for a broader effort to promote energy effective measures during the design and operating of office buildings.

1.2 The Role of Ventilation System

Ventilation systems satisfy air quality and thermal comfort requirements in office spaces by delivering conditioned air (return air plus outdoor fresh air). In North America, most offices are equipped with ceiling supply/return *mixing system* (MS), although some may have *underfloor air distribution* (UFAD) systems. Office space, with its spatial configurations and airflow/thermal states, is intertwined with ventilation system, resulting in an integrated indoor climate control system. Under such circumstances, the role that ventilation systems play in affecting occupants thermal comfort, IAQ, and energy demand for space conditioning is to be analyzed in detail in the following sections, so as to place the current work—simulation-based numerical optimization of ventilation system design and operation—in context.

Thermal comfort and ventilation

Thermal comfort is defined as "the condition of mind that expresses satisfaction with the thermal environment and it requires subjective evaluation" (ASHRAE Standard 55-2004). Factors such as unacceptable relative humidity, drastic vertical and horizontal temperature variation, radiant temperature asymmetry, and excessive draft (unwanted local cooling caused by excessive air movement at some part of the human body) (ASHRAE Standard 55-2004), may lead to dissatisfaction. Comfort level is also greatly affected by the individual's capability to control the local environment (Bauman et al., 1995).

As one of the constituent processes (sometimes referred to as the secondary system) of a *heating, ventilation, and air conditioning* (HVAC) system, a ventilation system is primarily responsible for air handling and energy distribution. By maintaining air temperature, humidity, and air speed at acceptable levels, it guarantees thermal comfort. Despite the fact that modern ventilation systems strive to offer us the capacity for subtle indoor climate control, thermal conditions in office spaces are still far from perfect. From year to year, the *international facility management association* (IFMA) announces survey data, identifying the fact that the predominant office occupants' complaints are "it's too hot and too cold, simultaneously" (IFMA, 2003). Thus, plenty room remains to ventilation system design and operation to enhance thermal comfort in office.

Energy consumption and ventilation

Triggered by the advent of the energy crisis in the early 1970s, energy efficiency of office buildings has been a major concern. Of the energy bill for office buildings, space conditioning contributes a major portion. In 2004, approximately 60% of the total energy consumed by Canadian commercial/institutional buildings was used for space conditioning (NRCan, 2005).

Generally, two types of building technologies have been adopted by building designers and operators to reduce energy costs of space conditioning. One is the minimization of thermal losses by using well insulated and sealed wall assemblies. As a result, newly constructed and existing buildings are being tightened up. The other approach is the adoption of high efficiency HVAC systems for cooling/heating generation and delivery and/or the minimization of ventilation rates. For example, many building designers and researchers have turned to advanced ventilation systems that

integrate flexible and responsive elements such as UFAD, passive swirl diffusers, and demand controlled ventilation. Such systems can supply air directly to where it is required and provide local control, which poses challenges to energy analysis due to the non-uniform temperature distributions created within the space. Energy simulation programs generally assume perfectly stirred room air conditions and uniform temperature distributions, and thus fail to provide the details that are necessary to analyze the energy performance of these systems. In contrast with this, *computational fluid dynamics* (CFD) techniques can effectively capture the temperature variations, which may advance the approach for energy efficiency evaluation.

Indoor air quality

IAQ in an office is "the physical, chemical, and biological characteristics of indoor air in non-residential workplaces with no internal industrial processes or operations that can affect the comfort or health of the occupant" (Nathanson, 1995). According to ASHRAE Standard 62-2004, a space is deemed to have acceptable IAQ when it has "air in which there are no known contaminants at harmful concentrations as determined by cognizant authorities and with which a substantial majority (80% or more) of the people exposed do not express dissatisfaction".

Space heating and cooling are relatively straightforward operations, which contrast with the more complex process involved in ventilation—determining the impacts of ventilation on IAQ. As previously mentioned, building construction and operation have shifted towards air-tightness and minimal ventilation rates ever since the energy crisis. Arguments against large amount of fresh air intake exist due to the additional costs occurring for filters, heat/cool generation, humidifying/dehumidifying process, and air

distribution. As a result, deterioration in IAQ has raised the problem of SBS, which reached a peak in the early 1980s in western countries. Some research (Pejtersen et al., 1999; Wargocki et al., 2000) revealed that the risk of SBS and associated sick–leave rates were strongly correlated to ventilation rates in office buildings. Milton et al. (2000) declared that the short-term sick leaves of 3700 employees in 40 office buildings were critically dependent on supply airflow rate.

In spite of the rising energy usage for ventilation, office worker dissatisfaction with IAQ is widespread, leading to demands for higher ventilation rates with regard to current standards (Wargocki et al., 2000). As recommended by ASHRAE Standard 62-2004, the minimum ventilation rate should be at or above 1.1 L/s/m^2 to maintain acceptable IAQ in an office. Some researchers even proposed a minimum fresh air supply flow rate of 17 L/s per person (or 1.7 L/s/m^2) to keep the indoor contaminant concentration in the office within an acceptable level (Rey and Velasco, 2000).

To sum up the above statements, trade-offs always exist between the energy used for ventilation and the benefits of ventilation to occupants' comfort and health. Further investigations of indoor environment in ventilated office spaces should orient to a holistic evaluation of thermal comfort, IAQ and system energy efficiency. Highly resolved modeling methods and systematic optimization approach should be developed for ventilation design and operation by codifying the basic notions and lessons from previous studies.

1.3 Optimization of Ventilation System Design and Operation in Office Environment

As previously mentioned, building designers are turning to advanced ventilation

systems that integrate flexible and responsive elements, which pose challenges to system design and operation. Although the accomplishments of previous studies on HVAC system control optimization have been significant, little work has been done to optimize the design configurations and operational states of ventilation systems in the office environment by integrating thermal comfort and air quality together with energy efficiency into the objective function.

The reason is threefold. First of all, in pursuit of improvement in IAQ, thermal comfort, and ventilation energy efficiency in office spaces, it would be necessary to acquire detailed information about the indoor airflow, the pollutant dispersion as well as the temperature variations resulting from various types of ventilated systems. Therefore, it is necessary to employ a highly resolved approach to the problem domain. Secondly, the ventilation performance in a particular office is highly dependent on a variety of geometric and thermal factors, such as ventilation approaches (overhead MS or UFAD), air supply/return terminal configuration, exterior and interior thermal states, contaminant source location and emission rate, office equipment and furniture configuration, supply air conditions, etc. Under this situation, a flexible modeling method has to be used to test a large design space. In addition, since the objective function of such an optimization problem is a nonlinear mixed-integer one with multi optimum, care should be taken to select an optimization algorithm fitting into the context.

In response to these needs, the optimization approach to be developed in the current study encompasses two essential components. The first one is a high-resolution indoor airflow and heat transfer investigation so as to capture the distribution of assessment indices pertaining to thermal comfort, IAQ, and energy usage. The other key component

of current work is the integration of an economical optimization scheme. The simulation-based optimization approach is to be devised with the ultimate goal of providing practical aid to conceptual ventilation design and regulation. Also, such a simulation-based method should offer flexibility in an attempt to predict, evaluate, and compare a wide range of objectives and constraints.

The subsequent sections set out to address the issues pertinent to these two components in detail. Based on that, the motivations and scope of current work are outlined.

1.3.1 Integration of CFD into the present optimization work

Better understanding of indoor air quality, thermal comfort and ventilation system energy efficiency requires detailed descriptions of airflow, temperature distribution, and contaminant dispersion in the problem domain. It is evident that the most reliable and realistic information could be collected through physical experiments. However, some limitations associated with taking measurements in the office space have impeded the universal applicability of this approach. The first one is the large amount of labor and high costs incurred during facility set-up and data recording in either mock-up or real office spaces. A typical chamber that mimics an office environment usually costs at least $300,000 US dollars (Yuan et al., 1999). Another drawback lies in the fact that it is sometimes impractical to retrofit the spatial configurations of office and ventilation system to represent various scenarios. On top of these, both the operating states of the ventilation system and the ambient thermal conditions have to be precisely maintained at a desired constant level to obtain accurate and conclusive results; however, this is not only expensive but also physically difficult due to the inevitable fluctuations in weather

and thermal conditions in field studies.

Alternatively, the objective of indoor environment evaluation can be realized by solving a set of conservation equations in terms of mass, momentum, energy, and chemical species. Due to expanding computer capabilities, numerical solution of these conservation equations is possible. This approach is known as the CFD technique. CFD, by name, is the numerical modeling of physical processes within fluids, including fluid movement, mass transfer, heat transfer, and chemical propagation.

During the last two decades, CFD methods have been used routinely in research to predict detailed room airflow patterns, highly resolved temperature distributions, and pollutant transport indoors, as evidenced by the large number of publications appearing in journals and conferences. Even in practice and in industry, CFD simulations have gained momentum in the design stage, as a useful tool aiding building design verification and comparison. In contrast to physical measurements, the CFD method is relatively inexpensive, applicable to any existing or conceived scenario, and can provide complete information. Consequently, the optimization approach was based on the use of CFD techniques to evaluate various ventilation system design configurations and operation states, with the hope that the near-optimal solution could be found thereby. The platform for implementing and demonstrating CFD simulation in this study was the Airpak package from Fluent Inc. (Airpak, 2002).

Despite the great potential of CFD techniques for indoor environment analysis, some issues had to be addressed before incorporating CFD into the optimization work. First, errors and liability concerns associated with CFD predictions are—as with any other simulation technique—inherent. Modeling and numerical issues such as mathematical

models, boundary/initial conditions, grid topology in computational domain, differencing scheme (spatial and/or temporal), and solution algorithm will have major influences on the calculation accuracy. Therefore, for any CFD simulation work, verification and justification exercises should be conducted through comparisons between the simulated and the measured data. Second, up to this point, the popular trend in the use of CFD for building modeling has been airflow prediction and corresponding comfort and air quality assessment; in contrast, issues regarding heat transfer and energy use have not been successfully addressed using CFD techniques.

In order to provide a holistic assessment of building performance, energy simulation tools are on their way towards expanding beyond the original thermal scope and the single-node room representation and advancing approaches on coupling CFD with building simulation. By doing so, energy simulation programs have become capable of capturing the spatial variations of thermal comfort related indices and indoor air contaminant concentration (Negrão, 1995; Clarke et al., 1995; Beausoleil-Morrison, 2000; Bartak et al., 2002; Zhai et al., 2002; Zhai and Chen, 2003, 2005). However, those coupling methods are still beyond the scope of practical application due to the demanding requirement on computer resources, the special treatment of the unequal converging time for different programs, and the special approach for handling the domain interface discontinuity. In light of this, the conflation of CFD and energy simulation is excluded from the scope of the current study; instead, a simplified approach is introduced in the subsequent chapter, which attempts to correlate the energy consumed by ventilation with the ventilation system operation states and CFD predicted room air conditions.

Once the CFD model has been set up appropriately and the credibility of predicted

objective indices (by CFD simulations) has been justified, optimization algorithms can be implemented to test possible design configurations and operation states, with the goal of searching for the best solution.

1.3.2 Optimization algorithms

As pointed out previously, the other important aspect of this simulation-based optimization work is how to select appropriate optimization algorithms.

Optimization algorithms in general

Optimization is an area of applied mathematics dealing with the analysis and solution of problems, intended to find the best set of controlled variables X, which can maximize or minimize the objective function $f(X)$, possibly subject to certain constraints on X. Constraints might be in the form of equality, inequality, and/or parameter bounds. Applications of optimization are very diverse, including problems encountered in all areas of mathematics, applied science, engineering, economics, statistics, and so on.

An optimization algorithm is a numerical method for finding the values of the optimum solutions. The tremendous progress in computer resources has resulted in the development of a wide variety of optimization techniques. The determination of an efficient and accurate algorithm for a particular problem depends not only on the problem complexity in terms of the number of design parameters and constraints but also on the nature of the objective function and constraints. For example, a linear problem, in which both the objective function and the constraints are linear functions, is commonly solved using the *Simplex* algorithm; an unconstrained nonlinear problem can be handled by the *steepest descent* method or the *Newton's* method; in the case of a nonlinear problem in which both the objective function and the constraints are nonlinear functions, it would be

necessary to employ an iterative solution procedure, and the *sequential quadratic programming* (SQP) method fits well into this type of problem; when many minima (or maxima) are likely in the searching space, global optimization methods such as *simulated annealing* (SA) and *genetic algorithm* (GA) appear to perform better in terms of finding the true global optimum.

Generally, optimization algorithms can be sorted into two main categories: conventional gradient-based methods and gradient-free direct search methods.

With the former category of method the objective function is often approximated by terminated first order or second order Taylor series expansion around an initial guessed value and then the local gradient information is used to establish a direction of search at each iteration until the optimum is achieved. A gradient based optimizer is efficient and accurate in searching for the optimum, but is in general prone to find a local optimum. Depending on the starting value, it would most likely get trapped at the nearest local optimal value.

To overcome this shortcoming, many global optimization strategies have been developed. Essentially, a global optimizer relies on a heuristic method rather than using derivatives to determine the search direction and step width; therefore, this school of methods are referred to as gradient-free direct search. When appropriately applied, such global optimization approaches as SA and GA can explore the search space better than gradient-based grid search and can avoid local traps; however, these approaches involve stochastic elements and thus may fail to find the absolute extreme and converge to a near optimal value instead. GA has been successfully applied to optimization problems where other classical methods fail, as stated by Goldberg (1989). One major negative attribute

of global optimization strategies is the relatively large amount of function evaluations that may slow down the convergence.

Optimization applications in previous building research

A wide variety of optimization approaches have been applied to the building related research. For example, SQP method has been employed to optimize the energy costs of a two-zone VAV heating system (House and Smith, 1995) and to optimize the control scheme for a cooling plant (Sun and Reddy, 2005); some other research employed a *conjugate gradient* method to develop optimal HVAC control strategies (Nizet et al., 1984). These are examples of the applications of gradient-based optimization algorithms; however, some issues related to such methods have discouraged the adoption of the gradient-based optimization method in building studies. For one thing, building phenomena are very often nonlinear mixed-integer ones (that is, with both continuous and discrete variables), which may lead to discontinuous outputs and thus cause problems for gradient-based methods (Wetter and Wright, 2003; Lu et al., 2005). Also, gradient-based methods are prone to find a local optimal, and the convergence speed and the value of final results are strongly dependent on the initial guess values in most cases (Wang and Jin, 2000). Due to these drawbacks, gradient-based methods turned out not to be well suited for building applications.

In contrast, gradient-free methods serve as better candidates for building optimization. For example, the *GenOpt* program—a generic optimization engine that can be used in conjunction with any text file type building energy simulation program—enables a wide selection of optimization methods, with the most predominant one being the *Hooke-Jeeves generalized pattern search* (Wetter, 2004). In addition to this, GA is characterized

as a gradient-free stochastic global optimization approach and has been successfully applied to the optimization of building thermal system design (Wright et al., 2002), to optimize HVAC control (Huang and Lam, 1997; Lu et al., 2005), to minimize chiller energy costs (Chow et al., 2002), and to improve green building design (Wang et al., 2005). The following advantages of GA have been described in previous studies: firstly, GA is capable of dealing with discontinuous variables and multi-modal problems, and is also able to tolerate noisy objective functions (Wright et al., 2002; Huang and Lam, 1997); secondly, it can find a sufficiently acceptable solution (near optimal solution) using less computing time, in comparison to other algorithms such as *mixed integer programming* method (Sakamoto et al., 1999), it can thus be incorporated into on-line optimal control; in addition, since no derivative information is needed during the search process, GA was also proven to perform well in conjunction with *response surface approximation* (RSA) methods (Chow et al., 2002; Lu et al., 2005); most importantly, GA is essentially stochastic, it can thus have better chance to explore the entire design space and reach the global optimum.

Optimization algorithm in current study

In the current case, the gradient-based approaches turn out not to be qualified candidates for building the optimizer. For one thing, it is critical to simplify the physical model before implementing gradient-based methods, so that the correlation between inputs and outputs can be explicitly formulated as differentiable equation(s). It is then possible to derive the approximation of the equation (using Taylor series expansion) and calculate the derivatives. This, however, is obviously not feasible here due to the complex nature of the current problem. On top of this, discrete variables (such as type of

ventilation system and type of diffuser) are imposed upon the CFD model and thus turn the problem in discussion to a mixed-integer one (which is also multi-modal the most likely). In light of this, it was reasonable to go with the direct search optimization strategies rather than with gradient-based methods; otherwise, the optimizer would either fail to work or easily get trapped by the local optimal value in the neighborhood of the initial guess point. Accordingly, GA was chosen as the optimization engine hereafter.

1.3.3 Response surface approximation

As a global optimization method, GA is relatively computationally expensive due to the substantial amount of fitness evaluations involved throughout the search process. In the current study, the value of the objective function was calculated based upon CFD estimates. The CFD simulations performed for the indoor domain usually converged in hours or even days, depending on factors such as the domain size, the nature of the flow regime, the air terminal geometrical complexity, and the computer capacity. When it comes to practice (e.g., in-situ design/operation decision making), such a large computational effort is obviously unattractive. Consequently, CFD is too computationally expensive to be directly applied into the current optimization search.

Driven by the need to extend the current approach to practical use (that is, providing prompt suggestions on ventilation design and operation), it was necessary to incorporate an approximation method into the GA optimization search, which could provide accurate prediction of system response (in response to the variations in the input variables) at affordable computing expense. This resulted in a low fidelity model for *response surface approximation* (RSA). Such a surrogate model, once built and validated using the inputs and outputs obtained from the high fidelity model (CFD simulation here), can be then

used in the place of CFD simulation inside the GA loop to represent the objective function and thus reduce the computational cost.

Though other RSA strategies (e.g. statistical regression and simple curve-fit) exist, the *artificial neural network* (ANN) technique has gained the greatest popularity in building related studies as a global RSA method. The word 'global' denotes that such an approach can represent the response of the system over the entire design space.

There have been a wide variety of applications of ANN techniques in building related studies. ANN techniques have been used to approximate and estimate the heating energy demand in commercial and residential buildings (Kreider and Wang, 1991; Waldemark et al., 1992; Olofsson et al., 1998; Mihalakakou et al., 2002), the energy cost of a cooling/heating plant (Curtiss et al., 1993; So et al., 1995; Massie et al., 2004), the overall building heat loss coefficient (Kreider et al., 1995; Olofsson and Andersson, 2002), the Z-transfer function coefficients (Chen and Chen, 2000) and thermal capacitance (Bloem, 1998) associated with the building envelope, and the characteristics of a non-linear VAV fan (Mei and Levermore, 2002). In particular, Chow et al. (2002) implemented an ANN in conjunction with GA to minimize the fuel consumption of a LiBr absorption chiller system, by controlling the inlet/exit temperatures in the chilled water and condensing water loops. It is worth mentioning that the optimization scheme that conflates CFD, ANN, and GA has also captured the attention of researchers in the area of aerodynamic studies of turbomachinery blade design and optimization (Mengistu, 2005).

It can be observed that relatively little research has integrated ANN techniques into the investigation of ventilation systems and indoor environment. One research reported using *feed-forward neural network* (FNN) to determine the optimal thermal comfort level

based on ventilation rate, occupant's behavior, and indoor air temperature, humidity, and velocity (Atthajariyakul and Leephakpreeda, 2004).

In the present work, an ANN model was established using the input-output data pairs generated by pre-conducted CFD simulations, and replacing CFD inside the GA loop to determine the value of objective indices. As a result, the overall computing time was significantly decreased and more affordable.

1.4 Research Objectives and Thesis Outline

The present research was targeted at the development of a robust and efficient simulation-based optimization method that could aid ventilation system design and operation for office space. Given the spatial configurations and thermal conditions in a particular office, the method searches for near optimal options and values of such controlled parameters as type of ventilation principle, diffuser type, number of diffusers per office, supply air temperature, amount of supply air, and placement of diffusers and return grilles, so as to achieve satisfactory thermal comfort and IAQ with minimum energy cost. The path taken to realize this objective can be broken down to the following key points:

- From the design and operation parameters of the ventilation system, extract those influential ones that have great impacts on the office environment. Such influential parameters are to be treated as the independent variables. Also, select appropriate indicators to evaluate comfort, IAQ, and ventilation energy costs in the context of office space, and specify the objective function for optimization accordingly.
- Build a reliable CFD model and perform extensive simulations based on the

validated baseline cases, in an attempt to accurately capture the impacts of all influential parameters on the built environment in a particular ventilated office space.

- Develop and test an ANN model to mimic the CFD module, and then incorporate it into the optimization search to provide fast and low order approximations of the objective metrics.
- Implement a GA to search for the best combination of controlled variables for an office space with specific outdoor temperature, interior heat load, and indoor contaminant emission rate, so as to provide satisfactory thermal comfort level and IAQ without sacrificing energy efficiency.

The framework of the numerical optimization scheme to be developed is briefly outlined in Chapter 1. Chapter 2 provides the technical basis for understanding the numerical details involved in implementing—the ANN technique for RSA and GA as the optimization engine. It is clear that an understanding regarding the mechanism of ventilation systems and the method used to quantitatively evaluate ventilation performance is necessary before implementing CFD simulation; therefore, Chapter 3 provides an overall introduction to the alternate ventilation principles commonly found in office buildings and also extracts the commonly treated influential parameters and objective indices from the literature. The objectives of the current study could only be realized by reliable CFD modeling of thermal and airflow phenomena, while the simulation results could only be justified by validating CFD predictions against data derived from experiments with baseline cases. Verification exercises were conducted and Chapter 4 presents CFD simulation results in comparison with data collected in mock-up

offices located in controlled environment chambers.

The training and testing of an ANN model for system response estimation are then demonstrated in Chapter 5. These are achievable when given the input-output data pairs from CFD simulations. Those influential parameters selected in Chapter 3 are treated as the input variables, whereas those commonly used objective indices related to occupant comfort, IAQ, and energy costs are specified as the model outputs. Due to the large number of influential variables (which meant a large number of CFD cases had to be explored), the issue regarding employing *Latin Hypercube sampling* (LHS) method to define design space is also addressed in Chapter 5. Furthermore, Chapter 5 presents the optimization results from GA, which incorporated the CFD-based ANN for fitness evaluation. Emphasis was placed on how to prescribe the objective function—by weighting and aggregating the different indicators into one performance index—and how to adapt the ventilation system design and operation parameters in response to variances in office conditions in an attempt to minimize the objective function. Finally, conclusions and recommendations for future work are summarized in Chapter 6.

In addition, CFD's essential concepts pertinent to modeling indoor airflow and heat transfer are described in Appendix A, with emphasis being placed upon the approaches adopted in the current CFD simulations. It is also worth mentioning that the validity and effectiveness of this ANN-based GA optimization method is demonstrated in Appendix B, through an example searching for the global minimum of a classic multi-modal optimization problem—the Rosenbrock function.

CHAPTER 2

NUMERICAL OPTIMIZATION

2.1 Introduction

As can be seen from Chapter 1, the two key elements of this study were indoor environmental modeling with CFD and numerical optimization. Essential issues pertinent to the former are to be treated later, while with respect to the latter, the numerical methods implemented in this study for computing the objective function and searching the optimum solution are introduced in this chapter, for the purpose of building the overall framework of this research.

Chapter 1 described GA as a suitable optimization approach in the context of building related studies, which can often be characterized as multi-modal problems with mixed-integer variables. Section 2.2 substantiates the suitability of GA for solving this type of problem by presenting the pertinent aspects of the conceptual basis of GA. Following this, Section 2.3 briefly covers the modeling and numerical elements involved in CFD simulation for indoor environment analysis.

Chapter 1 also raised the problem of the excessive computational expense of GA caused by a large number of fitness evaluations during the optimization search process. This is also partially due to the high computational costs associated with CFD simulation (which may take hours to reach convergence). It would be critical to integrate a new element into the context of current optimization method, so as to address this deficiency and move the optimization method forward. In response to this, ANN is introduced in Chapter 1 as a method for *response surface approximation* (RSA), with the intention of

reducing the computing time for objective function calculation without compromising accuracy. In the subsequent work, an ANN model was established with data generated by CFD simulations, so it could be used in place of CFD for fitness evaluation inside the GA loops. To do this, an understanding of ANN's theoretical basis was necessary. Section 2.4 describes the pertinent elements of ANN, including network topology, network training and calibration, improving the network's generalization, and training data preparation. Accordingly, the numerical optimization scheme is outlined in Section 2.5. Finally, a brief summary is provided in Section 2.6.

2.2 Genetic Algorithm (GA)

2.2.1 General introduction to GA

The Genetic Algorithm (GA) belongs to a class of probabilistic search algorithms, which combines elements of both direct and stochastic searches. The essence of this method is to strike a balance between exploration and exploitation.

GA maintains and operates on a set of potential solutions, called a population of individuals. By applying Darwinian principles of natural selection and implementing genetic operations, such as reproduction, crossover, and mutation, GA transforms a random initial population that is represented by a group of mathematical objects (each object has a corresponding fitness value) into a new population of offspring (Holland, 1975; Goldberg, 1989). Fitness evaluations and comparisons are then performed in the pool of offspring, based on which GA randomly selects individuals from the up-to-date population (parents plus offspring) to put in the mating pool as new parents. Then, GA re-applies the genetic operators to reproduce the next generation of children. By doing so

successively, GA modifies and updates a population of individuals and meanwhile keeps the size of the population unchanged. Such reproduction and fitness evaluation will continue until the termination criteria are satisfied (e.g., the maximum number of generations is reached or the best individual is found). During this searching process, the population "evolves" towards a near-optimal solution, as described by the natural selection rule "survival of the fittest". The individual achieving in the minimum (or maximum) value of objective function (corresponding to the highest fitness) is determined to be the final near optimal solution.

GA is suitable for general purpose optimization and has been successfully applied to a broad range of problems, especially to those problems where the objective function is discontinuous, non-differentiable, or highly nonlinear.

2.2.2 Key terminologies in GA

Before turning our attention to the implementation of GA, key issues pertinent to this numerical optimization algorithm are to be addressed, which include the population size, the variable representation, the variation operators, as well as the selection and replacement mechanism.

Population size

The population is an array of candidate solutions in one generation; equally, the number of candidates composing the population is the population size. Though large population size would necessarily result in excessive fitness evaluation and lead to high computation costs, it is still important to maintain sufficient candidates to ensure population diversity. When the population size is too small, it will increase the likelihood of the gene pool being dominated by some better performers, which would inevitably

narrow down the search space. When facing such a trade-off, the population size was set to 50 in this study, which worked reasonably well.

Representation

A candidate solution to a particular problem contains a group of controlled variables; a pool of candidate solutions composes the search space for GA. Generally, the representation of candidate solution inside a GA program can be binary code (as shown in Figure 2.1a), integer code, or real-valued (floating point) type (as shown in Figure 2.1b). In the current study, the majority of control variables complying with continuous distributions (as can be seen from Chapter 3) and the candidate solutions are encoded simply with a string of real numbers. This real-valued representation could also be considered as a cluster of genes. The fitness value of an individual is the value of the objective function resulting from this individual.

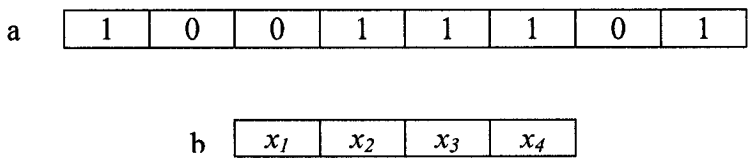

Figure 2.1: Binary (a) and real-valued (b) representation

Genetic operators

GA employs a suite of genetic operators to maintain a balance between exploration and exploitation. The evolutionary search process starts from an initial random population, which is then subjected to genetic operators including: reproduction, crossover, and mutation based on fitness evaluation. Accordingly, a new generation is produced. Brief descriptions of the basic genetic operators follow.

1. Reproduction (Elitism)

Candidates are selected for reproduction according to their fitness. The best

performers in the old generation make a few copies to ensure the survival of the fittest. By doing so, the best solution found so far would remain in the next generation. In this study, two individuals with the highest fitness values in the present generation were guaranteed to survive to the next generation; in other words, the elite count is set to 2.

2. Crossover

The crossover operator, sometimes referred to as recombination, combines two parents to form children for the next generation. This process combined with mutation, which is to be introduced next, plays a very important role in creating population diversity and thus is essential to the exploratory nature of GA. As controlled by crossover rate P_c, crossover operators are usually applied probabilistically to two individuals that are randomly taken from the mating pool formed by parents. The purpose of doing so lies in the fact that, if the offspring take the best characteristics of both the parents they will be more likely to thrive. A scattered crossover function was adopted in this work, which breaks the representation of each parent into two or more segments of contiguous genes, and the function randomly picks alternative segments from the two parents to create the children (as shown in Figure 2.2). As a result, two new individuals are produced, who might inherit the desired characteristics from the parents and become superior children (though that can not be guaranteed). The crossover rate was set to 0.8.

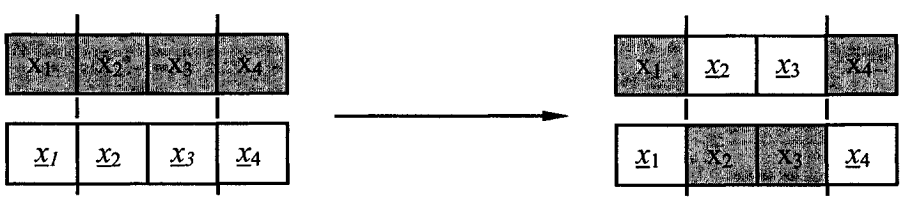

Figure 2.2: Scattered crossover (n-point crossover)

3. Mutation

The mutation operator introduces random changes to individual parents to form children. The mutation operator alters one or more genes in a chromosome of an individual. The mutation operator is targeted at producing new gene values and maintaining the diversity of the gene pool; as a result, the optimization search would possibly converge towards individuals with higher fitness than those presently exist. Because a real-valued representation was used, the mutation operation changed the value of each gene (as seen in Figure 2.3) guided by a mutation rate—P_m. The new value of the gene was uniformly and randomly drawn between the lower and upper bound of the corresponding variable, known as a *mutation-adapt-feasible function* (MATLAB, 2006). The mutation operation was performed to comply with a predefined probability P_m, the value of which was set to 0.2 in the present study.

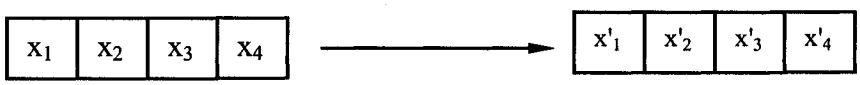

where x_i and x'_i ε [$LowerBound_i$, $UpperBound_i$]

Figure 2.3: Uniform adapt-feasible mutation

Parent selection

In this work, parents for creating the next generation were chosen from individuals in the current generation based on their scaled fitness values. It can be considered a fitness-proportional selection, which means that the number of individuals copied into the mating poor for crossover and mutation was proportional to the individuals' fitness. The selection method is named *stochastic uniform*. Specifically, this method lays out a line, and each individual from the generation corresponds to a portion of the line (Matlab,

2006); the length of the portion (corresponding to an individual) is proportional to the individual's fitness value. When performing the selection, the algorithm moves along the line at an even pace; at each step, it selects a candidate for crossover or mutation from the line section it lands on.

Survivor selection

It would be necessary to invoke a survivor selection process when the population size has to be maintained at constant level. For instance, the population size is fixed at 50 in this study; therefore, after reproduction, crossover, and mutation, survivor selection is performed to pick 50 high rank individuals from the up-to-date parents and offspring to enter the next generation. In other words, the fitness-based replacement selection mechanism is used for survivor selection.

Stopping criteria

Several criteria are set to determine when to terminate the optimization search, provided the optimizer is not stopped manually. When either of the following two conditions occurred, the algorithm stopped searching: 100 generations were reached or successive stall generations (generations with no improvement in the best fitness) exceeded 50.

2.2.3 Implementation of GA in the present study

To sum up the above statements, the following points outline the procedure involved in implementing GA in the present study, and the platform for implementing GA was MATLAB 7.1.

1. The algorithm began with random initialization of the population (50 individuals).
2. The algorithm then successively created new populations. At each step, the algorithm

used the candidates from the current generation to produce the next generation. In order to do this, the algorithm performed the following steps:

2.1 Scored the individuals in the current generation by evaluating their fitness (based on the calculated values of objective function), and scaled these fitness scores based on respective ranks to convert them into a consistent range;

2.2 Automatically, the two best performers in the current population that had the highest fitness were passed to the next generation as elites;

2.3 Selected parents based on their fitness, and produced children from the parents. Children were generated either by making random changes to a single parent—mutation, or by combining the gene segments of two parents—crossover.

2.4 Replaced the current generation of population with the parents and offspring possessing higher fitness, so as to form the next generation (with 50 individuals).

3. If no stopping criterion was satisfied, repeat Step 2 until—

4. The algorithm terminated when either of the stopping criteria was satisfied.

2.3 Office Indoor Environment Analysis Using CFD

CFD was not proposed exclusively for modeling indoor airflow, but as a universal numerical simulation technique instead. It has gained popularity in a wide variety of engineering areas, such as aerodynamics, hydrodynamics, design of gas turbine and combustion equipment, and environmental engineering, etc. Nielsen (1974) implemented a two-dimensional modeling of room airflow driven by a diffuser, which was marked the first application of the CFD technique to the indoor domain. Essentially, CFD employs particular numerical techniques to solve a set of nonlinear partial differential equations—conservation of mass, momentum, energy, and chemical species. By doing so, it enables

the description of fluid flow and related physical phenomena.

As previously mentioned modeling and numerical errors are inherent with CFD studies. Accuracy improvement and quality control of CFD simulations in indoor environment investigations requires an understanding of the primary sources of error. Factors that may significantly affect the precision of CFD calculations include the turbulence modeling method employed, the thermal and airflow boundary conditions prescribed, the differencing scheme used to treat the terms in the governing equations, the mesh quality (size and topology of computational grid), and the reliability of the solution algorithm.

The simulation results presented in subsequent chapters presume general familiarity with these modeling and numerical details; therefore, details of CFD are described in Appendix A.

2.4 Artificial Neural Networks (ANN)

2.4.1 ANN for RSA in the current study

It is straightforward that the reliability of the optimization result is critically dependent on two key elements: the robustness of the method used for optimization and the accuracy and efficiency of the model devised to predict objective indices. As previously discussed, the GA optimization approach was well suited for the problem under consideration, while validated CFD simulations built the foundation for optimization by providing credible predictions for indoor airflow and heat transfer (this is also discussed in detail in subsequent chapters).

However, Chapter 1 raised one problem associated with the direct integration of CFD

simulation into the context of GA. The obstruction was the computing time. It typically takes 17 to 20 hours of CPU time on a Pentium IV desktop computer (dual-processor) before the full-scale office CFD simulation reached convergence. Meanwhile, with the GA set up used, the population size was 50 and the number of generation limit was 100; accordingly, 5000 runs of the CFD program could have been required for a GA search. It was thus impractical to directly invoke CFD simulation inside the optimization loop for fitness evaluation.

One possible remedy to this problem was to establish a relatively inexpensive intermediate model for RSA. ANN techniques were employed in current study to provide low fidelity RSAs of the objective indices. In order to facilitate further optimization, input-output data sets extracted from CFD simulations were used to pre-train and test the ANN model. The platform for implementing and demonstrating the ANN model was MATLAB 7.1. Once the ANN model was validated against the results obtained from the high fidelity model (CFD in this case), it can be used in place of CFD inside GA loops to provide approximation of the objective indices and perform the fitness evaluation. As a result, the number of objective function evaluations and computing time was no longer the bottleneck in the optimization scheme.

2.4.2 Conceptual basis of ANN techniques

ANN technique is a RSA method that is based on some organizational principles resembling those of the human brain. Just as human brains learn from experience, ANN learns from data sets fed into it. An ANN model for response prediction can be established by training it with representative collections of data, which include both input and output variables for a specific system. Once validated with additional data from the

design space, the model may be considered a reliable information processing tool, which can accurately map the input information to the output information. The word "map" denotes the ability of ANN to learn, recall, and generalize from the training data sets. ANN techniques, with their remarkable ability to derive meaning from complicated and imprecise data, can be used to extract patterns and detect trends that are too complex to be recognized by either hand calculation or other computer techniques (Haykin, 1994).

Generally, ANN is composed of multiple layers of processing elements, known as neurons or perceptrons, which mimic the biological neurons of a human brain but work in a much simpler way. Each neuron is connected to its neighbors by different weights, and the magnitude of individual weight represents the strength of this connection. The weights are adjusted adaptively during the ANN training process, until finally the overall network can generate desired outputs when given the input information. Until then, the training of network is accomplished. The learning and generalizing ability of the network obtained is critically dependent upon its architecture, the quality of training data, and the training methods as well. These issues are briefly outlined next.

Network architectures

The architecture of ANN is one of the key factors ensuring the success of such a predictor. The term "architecture" includes the number of the layers, the number of neurons in each layer, the topology of the network, and the form of the transform functions (King, 1999).

As the basic functional elements in the human brain, biological neurons enable us to learn, recall, apply, and generalize our knowledge based on our previous experience. A typical neuron in our brain may be linked to 2×10^5 other neurons. The capacity of our

brain highly depends on the number of these elements and the complicacy of the linkage between them (Hassoun, 1995). Such biological neurons add the signals from other sources, perform certain nonlinear manipulation, and then pass the output as feedback to other functional cells. A Simplified sketch of a typical biological neuron is shown in Figure 2.4.

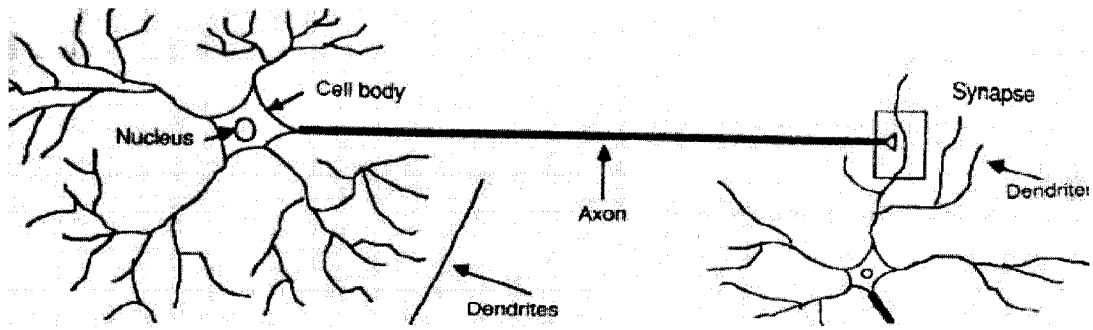

Figure 2.4: A typical biological neuron

Available:
http://www.doc.ic.ac.uk/~nd/surprise_96/journal/vol4/cs11/report.html#Introduction%20to%20neural%20networks

Functionally, the basic component of an ANN is a simplified version of a biological neuron. The conceptual operations performed in an artificial neuron are depicted in Figure 2.5.

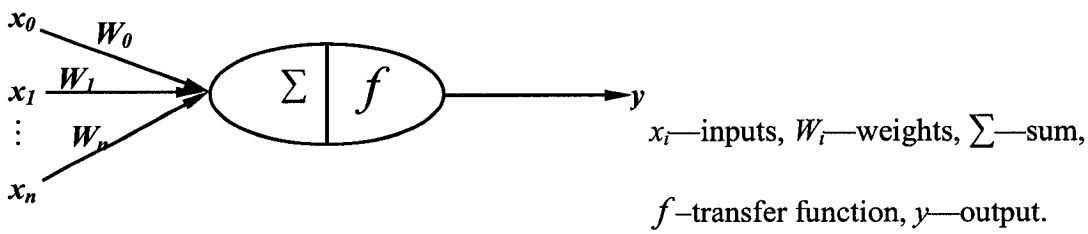

Figure 2.5: A typical processing artificial neuron

Inputs to each neuron from various sources are multiplied by a connection weight and these products are summed. The summation is then sent to a transfer function to calculate outputs from this neuron.

$$I = \sum_i (W_i x_i) \tag{2-1}$$

where i denotes the number of neurons in the previous layer that are connected to the current neuron, I is the summation of weighted input information.

The output from a neuron is then calculated using the transfer function,

$$y = f(I) \tag{2-2}$$

Obviously, the behavior of an ANN would be significantly affected by the input-output transfer function that is assigned to each unit. Though other non-linear transfer functions are available (e.g. log-sigmoid function and radial basis function), a hyperbolic tangent sigmoid function was selected in this study as the transfer function for the intermediate layer(s) (MATLAB, 2006),

$$f(I) = \frac{2}{1+e^{-2I}} - 1 \tag{2-3}$$

while a linear transfer function was assigned to all the neurons in the output layer,

$$f(I) = aI \tag{2-4}$$

where a is the coefficient in the linear transfer function.

Individual neurons are then assembled into layers; these layers are connected by weights and can thus be integrated into a network. It has been confirmed by previous applications of ANN that feed-forward neural networks with at least one hidden layer and sufficient hidden neurons can successfully approximate nonlinear functions of practical interest. In feed-forward ANNs, function signals travel from input to output (one way

only), and there are no feedback loops for function signals.

A multilayer feed-forward ANN was used in this study (see Figure 2.6 for the network structure). The current network consists of three or more layers of units: 1) a layer of "input" units, the activity of which represents the raw information fed into the network; 2) one or more than one layers of "hidden" units, and the activity of each hidden unit can be determined by the outputs from all the units in the previous layer, the weights corresponding to the connections between the previous layer and the current layer units, and the transfer function employed; 3) a layer of "output" units, and each unit corresponds to one of the system responses.

Trade-off always exists between the network accuracy and structural complexity (and thus the computing/training time). The most appropriate numbers of the hidden layers and the nodes in a hidden layer is case specific and can only be determined by exploratory calculations. The selection of input and output variables from the literature will be put forward in Chapter 3; the specification of these variables is left open temporally.

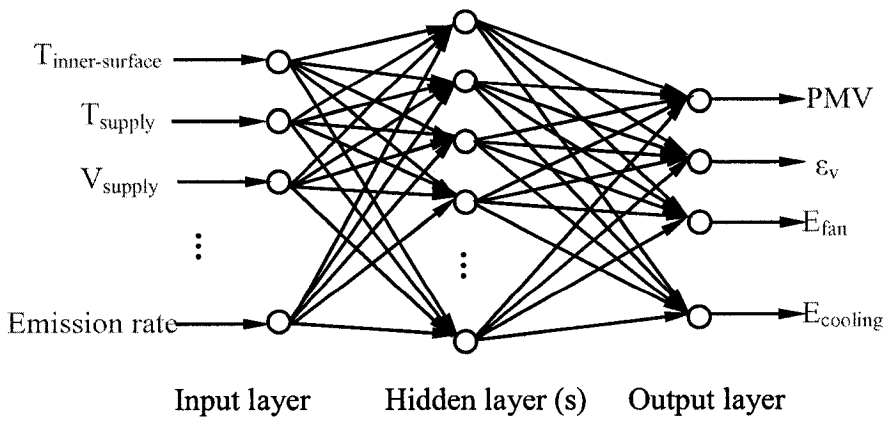

Figure 2.6: Topology of the feed-forward ANN in this study

ANN training

Analogous to the learning process of the human brain, an ANN learns from data received. This learning process is also referred to as "training". A trained ANN model can be thought of as an "expert" at analyzing the information that has been given to it. This expert can then be used to provide predictions when provided new input data of interest. During the training process, the connection weights inside the ANN are adapted under the guidance of certain algorithms, with the intention of enabling the network to map the target outputs to the inputs. The purpose of training is to determine the optimal weights which can minimize the error between the network's outputs and desired outputs. Generally, there are two categories of training methods: unsupervised training and supervised training (Haykin, 1994).

With unsupervised training, the network only learns from available input data without knowing the outputs. Unsupervised networks can be used, for example, to identify regularities and correlations in a cluster of input data (Haykin, 1994). This contrasts with the case of supervised training, where both the input and output data pairs are fed into the network; obviously, the supervised training fits the data pattern of this study and unsupervised training is excluded from the discussion hereafter.

Based on the available data, supervised training can be performed by certain algorithms, such as "perception" (Rosenblatt, 1961) and "back propagation" (Rumelhart et al., 1986). The back propagation algorithm has proven to be an efficient training algorithm for multilayer feed-forward ANN subjected to the supervised learning principle. The back propagation algorithm has also been extensively applied because it is well documented and thus convenient for implementation. Figure 2.7 depicts a portion of a

multilayer feed-forward ANN trained with a back propagation algorithm.

Figure 2.7: Two basic signal flows: forward propagation of function signals and back propagation of error signals

With this training scheme, the sum of squared error between the ANN outputs and target outputs is computed, and then the errors (as denoted by dashed arrows) are propagated backward to neurons in previous layers until they reach the input layer. Suppose the inputs to neuron j in the output layer at iteration n (corresponding to the nth training data set) are given by

$$x_j(n) = \sum_i \left(W_{ij}(n) y_i(n)\right) \tag{2-5}$$

where i denotes the neurons from the previous layer, y_i is the output from a neuron in the previous layer, W_{ij} is the weight connecting that neuron (neuron i) with neuron j in the output layer. Then, the values of outputs can be determined using the transfer function,

$$y_j(n) = f\left(x_j(n)\right) = f\left(\sum_i \left(W_{ij}(n) y_i(n)\right)\right) \tag{2-6}$$

The error signal associated with output neuron j can be calculated,

$$e_j(n) = y_{jD}(n) - y_j(n) \tag{2-7}$$

where y_{jD} is the desired output value for neuron j, which is supplied by the user. The *sum of squared errors* (*SSE*) is obtained by adding the squared errors over all neurons in the output layer,

$$SSE(n) = \sum_j e_j^2(n) \tag{2-8}$$

Based on this, the derivatives of *SSE* with respect to weights can be calculated and used to adjust each weight. The correction term $\Delta W_{ij}(n)$, which is defined by the delta rule (Haykin, 1994), is used to adapt $W_{ij}(n)$,

$$\Delta W_{ij}(n) = -\eta \frac{\partial SSE(n)}{\partial W_{ij}(n)} \tag{2-9}$$

where η is the learning rate used to moderate the training pace, and η can be set to a value between 0 and 1, depending on the gradient of the error surface.

An algorithm with a too small learning rate will take a long time to converge; whereas a learning rate that is too large may result in a training process bouncing around the solution surface and thus ending up with divergence. A small learning rate is desirable in the case of steep error surface, and vice versa. When no detailed information is available on the shape of the error surface, it is reasonable to employ a large learning rate to speed up the training convergence, provided no oscillation results. An effective way to adjust the learning rate to prevent divergence is: determining the change in weights by adding a momentum term that corresponds to the weight change in the last epoch (corresponding to the (*n-1*)th training data set).

$$\Delta W_{ij}(n) = -\eta \frac{\partial SSE(n)}{\partial W_{ij}(n)} + \alpha \Delta W_{ij}(n-1) \tag{2-10}$$

where α is a constant representing the influence caused by the weight correction in the previous epoch.

Finally, the weights connecting the output layer neurons and neurons in the second last layer can be updated by

$$W_{ij,new}(n) = W_{ij,old}(n) + \Delta W_{ij}(n) \quad (2\text{-}11)$$

The back propagation of the errors is performed throughout the ANN until the weights connecting the input layer neurons have been updated, and then one epoch is finished. This process is repeated until the error signal is driven to approaching a sufficiently small number.

Generalization capability of ANN

Essentially, back propagation training is a process of encoding the system input-output correlation. A well trained network has memorized the data sets fed into it, but its generalization capability remains to be justified. That is, the network should also be able to foresee and extend to new situations. When this fails, the problem of over-fitting occurs. Two methods are generally used in order to overcome this problem, one is early stopping and the other one is regularization (MATLAB, 2006), and both of them were adopted and implemented in the current study.

1. Early stopping

With the early stopping method, the available data sets are usually randomly partitioned into three groups. The primary subset is the training set, which is used for computing the gradient so as to update the network weights. The second subset is the validation set (typically about 20 percent of the available data). The errors associated with the validation set are monitored during the training process, and a rise in the validation set error indicates the occurrence of over-fitting. When the validation error increases continuously for a certain number of iterations, the training is stopped early. The third subset is used for network test (also about 20 percent of the data available). The errors calculated from the test data are compared to the validation error during the

training. The errors associated with the test data are usually used as a further check on the network's generalization capability, but do not have any impact on the training process. The early stopping training algorithm is implemented here in conjunction with a Levenberg-Marquardt back-propagation training function.

The flow chart of the ANN training, validation, and testing process with early stopping, which was devised and implemented in this study, is presented in Figure 2.8.

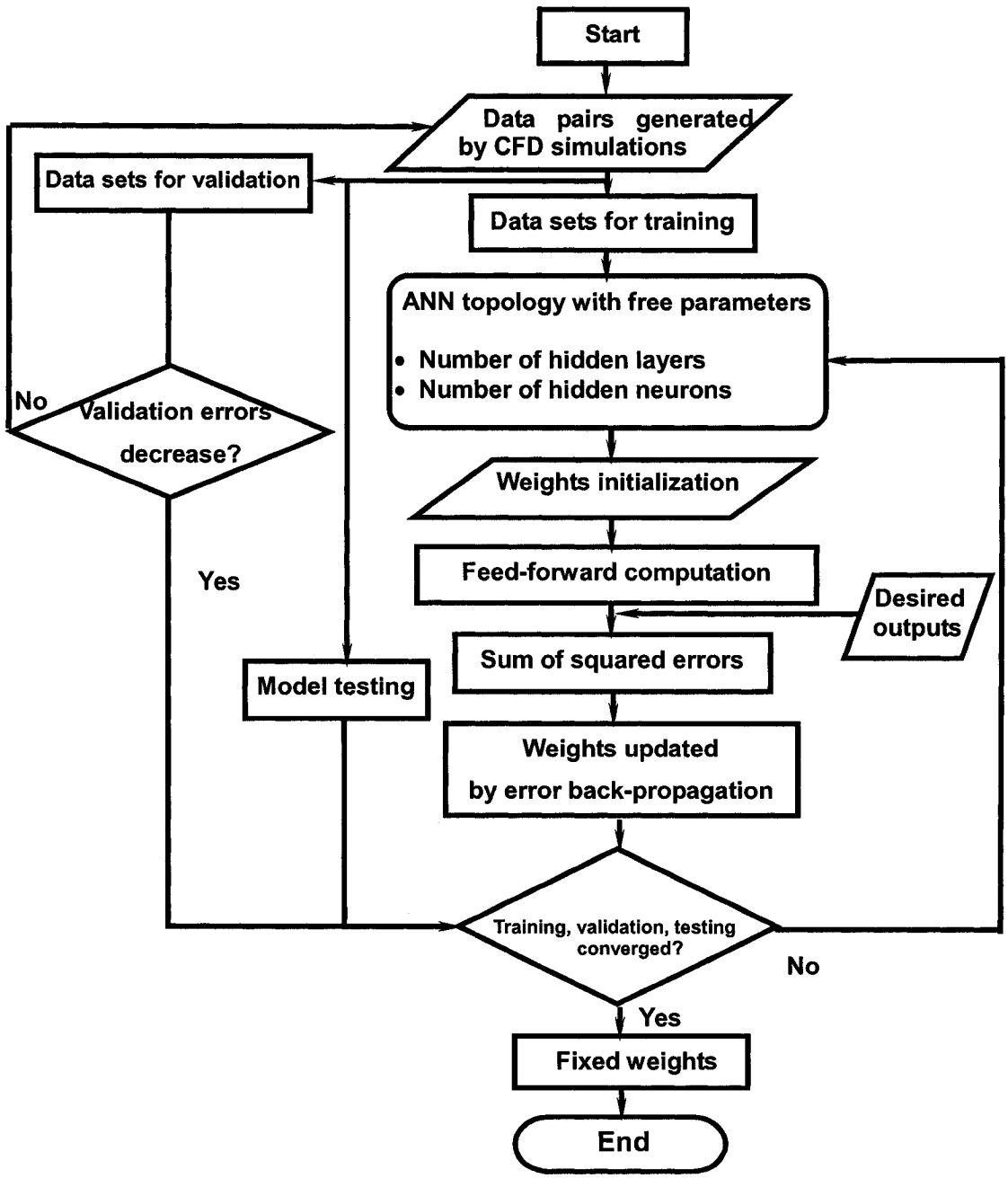

Figure 2.8: Flow chart for early stopping ANN training

2. Regularization

The regularization method involves adapting the error calculation function in response to the evolving error signals. The error calculation function is normally

prescribed as the sum of error squares over the training data set.

$$Error = SSE(n) = \sum_j e_j^2(n) \tag{2-12}$$

It is possible to improve the generalization of the network if such a function is modified by adding a term that consists of the mean value of summed squares of the up-to-date network weights.

$$Error' = \beta SSE(n) + (1-\beta)MSW = \sum_j e_j^2(n) + (1-\beta)\sum_i W_{ij}^{\ 2}(n) \tag{2-13}$$

β is the performance ratio, the value of which is left open to be determined by the user.

It is desirable to specify the optimal regularization parameters in an automated way. One approach to address this is Bayesian regularization (MacKay, 1992), in which the weights and biases of the network are assumed to be random variables complying with certain distributions. These parameters can be estimated using statistical techniques. It is stated in MATLAB (2006) that Bayesian regularization generally provides better generalization performance than early stopping. The reason is that Bayesian regularization uses all of the data rather than separating data into subsets for training, validation, and test. This becomes especially attractive when the size of the data set is not very large.

2.5 Framework of Numerical Optimization in This Study

The simulation-based optimization approach developed here breaks the problem under consideration into three sequential steps:

1. By varying the influential variables in the pre-validated template CFD model, perform sufficient CFD simulations to predict the system performance assessment indices in

response to the variations in the input data. This part of work can be considered as ANN training/test data preparation.

2. By exploiting the input/output data pairs obtained in the previous step, train and test an ANN model for quick response approximation. Such a model can be used in the place of CFD simulation inside the GA search loops for the purpose of computing the value of the objective function with less computational cost and comparable accuracy.

3. Apply GA to the established ANN model to search for the near-optimal set of controlled variables (parameters representing ventilation system design configurations and operational states) in an office space with particular geometrical configuration and thermal conditions, with the goal of achieving satisfactory comfort and IAQ without sacrificing the energy efficiency of the ventilation systems.

Of these three components, the first step can be carried out independently beforehand; while the ANN and GA are integrated into one numerical scheme to facilitate automated optimization search. Afterwards, the near-optimal combination of controlled variables obtained in step 3 is to be supplied to the CFD program to perform a verification case study; the simulation results can be used to illustrate the optimization result's preponderance and the accuracy of the low fidelity ANN model and thus can justify the validity of the optimization approach.

Figure 2.9 briefly outlines the implementation plan of the above numerical optimization methodology. One may notice from this flow chart that the topic of *Latin hypercube sampling* (LHS) is left open temporally, which will be addressed in Chapter 5 together with ANN training results.

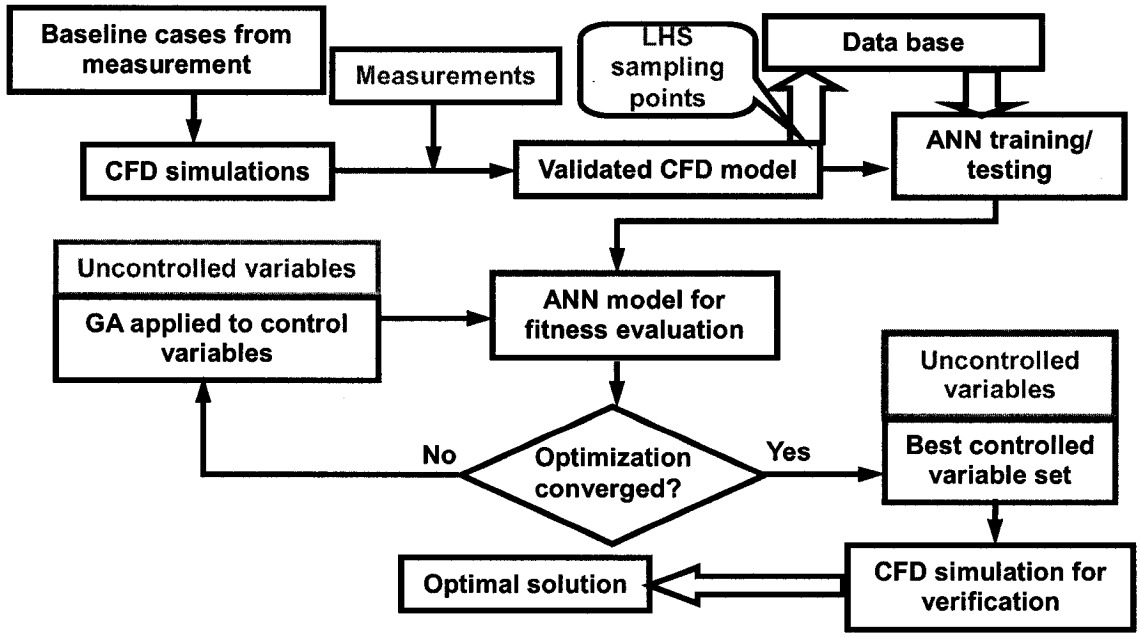

Figure 2.9: Flow chart of the simulation-based optimization approach

It is worth noting that such a simulation-based optimization scheme was not devised from scratch in the present work. Mengistu (2005) adopted a CFD simulation-based GA optimization approach to improve the turbomachinery blade shape, with the goal of maximizing the adiabatic efficiency and pressure ratio of the turbine. He also employed ANN techniques for RSA to cut down the computational expenses required by fitness evaluation. In addition to this, Chow et al. (2002) implemented an ANN-based GA approach to find the optimal set of parameters (regarding the mass flow rate and temperature in the chilled water and condensed water loops), to minimize the fuel and electricity consumed by an absorption chiller system. These studies have confirmed that numerical optimization combining ANN and GA could be an effective approach without explicitly formulating the objective function as ordinary mathematic equations and calculating the derivatives to guide the optimization engine.

2.6 Closing Remarks

Chapter 1 proposed the CFD-ANN-GA optimization approach for aiding the design and operation of office ventilation systems, while this chapter substantiated the applicability of GA and ANN as an optimization engine and for RSA by providing their respective conceptual basis.

Embedded key elements in GA including the population size, the mathematical representation of candidate solutions, the genetic operators, the method used for parents and survival selection, and the stopping criteria were described in Section 2.2. Also, the following topics regarding ANN techniques were addressed in detail in Section 2.4: how an artificial neuron handles the information given to it; what is the commonest ANN architecture in practical applications; how to train a network with an error back propagation mechanism; how to improve the generalization ability of an ANN model by integrating early stopping or regularization techniques.

After the numerical issues pertinent to GA and ANN were addressed, Section 2.5 presented the framework of the numerical optimization scheme that was used. As can be seen, the element of CFD, though a determinant factor affecting the efficiency, the accuracy, and the stability of the overall optimizer, has yet to be described. The conceptual basis of CFD is introduced in the Appendix A.

CHAPTER 3

EVALUATION OF THE OFFICE BUILT ENVIRONMENT

3.1 Introduction

Increasing awareness of the impacts of thermal comfort and IAQ on office workers' health and productivity has stimulated the evolution of ventilation systems in office buildings. Extensive studies, both experimental and numerical, have been—and continue to be—conducted in office-type spaces to examine and advance the performance of ventilation systems.

Chapter 1 claimed that CFD simulations of ventilated offices would provide a holistic evaluation of thermal comfort, IAQ and system energy efficiency. Accurate quantitative evaluation of the indoor environment can be only realized by considering reasonable independent variables and by selecting appropriate criteria to assess the objectives of interest. In response to this, the current chapter sets out to address such topics as: how the commonly employed ventilation systems affect the office environment; what criteria are suitable for the evaluation of comfort, air quality, and ventilation energy costs; and what the influential parameters are, in terms of representing the office environmental conditions and ventilation system design configurations and operating states.

Section 3.2 provides conceptual descriptions of alternate ventilation principles that are commonly used in office buildings. Section 3.3 then extracts the commonly employed evaluation indices with respect to the office comfort and air quality level from the literature. These indices are introduced in detail and their calculation methods are also described. Previously, it has been uncommon to predict ventilation energy cost using

CFD predicted data exclusively; however, the energy usage of a ventilation system is one of the major concerns herein. Therefore, the solutions to address this need are also put forward in Section 3.3, which describes how the fan power input and the space cooling energy consumption can be derived based on the data available from CFD calculations. After this, Section 3.4 surveys the literature for previously studied parameters that have proven to significantly affect the office indoor environment and ventilation energy consumption, and the commonly studied parameters are selected as the controlled states and input parameters in CFD modeling and in further optimization work. Finally, a brief summary regarding the above issues is provided in Section 3.5.

3.2 Alternate Ventilation Systems in Office Buildings

As previously mentioned, the most common ventilation systems in North American office buildings are MS with both supply and return air terminals located at ceiling level and UFAD systems with floor-mounted inlets and ceiling return vents. Overhead MS is the traditional ventilation principle, while UFAD has gained popularity in the building market over the recent decade.

3.2.1 Mixing System

With the concept of MS, conditioned air is delivered through ceiling level diffusers and is intended to be uniformly mixed with the room air before exhausting from ceiling return grilles, with the purpose of removing the surplus heat and gaseous contaminants. Previous studies have diagnosed some inherent problems associated with MS: first, it is difficult to achieve perfect mixing, which may result in stagnant regions within the flow field where high contaminant concentration occurs (Lin et al., 2005 (Part II)); second,

even when full mixing occurs, it could produce entrainment and recirculation inside the office and thus induce cross contamination between individual sources (office workers, equipments, furnishings, etc.); also, well-stirred indoor air resulting from MS might raise the issue of individual preference variations for micro-environment; furthermore, MS may increase the likelihood of air short circuit, that is, the supply air might flow to the return grilles (which are also located at ceiling level) without penetrating into and spreading through the lower occupied sub-zone and thus contribute little to contaminant and heat removal (Lehrer and Bauman, 2003).

In response to the growing demands for better indoor climate, MS is experiencing some advancement such as the incorporation of *variable air volume* boxes equipped with thermostats for flow rate control and the utilization of individually controlled jet nozzle diffusers (Zhou et al., 2005). Some of these newly integrated elements have dropped the fully-mixed assumption and resulted in a thermally non-uniform environment.

3.2.2 Underfloor Air Distribution System

Computer, network, and other types of information system devices are popular and even requisite in modern office buildings; therefore, there has been a growing tendency to use raised floors in office buildings with the goal of providing convenience and flexibility for cable accommodation and management. Such a tendency has promoted the broad adoption of UFAD systems in office buildings. It was estimated that, by 2004, approximately 35% of newly constructed office buildings would be built with raised floors and half of those would use UFAD (Bauman and Webster, 2001).

UFAD is also very often cited as an effective approach to overcome the aforementioned problems associated with MS and provide additional benefits. When

using this technology, air is directly delivered to the vicinity of the occupant at floor or desk level, through floor or partition/desk mounted swirl diffusers or perforated panels. Air is returned from grilles located at ceiling level, the same as with MS. This type of arrangement results in, to some extent, the mixing of the supply air into the lower part of the room. With a properly designed UFAD system, this mixing zone would be confined to the elevation of air throw, and air does not remix into this region after entering the upper uninhabited zone. As a result, this piston like upward airflow can expel the indoor air contaminants through ceiling exhausts and increase the ventilation efficiency. In addition, with the easily accessible air terminals, UFAD systems provide the occupants with the capability of *personal environmental control* (PEC) on supply air conditions such as air discharge orientation and air flow rate.

Aside from the above two categories of ventilation systems, *displacement ventilation* (DV) is also a popular technology that has been commonly used in industrial workshops in Scandinavia during the past 20 years (Yuan et al., 1999). With this principle, 100% outdoor air is usually delivered horizontally from low side wall diffusers at extremely low discharge speed and is exhausted at ceiling level. The low velocity allows the plume of warm air rising from heat sources to drive the piston-like upward flow and extract the indoor contaminants from ceiling exhaust grilles. However, using fresh air exclusively may be inadequate to satisfy the internal cooling load. Under certain conditions, air discharge of a DV system was proven to create recirculation and cross contamination in the occupied zones of a large office (Zhao et al., 2004). To overcome these shortcomings, recent research related to DV system in office environment has shifted towards discharging air with higher momentum (Lau, 2005; Lin et al., 2005), which demonstrated

a convergence of DV and UFAD. In light of this, discussions hereafter will mainly focus on overhead MS and UFAD systems. In comparison to MS, UFAD systems have the following attractive features, as summarized in the UFAD design guide (Bauman, 2003) and other literature.

Reducing energy use

UFAD, with its system arrangement, creates an upward airflow pattern and distinct temperature stratification. This airflow pattern and temperature distribution may produce energy savings, since heat generated from the internal heat sources will be captured by the upward plume and not mix with ambient room air. Further energy saving is possible with UFAD systems due to the high supply temperature (typically at or above 17 °C, in contrast to 13~15 °C with MS). Such a high supply temperature, on one hand, allows a high percentage of outdoor air usage and may extend the operation of economizer mode (an economizer mode uses 100% outside air for cooling purposes instead of mechanical cooling, provided that the temperature of outdoor air is low enough to satisfy the cooling requirements); on the other hand, it may decrease the chiller usage and improve the *coefficient of performance* (COP) of the chiller (the gain in chiller's COP was estimated by Ke and Mumma (1997) to be 1% for every 1.1 °C rise in supply air temperature).

Apart from the high supply air temperature, the low supply pressure required by UFAD (relative to that with MS) can offer further energy savings. UFAD systems often distribute the conditioned air through an underfloor plenum and use much less duct work compared to a typical MS; therefore, much lower supply pressure is required and the fan power input can be reduced (Webster et al., 2000).

Improving thermal comfort

Substantial experimental and numerical studies have demonstrated that, when properly designed, a UFAD system can maintain the indoor air motion, temperature stratification, and the horizontal temperature variations at comfortable levels (Loudermilk, 1999; Lau, 2005; Lin et al., 2005 (Part I)). Subjective survey results collected in a broadband center also revealed that UFAD could lead to higher degree of satisfaction, as 88% of panelists expressed preference for the thermal environment with the studied UFAD system over that with an overhead MS and 50% of them reported floor air supply enhanced their ability to perform their work (Webster et al., 2002). Additionally, as previously mentioned, UFAD provides the occupant with capability of *personal environmental control* (PEC). A field study on this topic (Bauman et al., 1995) concluded that the occupants who were given the ability to control local environment were almost twice as tolerant of temperature differences and thus expressed fewer thermal complaints.

Enhancing IAQ

In comparison with overhead MS, UFAD may result in lower contaminant concentration indoors (Sodec and Craig, 1990), higher air change efficiencies (Matsunawa et al., 1995), greater room average air change effectiveness (145% with UFAD vs. 100% with MS) (Olesen et al., 1994), a younger age of air at breathing level (Faulkner et al., 1995; Akimoto et al., 1999; Xing et al., 2001), and higher contaminant removal efficiencies (Lau, 2005). These improvements can be considered indicators of enhanced IAQ and ventilation efficiency. In addition, a subjective survey carried out in an office building with UFAD also reported a 50% cut in dissatisfaction with perceived air quality, relative to IAQ rating with MS (Shirai et al., 2003).

The reasons commonly cited for better IAQ resulting from UFAD are as follows

(Cermak and Melikov, 2005): on one hand, the high percentage usage of outdoor air can lead to a higher outdoor air change rate. Air change rate is the fresh air supply rate (per hour) divided by the indoor air volume. On the other hand, the plumes of warm air rising from heat sources and the upward airflow pattern can carry the chemical species or particles to the upper warmer zone and keep the more polluted air outside the breathing level.

It is worth mentioning that other potential benefits are ascribed to UFAD systems, including greater flexibility (with respect to MS) provided to building services and reduced life-cycle cost (Shute, 1995; Bauman and Webster, 2001; Bauman, 2003). But those issues are beyond the scope of the present study and thus no attempt is made to elaborate them here.

Notwithstanding, the realization of all these benefits with UFAD are highly dependent on many factors such as the quality of system design, installation, and commissioning, the post-occupancy building maintenance and operation, the occupants' awareness and education (regarding the features of the system), and the climate conditions. Some research reported that, using floor supply would increase the likelihood of local draft and excessive temperature stratification as well, due to the direct supply of cool air in the vicinity of occupants (Wyon and Sandberg, 1990); while another study even concluded that, in tropical regions, UFAD system is neither energy efficient nor cost attractive, due to the high cooling energy demand (resulting from both internal and external loads) and high ventilation rate requirement (Lin et al., 2005 (Part II)).

In light of this, it would be necessary to expand the current discussion to an overview of previous investigations of UFAD and MS in office environment, with the emphasis

being put on the commonly adopted criteria for comfort, air quality, and energy efficiency, as well as on the commonly studied influential parameters (in terms of system performance).

3.3 Criteria for Office Built Environment Evaluation

3.3.1 Thermal comfort and IAQ evaluation indices from literature

The literature was surveyed for indices appropriate for thermal comfort and IAQ evaluation in office environments. A wide variety of indicators can be seen in previous experimental studies and simulation-based analyses conducted in office-type spaces, from which the most frequently used ones are extracted and summarized in Table 3.1.

Performance evaluated	Index	Definition
Thermal comfort	Air Diffusion Performance Index (ADPI)	The percentage of points in the occupied zone that have air speed below 0.35 m/s and effective draft temperature between -1.7 °C and +1.1 °C (ASHRAE, 1990)
	Effective temperature	Temperature with the same effect as an imaginary sealed environment with relative humidity at 50%
	Equivalent Temperature (ET)	Temperature of an imaginary enclosure with the mean radiant temperature (T_{mrt}) equal to the actual still air temperature, where a person has the same heat exchange with the surrounding (Wyon, 1989)
	Mean Radiant Temperature (T_{mrt})	The uniform temperature of an imaginary enclosure in which the radiant heat transfer from the human body equals the radiant heat transfer in the actual non-uniform enclosure (calculated as the average temperature of the objects and its surrounding surfaces)
	Percentage of people dissatisfied due to draft (PD)	PD is a function of turbulence intensity, temperature, air velocity (Fanger et al., 1989)
	Operative temperature	The average of dry bulb temperature and T_{mrt}

	Predicted Mean Vote (PMV)	PMV of a large group of people (Fanger, 1970; ISO7730, 1994) is a function of human activity, clothing, and thermal environmental parameters
	Predicted Percentage of people Dissatisfied (PPD)	PPD with the thermal surrounding (Fanger, 1970; ISO 7730, 1994) is a function of human activity, clothing, and thermal environmental parameters
IAQ	Air Change Effectiveness (ACE)	$ACE = t_{return}/t_{bl}$, where t_{return} is mean age of return air, t_{bl} is mean age of air at breathing level (Faulkner et al., 1999)
	Air Change Rate (ACH)	ACH is defined as fresh air supply rate (per hour) divided by indoor air volume
	Age of air	The average time required for air to reach a given point after it enters the room (Etheridge and Sandberg, 1996)
	Air change efficiency	Ratio of nominal time (volume of indoor domain divided by fresh air supply rate) to room mean age of air (Sutcliffe, 1990)
	Contaminant Removal Efficiency (E_c)	$E_c=(C_{return}-C_{supply})/(C_p-C_{supply})$, where C_{return} is the contaminant concentration in the return air, C_{supply} is the contaminant concentration in the supply air, C_p is the contaminant concentration at the measurement point
	Personal Exposure Effectiveness (E_P)	$E_P=(C_{I,O}-C_I)/(C_{I,O}-C_{PV})$, where $C_{I,O}$ is the contaminant concentration in the inhaled air without personal ventilation, C_I is the contaminant concentration in the inhaled air, C_{PV} is the contaminant concentration in personalized air (Melikov et al., 2002)
	Ventilation Effectiveness (E_v)	$E_v=(C_{return}-C_{supply})/(C_{ws}-C_{supply})$, where C_{ws} is the average contaminant concentration in a workstation (Awbi, 2003)
	Re-inhaled Exposure Index (E_{RI})	$E_{RI}= C_I/ C_E$, where C_E is the contaminant concentration in the exhaled air (Melikov et al., 2000) and C_I is the contaminant concentration in indoor air

Table 3.1: Office thermal comfort and IAQ assessment criteria

It is worth noting that some of these indices, as reported in literature, do not fit the performance analysis of particular ventilation principles. For example, MS was found to outperform UFAD by far in terms of ADPI; however, a study pronounced that ADPI

would be an inappropriate index for those systems delivering conditioned air in the vicinity of occupants (Arens et al., 1991).

The selection of indices to quantify ventilation performance and to evaluate the office environment mainly depended upon two factors: applicability and availability. Applicability indicates whether or not the indices are appropriate for evaluating the performance of the ventilation systems under consideration and whether or not they (collectively) can provide a holistic evaluation to cover all the issues of interest; whereas availability means whether or not these indices can be derived from CFD simulations. The baseline CFD simulations presented in subsequent chapters were validated against experimental measurements, thus the availability of a particular independent variable in CFD results was exclusively determined by the experimental design, the facilities, and the objective measurements.

From the assessment criteria listed in Table 3.1, the following indicators were selected for thermal comfort and IAQ evaluation in ventilated office environments. These were calculated based on output quantities from CFD simulation and were integrated into the objective function for optimization.

3.3.2 Indices for thermal comfort evaluation in the current study

The PMV-PPD model

Maintaining the indoor thermal conditions at comfortable levels is the primary design objective of a ventilation system. The prediction of comfort level has been standardized over the last four decades. The PMV-PPD model (Fanger, 1970) is the most frequently used and best-understood model for quantitative thermal comfort analysis.

PMV reflects the mean vote of a large group of occupants who are exposed to a given

combination of thermal parameters. PMV index evaluates thermal environment in an indoor space by using a thermal sensation range scale: -3 (cold), -2 (cool), -1(slightly cool), 0 (neutral), +1 (slightly warm), +2 (warm), +3 (hot). PMV is defined as a function of six thermal variables related to the indoor air conditions and human activitues, including air temperature, air humidity, air velocity, *mean radiant temperature* (T_{mrt}), clothing insulation level, and human activity. The value of PMV can be determined from the following equation (ISO 7730, 1994)

$$PMV = (0.303\exp(-0.036M)+0.028)L \tag{3-1}$$

where L is the thermal load on the human body (W/m^2) and

$$\begin{aligned} L = {} & M - W - 3.05\times10^{-3}[5733 - 6.99(M-W) - P_v] - 0.42(M - W - 58.15) \\ & - f_{cl}h_c(T_{cl} - T_{indoor}) - 1.7\times10^{-5}M(5867 - P_v) - 0.0014M(34 - T_{indoor}) \\ & - 3.96\times10^{-8}f_{cl}\left[(T_{cl}+273)^4 - (T_{mrt}+273)^4\right] \end{aligned} \tag{3-2}$$

where M is the metabolic rate per unit body surface area (W/m^2), W is the external work (W/m^2) (equals to zero in most cases), P_v is the local partial water vapor pressure in air (Pa), f_{cl} is the ratio of the area of clothed body to the surface area of the nude body, h_c is the convective heat transfer coefficient between the outer surface of clothing and the ambient air ($W/m^2°C$), T_{cl} is the outer surface temperature of clothing (°C), T_{indoor} is the local indoor air temperature (°C), and T_{mrt} is the radiant temperature (°C) The partial water vapor pressure is obtained from

$$P_v = \frac{P_s \times RH}{100} \tag{3-3}$$

with P_s being the saturated water vapor pressure at local temperature (Pa) and RH is the relative humidity in local air. Furthermore, T_{cl}, h_c, and the f_{cl} can be determined using the following conditional equations:

$$T_{cl} = 35.7 - 0.028(M - W) - I_{cl}\left\{3.96\times10^{-8} f_{cl}\left[(T_{cl}+273)^4 - (T_{mrt}+273)^4\right] + f_{cl}h_c(T_{cl} - T_{in})\right\} \quad (3\text{-}4)$$

$$\begin{cases} h_c = 2.38\times(T_{cl} - T_{in})^{0.25} & \text{for } 2.38\times(T_{cl} - T_{in})^{0.25} > 12.1\times\sqrt{V} \\ h_c = 12.1\times\sqrt{V} & \text{for } 2.38\times(T_{cl} - T_{in})^{0.25} < 12.1\times\sqrt{V} \end{cases} \quad (3\text{-}5)$$

$$\begin{cases} f_{cl} = 1.00 + 1.290 I_{cl} & \text{for } I_{cl} < 0.078 \\ f_{cl} = 1.05 + 0.645 I_{cl} & \text{for } I_{cl} > 0.078 \end{cases} \quad (3\text{-}6)$$

where V is the local air velocity (m/s) and I_{cl} is the thermal resistance of the clothing ($m^2°C/W$).

It should be noted that PMV can not precisely indicate what percentage of the occupants are expected to be dissatisfied; notwithstanding, even when the PMV index is neutral (which is supposed to represent the ideal thermal conditions), there still remains some people dissatisfied with the thermal environment due to the variations in individual preference. To account for this type of subjective difference, Fanger (1970) proposed another index—PPD, which can be determined from PMV value.

$$PPD = 100 - 95\exp(-0.03352PMV^4 - 0.2179PMV^2)(\%) \quad (3\text{-}7)$$

PPD represents the percentage of people who express thermal sensation more than slightly warm or cool. Correlation between PPD and PMV indicated that even when PMV is equal to zero, PPD is 5%, allowing for the fact that there always exist some people who are dissatisfied. According to the recommendation of the comfort standard ISO 7730 (1994) and ASHRAE Standard 55-2004, a PMV value between −0.5 and +0.5 corresponds to the situation that about 90% of people feel comfortable (PPD ≤ 10%).

Equivalent temperature

Despite the provision of acceptable whole-body comfort, UFAD systems are

sometimes found to cause asymmetric thermal sensations, if not designed properly. That is, even if an individual expresses global comfort, he/she may still experience discomfort at a particular part of his body. An indicator named *equivalent temperature* (ET) was proposed to appraise thermally non-uniform environments.

ET was originally introduced to study the highly non-uniform micro-climates encountered in automobiles (Wyon, 1989). ET integrates the independent effects of air temperature, air velocity, mean radiation, and solar load on heat loss/gain from the occupant body into a single physical quantity. It is defined as the temperature of a uniform enclosure in which a human body would experience the same rate of heat loss as in the actual thermally non-uniform environment. It was claimed that if the variations of ET over the entire body are controlled in the range of -2 °C to 2 °C, there is no excessive thermal non-uniformity over the entire body.

The applications of ET have not been restricted to vehicle conditions. Previous research also used ET to account for the spatial variations of comfort sensation in office-type spaces (Fukao et al., 2002; Nilsson and Holmér, 2003). Both studies calculated the value of ET based on the heat loss rate at each body segment of a thermal manikin in office environments equipped with UFAD and MS. Nilsson and Holmér (2003) also conducted a subjective survey and introduced an index named *mean thermal vote* (MTV) based on the thermal sensation rated by the panelists. The regression of MTV on ET demonstrated a good agreement between the survey results and the data measured from the manikin.

For each part of the human body, ET can be calculated using the following equations (Bauman et al., 2000),

$$ET = T_s - I_{cl} \times Q_t \quad (3\text{-}8)$$

where T_s is the skin temperature (°C), and Q_t is the local heat loss rate from skin surface (W/m^2).

ET was included in the objective function to quantify asymmetric sense of thermal sensation, a risk frequently associated with UFAD system.

Head to ankle temperature difference and local air velocity

UFAD strategies supply cooler air to the lower region of the office and produce distinct temperature stratification; however, excessive temperature gradient along vertical direction may result in complaints. According to ASHRAE Standard 55-2004 and ISO 7730 (1994), the temperature difference between the head and the ankle level should not exceed 3 °C, which corresponds to 5% dissatisfaction. It is necessary to maintain this vertical temperature difference at or below the recommended value to avoid "cold feet and warm head" complaints.

In addition to the above-mentioned indices for comfort evaluation, it was suggested by ASHRAE standard 55-2004 that the local air speed near an office worker should be controlled at or below 0.25 m/s to avoid annoyance and distraction.

The ET difference between the two sides of an individual occupant, the head to ankle temperature difference ($\Delta T_{HeadToAnkle}$), and the local air velocity near the occupant were integrated into the penalty terms in the objective function for optimization. When these three indices exceeded the recommended values, the penalty term was set to a relatively large positive number (since GA intends to minimize the objective function here).

3.3.3 Indices for IAQ evaluation in the current study

Concentration of Carbon Dioxide (CO_2)

Concentration of CO_2 has been the most important indicator for IAQ monitoring and studies (Stonier, 1995; Persily, 1997). Previously, CO_2 concentration measurements were conducted in office buildings to estimate ventilation adequacy (Cheong, 1996). Though CO_2 concentration does not provide a holistic evaluation of air quality, high CO_2 concentrations in offices could be an indirect indication of inadequate ventilation. The basic premise is that if the surplus CO_2 can't be adequately removed by ventilation, then other indoor contaminants may accumulate proportionately.

The CO_2 generation rate from a person who is performing moderate office work is at 0.31 L/min (ASHRAE, 2001). CO_2 concentrations in office buildings typically range from 350 to 2500 ppm (Seppänen et al., 1999) while, CO_2 concentration in outdoor air is approximately 350 ppm. The minimum ventilation rate specified in the Standard ASHRAE 62-2001 is 8 L/s per person (ASHRAE, 2001). As indicated by these numbers, the allowable indoor CO_2 level in office spaces would be at or below 1000 ppm (approximately).

Seppänen et al. (1999) indicated that the risk of respiratory organic irritations would possibly increase by a factor of six when indoor CO_2 concentrations in office were increased by 420 ppm above the outdoor level, or even if the maximum indoor CO_2 concentration requirement ($\leq$ 1000 ppm) was satisfied. Also, they indicated that reducing the CO_2 concentration to 800 ppm or less can substantially improve occupant's satisfaction with IAQ and lower the related health risks. Similar conclusions were obtained by another study (Charles, et al., 2005), which found that the evaluation of IAQ

was improved as CO_2 concentration decreased (data cited was from 1100 ppm to 470 ppm); furthermore, when the CO_2 concentration went below 650 ppm, the majority of people would express satisfaction.

CO_2-based Ventilation Effectiveness (ε_v)

The calculated CO_2 concentration distribution can be further integrated into a dimensionless index—Ventilation Effectiveness (ε_v). ε_v is calculated from the equation below, which is slightly different from the original definition (Awbi, 2003). The CO_2 concentration at breathing level is used here instead of the average concentration throughout the workstation.

$$\varepsilon_v = \frac{c_{return} - c_{supply}}{c_{br} - c_{supply}} \tag{3-9}$$

where c_{return} is the CO_2 concentration in the return air (ppm), c_{supply} is the CO_2 concentration in the supply air (ppm), and c_{br} is the CO_2 concentration at breathing level near the occupant (ppm).

In the current study, two boxes were placed in the office studied, releasing CO_2 and heat to the ambient air at adjustable rates (see Chapter 5 for details). These boxes mimicked the behavior of office equipment (such as photocopier, printer, fax machine, etc.). The transport of CO_2 in room air was modeled by the CFD program. The optimizer searched for better system design and operation parameters that decreased the CO_2 concentration at breathing level and enhanced ε_v as much as possible.

3.3.4 Accounting for ventilation energy usage in the current study

A popular trend in CFD simulation of office environments is the prediction of airflow; in contrast, issues with regards to heat transfer and energy usage have not been

successfully addressed using CFD techniques. A common approach to account for cooling energy consumption is by making use of the operational parameter of the chiller. For example, Sekhar et al. (2003) applied an integrated IAQ-energy audit method to office buildings in Singapore, in which the product of chilled water flow rate and change in chilled water enthalpy was used as the energy performance index.

Based on the survey of previous experimental and numerical work on quantifying energy efficiency of ventilation systems, this section sets out to describe the indices used in the current study to determine energy required by ventilation. Those indices can be derived from the outputs estimated by CFD calculation. The energy usage of the ventilation system can be divided into two main parts, fan power input and cooling energy consumption.

Fan energy consumption

In modern office buildings, most ventilation systems employ an all-air mode for cooling/heating distribution; therefore, the power input into supply (exhaust) fans may be a significant portion of the total energy required by the mechanical system. For example, in the case of typical overhead MS, supply fans may consume up to 40% of the overall energy usage by ventilation. Therefore, it is important to look for ways to reduce this portion as much as possible. It was often claimed that the distribution ductwork could be reduced with UFAD systems, which could shrink the electricity consumption by fans. The discussions herein (related to fan energy uses) mainly focus on UFAD and MS systems equipped with pressurized (passive) *variable air volume* (VAV) air terminals. The word "pressurized" stands for the fact that conditioned air is distributed by central

fans and then discharged through passive diffusers. Thus, fan energy consumption in a ventilation system can be translated into central supply fan(s) energy inputs.

Principally, we know that fan power input (W) can be determined using the following expression

$$E_{fan} = \frac{\Delta P \times \dot{V}_{air,total}}{1000\eta_{fan}} \tag{3-10}$$

where ΔP is the pressure rise through the supply fan (Pa), $\dot{V}_{air,total}$ is the overall volumetric flow rate of supply air (L/s), and η_{fan} is the fan efficiency.

It is straightforward and understandable that, in the present study, the value of $\dot{V}_{air,total}$ can be directly extracted from the CFD model (actually, the volumetric flow rate through the central fan is the summation of flow rate through each of the diffusers); whereas the pressure rise and fan efficiency remain to be determined, and how to prescribe the values of ΔP and η_{fan} deserves further specification.

In the case of an overhead MS, a typical central fan is designed to provide a pressure of 750 Pa to deliver air, of which about 125~250 Pa might be required to move air through the VAV box, reheat coil, and ductwork. This is in contrast with the situation in a UFAD system with equivalent capacity—no ductwork is involved (only a trunk duct is necessary) and the conditioned air is supplied through a pressurized plenum. With this type of system configuration, a large portion of pressure loss could be avoided with UFAD. As indicated in a previous study (Webster et al., 2000), it would be reasonable to assume that the central fan static pressure requirements in an UFAD system could be cut down by 25% relative to that in a MS. In this study, the static pressure rise via the central

fan in the MS is assumed to be at 750 Pa while, with the UFAD system, 562.5 Pa is the static pressure rise assigned to the central fans (25% reduction).

The magnitude of fan efficiency is often treated as a function of pressure rise and amount of air passing through the fan. The UFAD design guide (Bauman, 2003) cited the following examples to provide a demonstration of the supply fan performance: when a central airfoil fan with a diameter of 0.76 m is operating at 750 Pa and supplying air at 9700 L/s, it would result in a combined efficiency (efficiency of the fan plus that of the motor) of 76%. When the same central airfoil fan is operating at 623 Pa for the same air flow rate (9700 L/s), it would work under an overall efficiency (motor plus fan) of 67%. In the case of a forward curved fan with small size (with a diameter of 0.46 m), it supplies air at 1460 L/s and provides a 62 Pa pressure rise with a combined fan and motor efficiency of 38%. These numbers indicate that, when the flow rate through a fan holds constant, the overall efficiency of a fan decreases as the pressure rise drops. Also, the overall efficiency value of a small size supply fan is lower than that of a large fan working at higher static pressure and higher supply flow rate.

Given the above numbers, the efficiency of the central supply fan in the current study was characterized by relating the efficiency to overall supply flow rate. Since the pressure rise via the supply fan in this study was assumed to be at a constant level, its effect on fan efficiency is dropped here. Accordingly, the overall efficiency of the supply fan within the allowable flow rate range (80~160 L/s) was calculated using the following correlation:

$$\eta_{fan} = \frac{\dot{V}_{air,total}}{400} + 0.25 \qquad (3\text{-}11)$$

This correlation was established based on the assumption that when the total supply air flow rate is 160 L/s, the resulting combined fan energy efficiency isat 65% while,

when supply air flow rate is reduced to 80 L/s, the combined fan energy efficiency is 45%. The intermediate values can be approximated using a linear interpolation between the two extremes.

Cooling energy consumption

The flow chart of chiller, cooling coil, and supply fan is shown schematically in Figure 3.1.

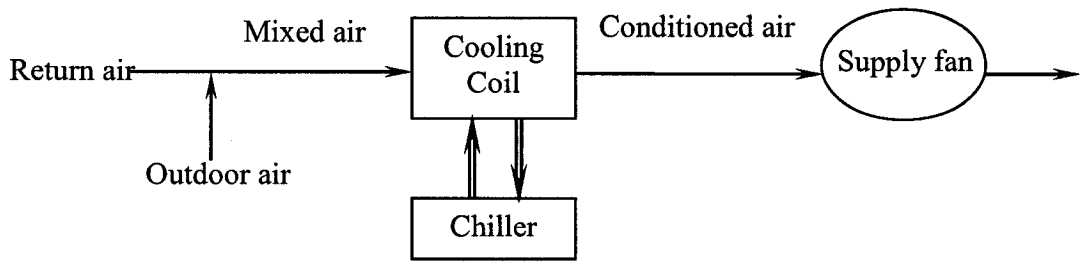

Figure 3.1: Sketch of chiller, cooling coil, and supply fan

Cooling coils remove the sensible heat load produced within the conditioned space and offsets the humidity and temperature in the outdoor fresh air. In light of the previous methods used for energy usage prediction with alternate ventilation systems (Bauman, 2003; Xu and Niu, 2006), it is clear that the cooling energy requirement can be subdivided into two portions,

$$Q_{cooling} = Q_{space} + Q_{vent} = \dot{m}_{air,total} c_p \left(T_{return} - T_{supply}\right) + \dot{m}_{fresh} (h_{out} - h_{return}) \quad (3\text{-}12)$$

where $Q_{cooling}$ is the total cooling load (W), Q_{space} is the cooling energy portion used to remove sensible heat load in the indoor space (W), Q_{vent} is the cooling energy portion used to condition the outdoor fresh air to return air states (W), $\dot{m}_{air,total}$ is the total mass flow rate of supply air (outdoor fresh air plus the re-circulated portion of return air) (kg/s), c_p is the specific heat of air (J/kg°C), T_{return} is the temperature of return air (°C), T_{supply} is

the temperature of supply air (°C), $\dot{m}_{fresh}$ is the mass flow rate of outdoor fresh air (kg/s), h_{out} and $h_{returnt}$ are the specific enthalpy of the outdoor air and return air (J/kg), respectively. The value of enthalpy (J/kg) is given by,

$$h = 1.01T + 0.001d(2500 + 1.84T) \tag{3-13}$$

where d is the humidity ratio (moisture content) of the air (kg water vapor/kg dry air), based on this, the equation of Q_{vent} can be translated to,

$$Q_{vent} = \dot{m}_{fresh}[1.01T_{out} + 0.001d_{out}(2500 + 1.84T_{out}) - 1.01T_{return} - 0.001d_{return}(2500 + 1.84T_{return})] \tag{3-14}$$

where T_{out} is the temperature of the outdoor air (°C), d_{out} is the humidity ratio in the outdoor air(kg/kg), T_{return} is the temperature of the return air (°C), d_{return} is the humidity ratio in the return air (kg/kg).

Accordingly, the total energy consumed by cooling can be determined provided that the operating states of the ventilation system, the return air conditions, and the outdoor air states are specified. Thermo-physical quantities such as the supply air temperature, the flow rate of supply air, the mean humidity ratio indoors, the return air temperature, the outdoor air moisture content, and the temperature would be treated as the independent variables in this analysis.

One thing requiring explanation is, due to the absence of measured data regarding the room air humidity (for the verification of the CFD simulation results), the transport of water vapor was excluded from the current CFD study; instead, the relative humidity throughout the room is assumed to be maintained at a constant level around 40%. That said, the relative humidity existing in the supply air is presumed to be equal to that in the

return air, and there is no latent heat load generated within the indoor space. The outdoor relative humidity is assumed to be at 70%. Based on the values of relative humidity and corresponding temperature, the moisture content in return air and outdoor air can be determined.

It is the chiller that manages the cooling generation in an HVAC system. $E_{cooling}$ (W), the cooling energy requirement (which equals the power input into the chiller), is given by,

$$E_{cooling} = P_{chiller} = \frac{Q_{cooling}}{COP} \tag{3-15}$$

where $P_{chiller}$ is the power input into the chiller (W), *COP* is the chiller's coefficient of performance.

It is straightforward that when ventilation system is operating with a higher supply air temperature, the chiller energy consumption will be cut down; however, higher supply air temperature may further decrease the chiller energy usage due to the associated positive influence on *COP*. The *COP* of a chiller is defined as the ratio of the cooling load to the electricity power (or fuel) consumption. For a particular chiller, the value of *COP* may depend upon such thermo-physical parameters as the chilled water temperature, the outdoor air temperature, the outdoor air humidity, the cooling load, the supply air temperature in ventilation system, etc., though the quantitative correlation between *COP* and these variables is case specific and can not be readily prescribed. Within the scope of present research, only the effect of supply air temperature on chiller *COP* was taken into consideration.

Based on a previous study (Ke and Mumma, 1997), it would be reasonable to assume the improvement in *COP* to be 1% for every 1.1°C increase in the supply air temperature.

In this study, a reference *COP* value of 3.0 was associated with a baseline supply air temperature of 13 °C; any increase of supply air temperature increased *COP* as follows,

$$COP = COP_{ref} + \frac{(T_{sup\,ply} - T_{ref})}{1.1} \times 0.01 = 3.0 + \frac{(T_{sup\,ply} - 13)}{1.1} \times 0.01 \quad (3\text{-}16)$$

As a supplement to the above statement, the following assumptions were imposed on the energy analysis for the ventilation system:

- The energy used by condenser water pump, chilled water pump, and fans in cooling tower were excluded.
- The cooling coil and chilled water heat exchanger were presumed to work under perfect condition, that is, the heat transfer efficiency in each component was assumed to be 1.
- The ducts were assumed to be perfectly tight and airflow through the ductwork was adiabatic; there was no temperature gradient along the duct when there was no other energy generation equipment; the return air temperature was equal to the local air temperature in the vicinity of the return grille.
- The effect of fan power on the supply air temperature was neglected.
- Air density and specific heat were set to constant values, at 1.205 kg/m^3 and 1005 J/kg°C, respectively, as 20 °C is taken as the reference temperature (Available: http://www.engineeringtoolbox.com/air-properties-d_156.html).

3.4 Influential Parameters

In CFD simulation-based optimization work, it is necessary to abstract the complexities of the real flow field and the thermal boundary in a ventilated office space to a manageable degree; therefore, selecting which parameters to include and exclude as

input variables in CFD simulations and as controlled variables in GA optimization is a common decision faced by the program developer or user. Prior to implementing extensive CFD simulations in the current study, a literature survey of influential parameters (regarding the geometric features, the thermal/airflow conditions, and the system configurations, etc.) commonly studied in a ventilated office environment was conducted.

3.4.1 Influential parameters in the literature

As identified in the literature, a broad range of factors affect the airflow pattern, thermal conditions, and contaminant dispersion in a ventilated office space. Whether or not a physical parameter influences the indoor thermal environment and the extent to which it can affect the indoor environment depends upon the air distribution method, the experimental conditions, the goal of the simulation exercise (or, the objective indices being specified), and/or the design of the numerical model. Results from different sources report conflicting observations regarding the influence of a particular parameter on indoor environment.

For example, Huo (1997) found the airflow pattern and mean age of air in an office-type test chamber, which was served by ceiling mounted linear and square diffusers, were not sensitive to the workstation partition height and the partition bottom gap under the test conditions; while Lee and Awbi (2004) reported that the *air change efficiency* and *ventilation effectiveness* in an environment chamber equipped with a MS were sensitive to partition height and partition gap underneath.

In some research, it was concluded that the air distribution pattern and *air change efficiency* with MS was not sensitive to the studied supply diffuser type (linear/square

grille), the partition height/bottom gap, and the location of supply/return grilles under the test conditions (Haghighat et al., 1996); in contrast, some other studies (Shaw et al., 1993 (Part I&II); Lee and Awbi, 2004) reached different conclusions that the airflow pattern and *air change efficiency* with the studied MS was significantly influenced by the following parameters: the diffuser type, the internal heat source, the furniture presence, and the partition height/gap underneath.

Despite the above disagreements, the majority of previous studies agreed that the contaminant transportation pattern highly depends on the airflow pattern in the flow field (Huo, 1997; Cheong et al., 2003; Lee and Awbi, 2004; Lau, 2005). In addition, Cheong et al. (2003) found that the location of the emission source, the furniture layout, and the partition presence would significantly influence the distribution of contaminant in an office with MS. Any confined space produced by partitions and furniture would lead to build-up of contaminants. The exhaust vents situated at ceiling level were found to have minimal effects on comfort and IAQ, except for those cases when air was exhausted from the return grilles at high speed. The supply air terminal location and the number of supply diffusers were found to have impact on the overall comfort levels (Lau, 2005).

By taking thermal comfort and IAQ as objectives, Lau (2005) carried out a non-heat-load parametric study with UFAD in an office-type chamber and found that the air change rate, the supply air velocity, the supply air temperature, and the number of diffusers per office were the parameters of the most importance; the location of partition and return grilles were found to have moderate impact; and the changes in the diffuser location and the furnishings placement hardly affect the indoor environment.

It should be mentioned that some research even integrated physical quantities into

non-dimensional groups to study the influence of such parameters on indoor airflow and thermal conditions. Examples include Archimedes number (Di Tommaso et al., 1999), thermal length scale (Wan and Chao, 2005), etc. In this study, discussion will not focus on indices like these, due to the data available in the experimental results.

The above studies are just a few examples extracted from the extensive research on indoor environment analysis in ventilated offices. By summarizing the literature on influential parameters pertaining to office thermal comfort and IAQ, the subsequent subsection puts forward the parameters examined in this study.

3.4.2 Parameters to be examined in the current study

Based on the review of related work, the parameters listed in Table 3.2 were selected for this study. The upper and lower bounds of each parameter were also defined based on the geometric and thermal conditions commonly found in a typical office.

Category	Parameter	Design range
Office related	Outdoor air temperature	25 °C~40 °C
	Inner surface temperature	20 °C~35 °C
	Internal heat load density	25 W/m^2~45 W/m^2
	Contaminant (CO_2)emission rate	0.3 L/min~1.5 L/min
Ventilation system related	System type	UFAD and MS
	Diffuser type	Passive swirl diffuser/ perforated grille type diffuser
	Number of diffusers with UFAD	2 diffusers per room
		4 diffusers per room
	Number of diffusers with MS	1 diffuser per room
		2 diffusers per room
	Distance from diffuser to occupant	0.5 m~2.0 m
	Distance from return grilles to contaminant source	0.5 m~2.5 m
	Outdoor air supply flow rate	Maintaining the CO_2 concentration in supply air at 400 ppm
	Overall supply air flow rate	80 L/s~160 L/s
	Supply air temperature	UFAD: 15 °C~22 °C
		MS: 13 °C~18 °C

Table 3.2: Design space of input parameters for CFD simulation

3.6 Limitations of the Scope of the Current Work

Although this study attempted to span a wide range of input parameters, it was not possible to address all the influential parameters within the scope of the current work. The bottleneck appeared to be twofold: the availability of computer resources and experimental data. Specifically, one should be aware of the following limitations of the current study:

- The office scenarios considered in this work have excluded the impact of solar radiation passing through exterior window (there was no exterior window in the test chambers) to the indoor domain. The reasons are twofold. Firstly, the majority of existing CFD programs can not efficiently capture the behavior of the solar radiation (though some methods are claimed to be available with Airpak, as stated in Appendix A). Secondly, the current office-type test chambers are usually unglazed; therefore, it is often infeasible to obtain reliable data to validate those cases with solar radiation imposed upon the room air.
- The CFD simulations were performed under steady state conditions in the current study, and the computational domain has been confined to a single office with two occupants. Should adequate computer resources become available, it would be necessary to include transient condition into consideration and to expand the problem domain to a larger area of open-plan offices (with cubicles) or even to a whole office building.
- The current study has focused on the peak load of cooling season (which is the common case in the core zone of an office building), though the heating energy requirement of an office building is much higher than the cooling energy requirements in Canada due to the long heating season. During the heating season, it would be common to integrate a hydronic system along the perimeter of an office to offset the heating load through building envelope, but in the controlled environment chamber where the measurement was taken (for the verification of CFD simulation results), this type of system was not installed; therefore, heating season was excluded from the scope of the current work.

- The internal lighting load was set to about 20 W/m^2 with the intention to mimic the conditions in the environment chamber, which was much higher than the value in an actual office scenario (11 W/m^2 as specified in ANSI/ASHRAE-IESNA 90.1-2004); also, the power of the heat sources added into the office space may differ from a typical office equipment.
- CO_2 released from two boxes at fixed locations was taken as the only indoor contaminant; however, other types of gas phase pollutants and other possible placement of contaminant source (e.g., area-type sources as carpet or painted wall/surfaces) are commonly encountered in office spaces.
- In addition, the impact of internal partitioning (e.g., partition height and location as well as air gap underneath, etc.) has been excluded here due to the absence of data for validation. In the literature, partitions were identified as a key factor affecting the room air distribution; therefore, this topic would be worthy of addressing in further CFD investigations and optimization work concerning office indoor environment.

3.7 Closing Remarks

Chapter 1 claimed that this study sought a holistic evaluation of thermal comfort, IAQ, and ventilation system energy efficiency. To set the stage for CFD and experimental work in the subsequent chapters, it was necessary to understand the ventilation approaches commonly used in office buildings and how to characterize their influences on office environment.

This chapter started with a comparative introduction of two common ventilation approaches in office buildings: UFAD and MS, which underlined the contributions of

UFAD systems to improve office comfort level, IAQ, and energy efficiency.

In order to evaluate thermal comfort and IAQ in a quantitative way, PMV-PPD, *equivalent temperature* (ET), *head-to-ankle temperature difference* ($\Delta T_{HeadToAnkle}$), air velocity in the vicinity of the occupant, CO_2 concentration distribution, and CO_2-based ventilation effectiveness were selected as the criteria for performance assessment. The selection of these indices is, on the one hand, based on discussion in the literature, on the other hand, according to the information available from the CFD simulation. The theoretical basis of these indices and calculation methods were also described.

There have been a significant number of numerical and experimental investigations of office thermal comfort and IAQ with different ventilation technologies, but energy use of ventilation systems has not been adequately treated in previous CFD studies. How to quantify the energy consumption of a ventilation system in response to the operating states deserves further investigation. This chapter also described how to account for the energy use by taking both the fan power input and cooling energy requirement into consideration. These indices can be determined from the CFD solution—the supply air conditions and the outdoor air conditions are input information into the CFD program, whereas the return air states are predicted by CFD.

Prior to commencing the CFD simulations, it was also necessary to identify those parameters that would significantly affect the office environment. Previous studies (though sometimes provided conflicting opinions) suggested that outdoor temperature, inner surface temperature, internal heat load density, contaminant emission rate (CO_2 here), system type (UFAD vs. MS), diffuser type, number of diffusers, distance from diffusers to occupant, distance from return grilles to contaminant source, outdoor air

supply flow rate (ventilation rate), supply air flow rate, and supply air temperature would reasonably cover the design variables of practical problems. Consequently, these were chosen as the input variables for the CFD simulations.

Since not all influential variables could be addressed in the current study due to the limitations on computer resources or the absence of experimental data, the limitations of the scope of the current study were also put forward in this chapter.

CHAPTER 4

VERIFICATION OF CFD SIMULATIONS OF OFFICE ENVIRONMENT

4.1 Introduction

Appendix A substantiates Chapter 1's claim that CFD is well suited for indoor airflow and heat transfer modeling by providing the technical basis of CFD; Chapter 3 described how to quantify the comfort level, IAQ, and ventilation energy costs in a office space by making use of data derived from CFD calculations. The stage has been set for CFD simulation; however, questions regarding the credibility of CFD predictions have yet to be fully addressed. Appendix A also suggests that care should be taken when selecting the turbulence modeling method and numerical approach for CFD simulations, so as to increase the accuracies of CFD predictions. A guest editorial in *Indoor Air* suggested that, whenever possible, CFD simulation results should be validated against corresponding measurements or standard test cases with similar features, for the purpose of quality control (Sørensen and Nielsen, 2003).

In response to this, this chapter sets out to demonstrate the validity of CFD simulations conducted in this research, by comparing the CFD estimates with experimental data obtained from mock-up offices. Two full-scale office-type test chambers, one located in south China and the other located in Denmark, were the subjects of the comparison. The experimental facilities enabled the comparative investigations of the performance of UFAD and MS, and results from representative cases are presented. The validated cases then served as the baseline cases for further CFD exercises (ANN

training/testing data preparation).

Later on, Section 4.2 describes the experimental facilities and measurement design in the two environment chambers. Prototype CFD models created in Airpak are briefly introduced in Section 4.3, with emphases being placed on the mimicking of diffuser boundary conditions. Verification is then treated in Section 4.4. The case studies allowed performance comparison between alternate ventilation principles and alternate air terminals. Also, investigative simulations were conducted by implementing two separate turbulence models, in an attempt to appraise the applicability and efficiency of these two models within the context of the verification cases. Finally, closing remarks are provided in Section 4.5.

4.2 Test Chambers for Data Collection

Experimental data for CFD verification must contain detailed information about the flow field, the thermal conditions, the air jet boundary conditions, and the geometric configurations of the space as well. Two sets of experimental data are used here for CFD verification. One set of data was derived by conducting measurements in a full-size mock-up office served by UFAD and MS with grille-type diffusers (Zhou et al., 2006) while; in the case of UFAD and MS with passive swirl diffusers, the current study draws upon data collected by Cermak and Melikov (2005) to demonstrate the accuracy of CFD predictions. Clearly, these experimental facilities enabled the analysis of alternate ventilation systems (UFAD and MS) and different diffuser types (grille-type and swirl diffusers). A description of the experimental facilities and measurement setup is provided first.

4.2.1 Experimental facilities with grille-type diffusers

Controlled environmental chamber

The experimental work presented here was carried out in the Advanced Underfloor Ventilation Research and Development Center at the Hong Kong University of Science and Technology—a real-size office type experimental chamber (see Figure 4.1). The chamber was 6.0 m in length and 4.8 m in width, with a clear space of 2.4 m measured from the raised floor to the false ceiling. The 100 mm thick side walls of the chamber were constructed of two layers of gypsum board on both sides of a 64 mm thick fiberglass insulation layer; in an attempt to segregate the indoor environment from the impact of surrounding temperature fluctuations. The gypsum boards were coated with white emulsion paint. For both floor and ceiling, a 25 mm thick polyurethane insulation layer was adhered to the inner surface of the concrete slabs, as shown in Figure 4.2. Gypsum boards coated with white paint were also adhered to the ceiling. The access floor panel was constructed with 25 mm thick marble tiles above an underfloor plenum 300 mm deep. Each marble tile was of standard size of 0.60 m×0.60 m.

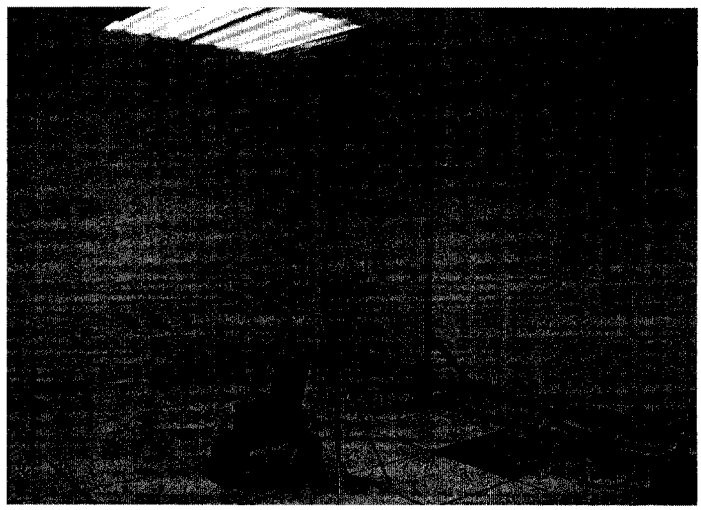

Figure 4.1: Test Chamber in the Advanced Underfloor Ventilation Research and Development Center at the Hong Kong University of Science and Technology

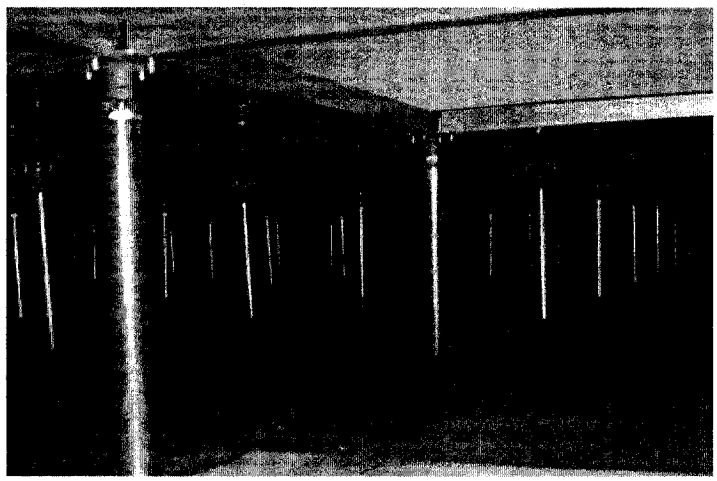

Figure 4.2: Underfloor plenum and insulation layer on the slab

During the experiment, the room was furnished with a background light and a desk with a personal computer. The power level and placement of internal heat sources resembled those in a typical office. Table 4.1 presents the sensible heat gains from these

sources. The nominal power consumptions of this equipment was recorded and assumed to be the heat released to the ambient air (radiation plus convection).

Internal source	Sensible heat gain (W)
Occupant	1×75
Computer monitor	1×75
Computer tower	1×75
Ceiling light fixtures	18×36
Total	873 (30.3 W/m^2)
Hot plate (optional)	2×500
Total (with two hot plates switched on)	**1873 (65 W/m^2)**

Table 4.1: Summary of internal heat sources in the test chamber

Two rectangular hot plates, with the dimension of 0.20 m×0.05 m, were added to the room as extra heat sources. As shown in Figure 4.3, the hot plate consisted of variable power electric resistance coated with a ceramic glaze, and it was supported by asbestos bricks (0.1 m above the floor). The power to each hot plate was varied up to 500 W, and the power input was controlled and monitored by a power analyzer (Fluke 41B, Everett, WA, USA). When switched on at full load, they would increase the internal heat load density in the room from 30.3 W/m^2 to 65 W/m^2.

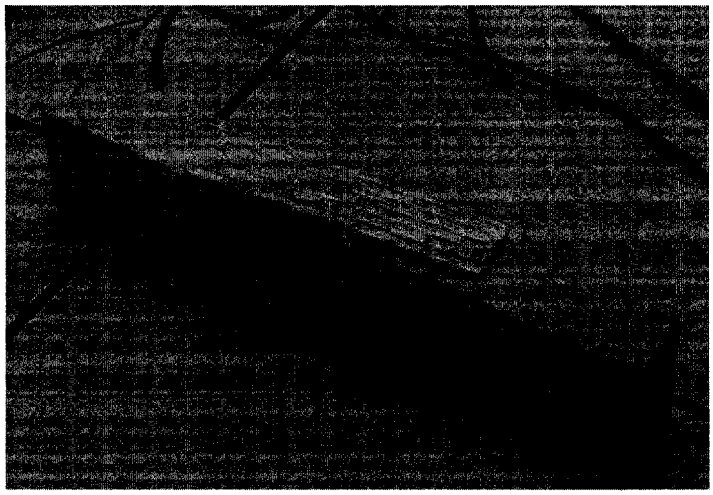

Figure 4.3: Extra heat source

Ventilation systems

The test room contained both a ceiling supply/return MS and a floor supply/ceiling return UFAD system. Near the center of the room, a pair of rectangular openings with the dimensions of 0.59 m×0.21 m was installed at the ceiling level as the MS air inlets. Air exited the room through 4 return grilles at ceiling level. These 4 grille-type return vents with the dimension of 0.59 m×0.21 m were used for both the MS and the UFAD system. The air outlets were covered with panels made of slim aluminum bars, resulting in an effective aperture ratio of 0.7.

The UFAD system supplied air through two floor mounted grille-type diffusers, which were also located near the center of the room, as can be seen in Figure 4.1. The floor air terminals were covered by 0.59 m×0.21 m perforated panels, with an effective area ratio of 0.55 (shown in Figure 4.4). With UFAD, the conditioned air passed through the pressurized underfloor plenum prior to being discharged from the diffuser. This

contrasted with the case of MS, for which the air terminals were connected to the *air handling unit* (AHU) by ducts.

The total supply air flow rate from ceiling and floor diffusers could be set up to 420 L/s. Throughout the experiment, the amount of air coming out from the each diffuser was fixed at 140 L/s by the AHU, while the supply air temperature was manually controlled by adjusting the temperature set-point in the AHU. In response to the signal sent by the temperature sensor located in the supply air duct, the microcontroller regulated the flow rate of chilled water through the cooling coil inside the AHU.

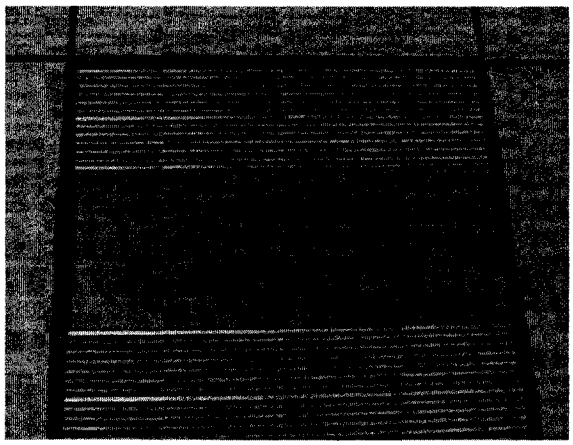

Figure 4.4: Floor air diffuser

Measuring instruments

The test room was instrumented with thermocouples and thermal comfort transducers, which enabled the following readings to be recorded:

- As shown in Figure 4.5, the inner surface temperature at the walls, ceiling and floor were measured using T-type thermal couples (OMEGA, Stamford, CT, USA). The thermocouples were pre-calibrated against an air temperature transducer (Innova MM0034, Ballerup, Denmark); the latter has an accuracy of 0.2 °C within the

measurement range from 5 °C to 40 °C. The thermocouples were covered with aluminum foil tape (with a low emissivity in the long-wave spectrum) to minimize the radiant exchange with the surroundings.

- At four measurement positions along the centre axis of the test room (shown in Figure 4.8 below), air temperatures and air velocities at six vertical levels (0.1 m, 0.6 m, 1.1 m, 1.7 m, 2 m, 2.2 m) were recorded using thermal couples and a heated-sphere omni-directional anemometer (Innova MM0038, Ballerup, Denmark), respectively. The measurement accuracy of the anemometer is 0.05V + 0.05 m/s when the local air velocity reading V is lower than 1 m/s.
- For the air throw from the diffusers, the instant air velocity and mean air velocity variations with height were measured, which allowed the determination of discharge velocity, local turbulence intensity, terminal velocity, and decay constant, so as to fully characterize the discharge airflow from the diffusers.
- In order to determine the comfort level, ambient relative humidity in the test room was monitored by a humidity transducer (Innova MM0037, Ballerup, Denmark) with an accuracy of 0.5 °C (*dew point temperature* T_{dew}) when (T_{air}-T_{dew}) < 25 °C. Also, the ambient temperature was recorded using the air temperature transducer (Innova MM0034, Ballerup, Denmark).

Table 4.2 shows more detailed information regarding the measuring ranges and accuracies of the instruments; and the transducers are shown in Figure 4.6.

Measurement objective	Instrument	Measurement range	Accuracy	Response time
$T_{ambient}$	Temperature transducer MM0034	-20~50 °C	±0.2 °C (from 5 °C~40 °C)	20 s to 50% of step change
RH	Humidity transducer MM0038	$(T_{air}-T_{dew})$ < 25 °C	±0.5 °C (T_{dew})	N/A
V	Omni-directional anemometer MM0037	0~10 m/s	±(0.05V + 0.05) m/s when V < 1 m/s	< 0.2 s to 90% of step change
T_{air}/T_{surf}	T-type thermal couple	N/A	Calibrated against MM0034	5 s

Table 4.2: Summary of instruments specifications

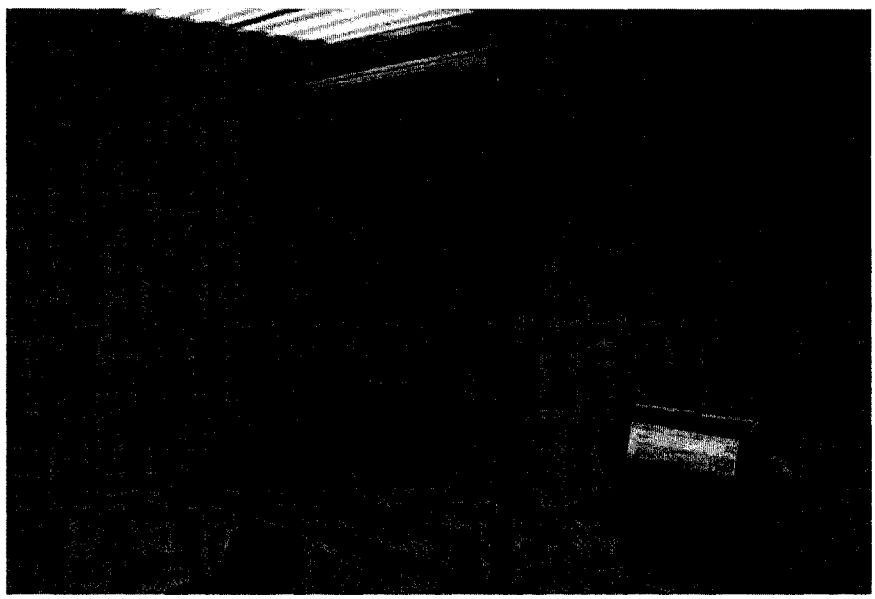

Figure 4.5: Instruments set up in the mock-up office

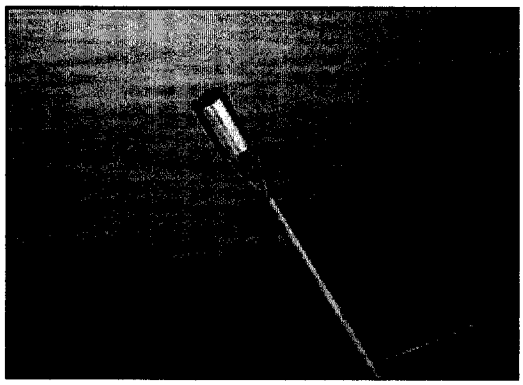

(a) Temperature transducer MM0034

(b) Humidity transducer MM0037

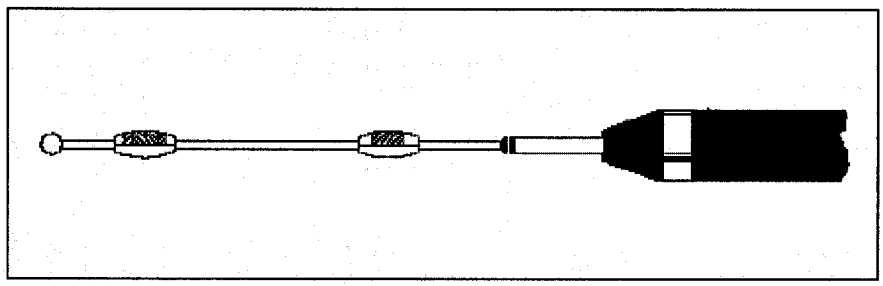

(c) Air velocity transducer MM0038

Figure 4.6: Transducers (Innova, Ballerup, Denmark)

Temperature, air velocity, and humidity transducers were connected to a thermal comfort data logger (Innova 1221), and the outputs were recorded every 1 s. Also, a PC-based data logger system (SCXI series, National Instruments, Austin, USA) recorded the outputs of the thermocouples every 5 s. Once steady conditions within the room were achieved, the final readings of the objective parameters were the time-mean quantities by taking averages over a time period of 180 s. The experimental instrument set-up in the mock-up office is presented in Figure 4.5.

Procedure

The room was monitored over a three-day period. During that period, the supply air flow rate was maintained at a constant level while, the test room thermal conditions and

supply air temperature were varied during the measurement period and experiments repeated to capture the impacts of inner surface temperature, internal heat load, supply air temperature, and the ventilation systems on the indoor flow field.

The experiments were divided into two stages according to the ventilation system in service. In the first stage, when air was supplied through UFAD, the three experiments spanned realistic ranges of supply air temperature, inner surface temperature, and internal heat load density. The second stage of experiment (one case study) was targeted at comparing the resulting flow field from overhead MS with that produced by UFAD (obtained in the first stage). Other than as explicitly specified, the setups and conditions were almost identical for all four cases. The experimental conditions and operational states of ventilation systems for the 4 cases are briefly summarized in Table 4.3.

The CFD simulations in this study were performed under steady state conditions; therefore, it was preferable to take measurements under steady state conditions (regarding the airflow field and the room fabric surface temperature).

For each case, the first step was to start the ventilation system to condition the test room; the data acquisition system was also switched on to trace the temporal variation of room air temperature. In order to achieve steady room air conditions, data collection took place 5~10 hours later, depending on the supply air conditions, outdoor air temperature, and the internal heat load density level. At all the measurement points, a temperature variance less than 0.1 °C within a half hour duration was considered as the indication of reaching steady state.

Case No.	System type	Supply air T (Set Point) †	Inner surface temperature	Extra Heat source Presence
1	UFAD	21 °C	24.2 °C	No
2	UFAD	19 °C	23.5 °C	No
3	UFAD	21 °C	25.5 °C	Yes
4	MS	20 °C	24.8 °C	No

† The air temperatures at the supply diffusers deviated from the set-point temperature in the AHU, due to the heat exchange between the supply air and the plenum envelop.

Table 4.3: Experimental conditions for the designed cases

4.2.2 Experimental facilities with passive swirl diffusers

Grille-type diffusers are the commonest type of air supply terminals in practice, and the modeling of them has been substantially treated in previous CFD studies in the indoor domain. Passive swirl diffusers have gained momentum in office building applications recently, and two advantages are frequently associated with such diffusers. Firstly, the occupant can have direct control over the amount of air supply by rotating the face of a swirl diffuser. Secondly, the strong entrainment effect produced by swirling air discharge is often claimed to be a remedy to local draft, especially in the case of UFAD systems.

Unlike grille-type diffuser, the modeling of swirl diffusers in CFD simulation is usually considered a challenge. Therefore, this topic is addressed in the current study. This objective was realized with the help of measured data provided by Cermak and Melikov (2005) for a mock-up office served by passive swirl diffusers (both ceiling and floor mounted).

In this case, a 4.80 m×5.40 m mock-up office was located within a larger enclosure maintained at a similar temperature, to minimize the temperature gradient (heat transfer) across the office wall assemblies. The mock-up office consisted of two fully-furnished workstations, and each of them accommodated a breathing thermal manikin in business

attire. Figure 4.7 shows the configuration of the mock-up office. 4 passive swirl diffusers with diameters of 200 mm (TROX, type FBM-3-EU-K/200-SM) were installed in the raised floor. Alternatively, conditioned air could be also introduced to the test room through a ceiling mounted swirl diffuser (TROX, type RFD-R-D-US/250), which had a face diameter of 350 mm. With either UFAD or MS, air was extracted from 4 circular return vents at ceiling level.

During this experiment, in addition to velocity and temperature measurements, tracer gas was injected into the test room in order to compare the ventilation efficiency of the two ventilation systems. Rectangular grid tubing, as the dosing apparatus, was designed to release CO_2 tracer gas uniformly over the floor area. This was in an attempt to mimic the emissions from the floor covering material. In this test room, the fabric assemblies, insulation levels, internals heat gains, and contaminant emission rate are typical for offices. The experimental conditions inside the chamber are briefly summarized in Table 4.4.

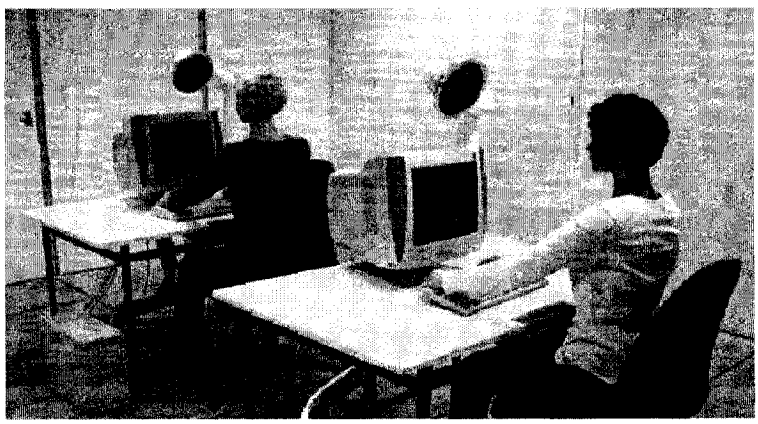

Figure 4.7: Configuration of workstations and manikins (Cermak, 2004)

Condition	Description
Room dimension (m) (L×W×H)	4.8×5.4×2.6
Ventilation system	UFAD/MS
Wall temperature (°C)	25
Supply air temperature (°C)	18
CO_2 concentration in supply air (ppm)	400
Overall supply air flow rate (L/s)	80
Dose of tracer gas CO_2 (mL/s)	24
Heat gain from heat sources (W)	Breathing thermal manikin 2×75
	Computer tower 2×74
	Computer monitor (CRT, 17") 2×70
	Desk lamp 2×55
	Ceiling light fixture 6×6

Table 4.4: Conditions in the environment chamber with swirl diffusers

4.3 CFD Models

4.3.1 CFD models of test rooms

Two prototype CFD models of the above test rooms (with both MS and UFAD system) were created in Airpak (see Figure 4.8 and Figure 4.9). The models include the air terminals, the furniture, the heat sources, the occupants (or thermal manikins), and the contaminant sources (in the case with swirl diffusers).

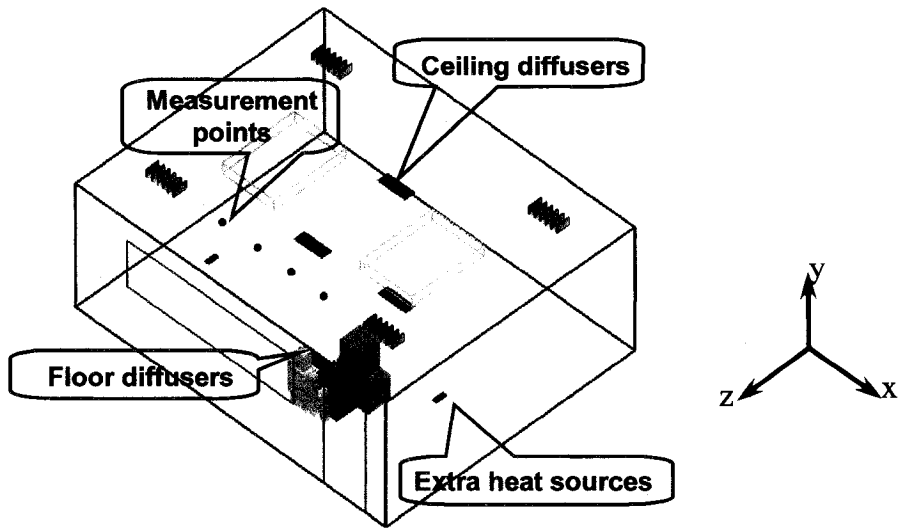

Figure 4.8: Prototype CFD model of the mock-up office with grille-type diffusers

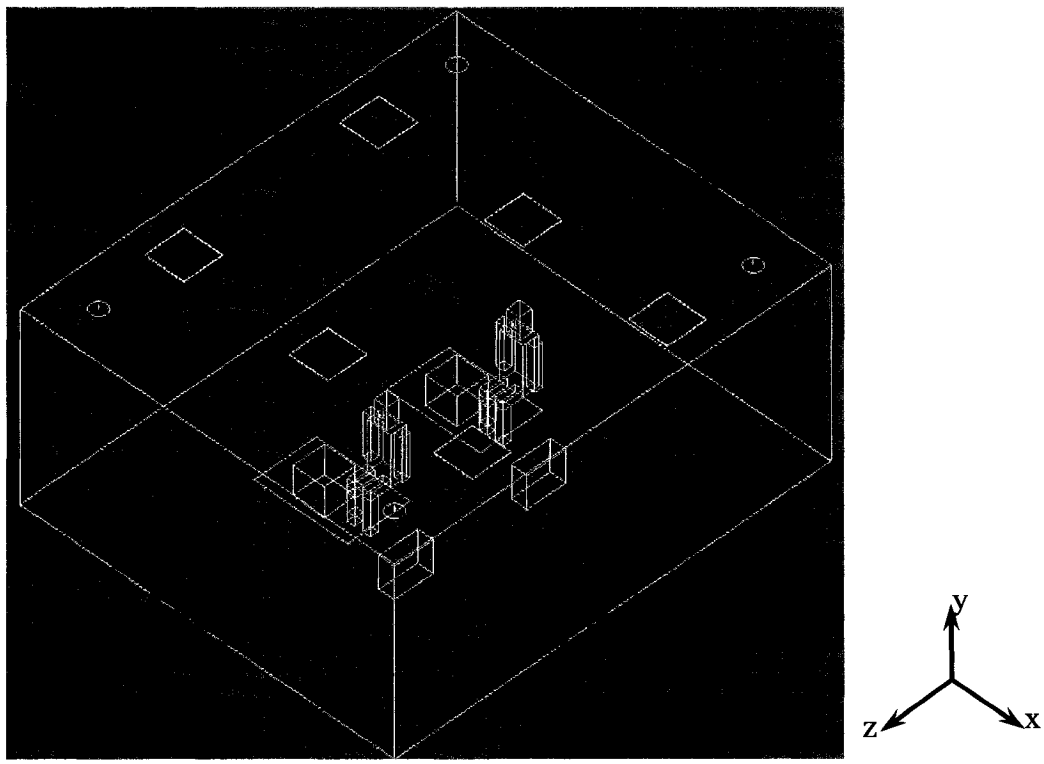

Figure 4.9: Prototype CFD model of the mock-up office with swirl diffusers

The following assumptions were made when creating the models:

- The domain boundary was placed at the internal surfaces of the test room envelop

assemblies, thus the solid masses of fabrics were excluded from the computational domain; the influence of surrounding thermal conditions was represented by the inner surface temperatures at exterior walls.

- Zero infiltration/exfiltration rates were assumed, as the test rooms were tightly sealed.
- No humidity data was provided in the mockup-office with swirl diffusers, so 40% was assumed to be the relative humidity in the office when calculating the thermal comfort.

4.3.2 Modeling the diffusers

Since the room airflow in an office space is primarily driven by air inlet diffusers, it is important for CFD simulations to accurately characterize the air throw from the diffuser as well as the penetration and spread of the air jet to other parts of the room. Due to the large scale differences between the room dimension and the diffuser size, it is often infeasible to copy the detailed geometric feature of a diffuser into a CFD model. In essence, the art of diffuser simulation is to abstract the complexities of diffuser geometry and air throw to a model of reasonable representation, with the goal of generating the desired airflow pattern (see Appendix A for a literature survey of the issue of diffuser modeling).

Modeling grille-type diffuser

Since the modeling of grille-type diffusers has been substantially addressed in previous CFD studies of the indoor domain, no attempt was made in this study to advance the treatment. A common approach for modeling grille-type diffusers is mimicking the diffuser using rectangular openings with appropriate effective areas, which was also

employed in the current study.

Originally, in some investigative simulations, each grille-type diffuser was modeled as a single perforated panel. When defining the boundary conditions at such diffusers, the CFD calculations resulted in much lower velocities at the measurement points in comparison with the measured data. The measurement points were located at the center of the room (away from the diffusers); therefore, the relatively low velocities estimated by CFD indicated that this diffuser modeling method underestimated the airflow induced by the supply air jet. Therefore, the following improvement is required to address this problem: the face area of a diffuser was resolved into 5 rectangular slots along the short edge (as shown in Figure 4.10), and various air throw orientations are assigned to each of the slots. As a result, the entrainment effect was better captured.

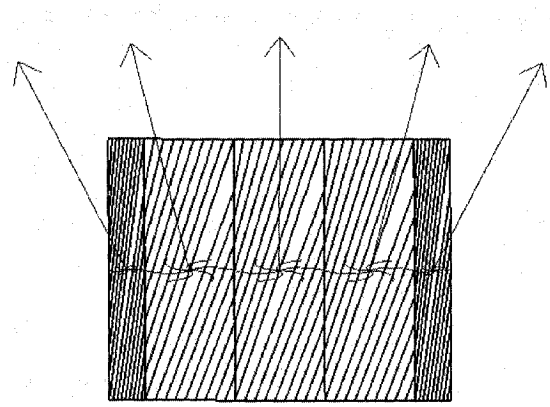

Figure 4.10: Modeling grille type floor diffusers

Modeling swirl diffuser

CFD simulations were also conducted in this study to address the modeling of room air driven by swirl diffusers. Some previous studies have been conducted to tackle this problem. A common approach was to approximate the round supply device by a group of rectangular segments and a different air throw orientation was assigned to each segment

(Srebric and Chen, 2002; Lau, 2005).

In the current study, a circular opening was devised to mimic the swirl diffuser face area. A prototype model of the floor swirl diffuser is shown in Figure 4.11. It should be mentioned that the ceiling swirl diffuser was simulated using a similar approach. In order to simulate the vortex-type airflow, the face of the diffuser was divided into six equal-sized sectors. Each sector shared 1/6 of the total amount of supply air, while the tilt angle of the air jet varied from one sector to another. In both horizontal and vertical directions, the azimuths of airflow from each of the sectors were determined based on the discharge airflow pattern obtained from the smoke visualization (shown in Figure 4.19 below).

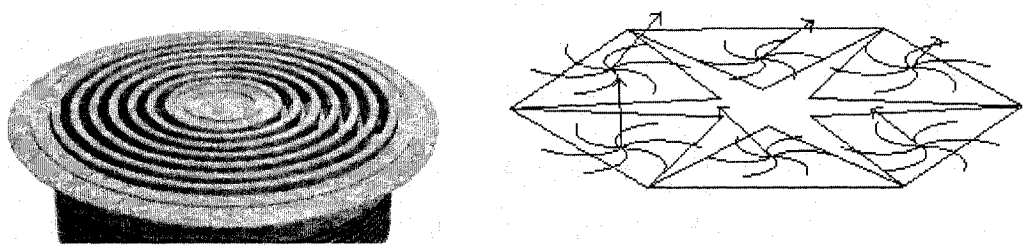

Figure 4.11: Modeling floor swirl diffusers

As mentioned in Appendix A, the mesh was locally refined at the supply diffusers by increasing the grid count number according to the geometric feature and airflow/thermal states of the objects. For example, for a floor mounted swirl diffuser (diameter = 0.20 m) supplying air at a flow rate of 80 L/s, the grid count number along the radius was set to equal to 6, and the total number of cells generated on the surface was 98 cells.

4.4 Verification of CFD Simulation: Results and Discussions

The CFD simulation program was assessed for its capacity to predict the temperature, velocity, and tracer gas concentration (where applicable) profiles in the flow field where the measurements were taken. The comparisons of the simulated and monitored flow field provided some interesting observations, which are presented in the subsequent sections.

4.4.1 MS and UFAD with grille-type diffusers

Simulations covering the four cases listed in Table 4.3 were performed with the aforementioned base model. In addition, a decision regarding the turbulence model selection was required: should the *renormalization group* (RNG) k-ε model (Yakhot and Orszag, 1986) be employed to capture the flow field features or was the indoor zero-equation model (Chen and Xu, 1998) adequately accurate? Such a decision also considerably affected the computational effort; therefore, a number of exploratory simulations were performed to examine the applicability, accuracy, and efficiency of these two turbulence models.

RNG k-ε model vs. indoor zero-equation model

Both the RNG k-ε model and the indoor zero-equation model were implemented for all the four cases listed in Table 4.3. The computation platform for the CFD simulation was a dual-processor Pentium IV workstation (Dell Precision 670) at 3.4 GHz speed. When using the RNG k-ε model, the CPU time required for a steady-state simulation to reach convergence was about 17 hours; in the case of the indoor zero-equation model, the computational time was reduced to approximately 5 hours. This is understandable as the

indoor zero-equation model does not require the solution of transport equations for the *turbulent kinetic energy* (k) and the *dissipation rate of turbulent kinetic energy* (ε).

Figure 4.12 plots the predicted (by both turbulence models) airflow patterns in the transverse plane in the middle of the chamber (x = 3) for case 1. The vertical profile of the axial jet velocity is plotted in Figure 4.13, which demonstrates the decay tendency of the supply air jet above the floor supply diffuser.

The airflow patterns (Figure 4.12) clearly demonstrate that the CFD predictions are sensitive to the turbulence modeling method being used. With the indoor zero-equation model, the discharged air jet decays faster when approaching the ceiling level: the centerline jet velocity at the height of 2.3 m is 0.23 m/s (see Figure 4.13) while, the predicted velocity at this point was found to be at 0.6 m/s in the simulation results of the RNG k-ε model. The latter is very close to the actual measured value of 0.62 m/s (see Figure 4.13). Such a high terminal velocity (0.62 m/s) indicates a diffuser throw greater than the height of the room, and this also explains the high velocity occurring in the upper region of the room, which is to be discussed later on.

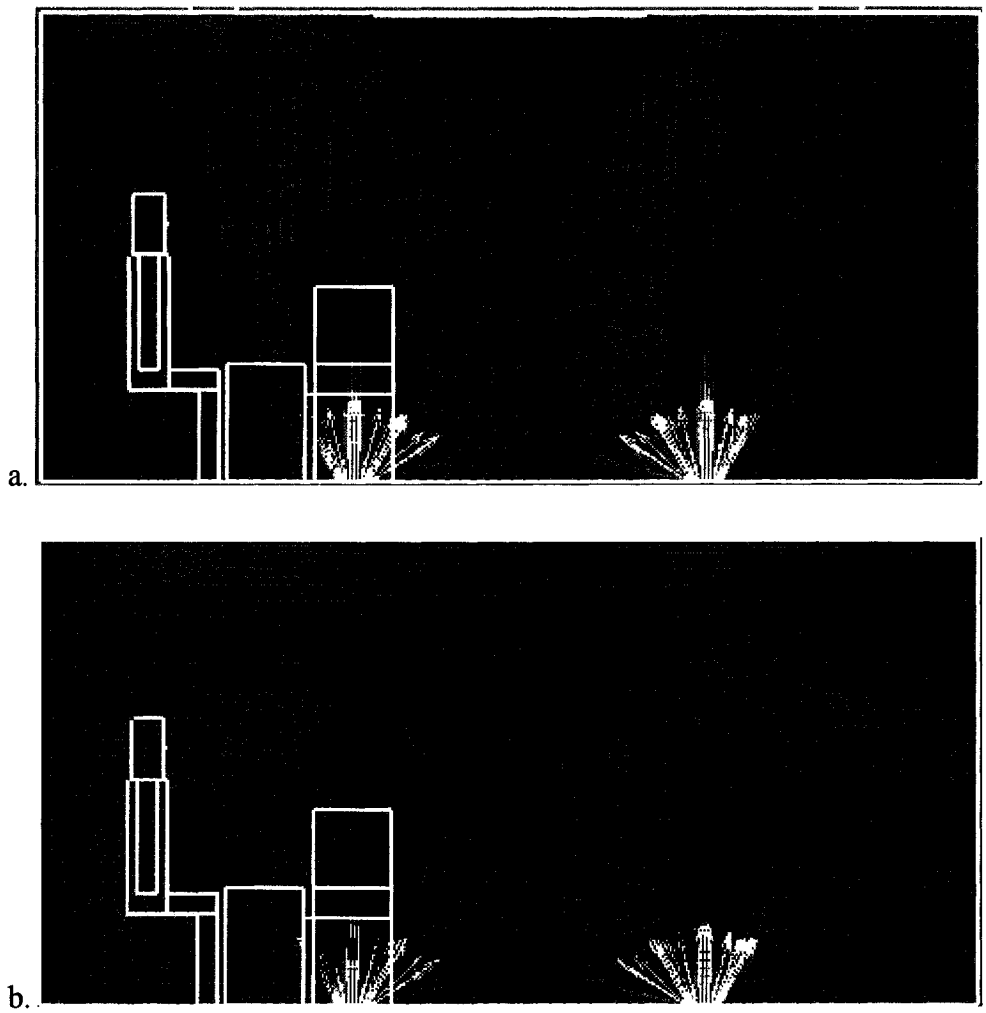

Figure 4.12: Predicted airflow pattern (case1): a. with the RNG k-ε model; b. with the Indoor zero-equation model

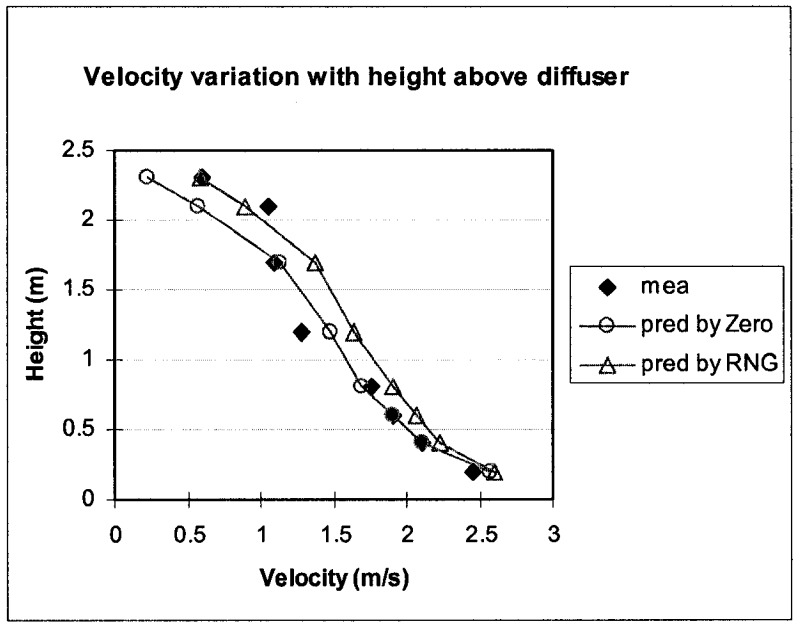

Figure 4.13: Vertical profile of axial jet velocity (case 1)

In addition, Figure 4.14 and Figure 4.15 present the predicted velocity and temperature results (by both the RNG k- model and the indoor zero-equation model) at the four measurement locations for case 1, and the measured data are also presented for comparison purpose. As can be seen from these figures, at all the measurement positions, RNG k-ε model produced relatively low air temperatures (about 0.6 °C lower than the experimental data), while the indoor zero-equation model overestimated the air velocities.

Two reasons may attribute to the above phenomena.

1. Prescription of μ_t

Strictly speaking, the RNG k-ε model is only valid for fully turbulent flow; however, weakly turbulent or even re-laminarized regions are often encountered in room air domain (especially in those regions remote from the supply diffusers). With RNG k-ε

model, the turbulent viscosity μ_t (Pa·s) was calculated by

$$\mu_t = \frac{C_\mu \rho k^2}{\varepsilon} \tag{4-1}$$

where C_μ = 0.085 is an empirical constant, ρ is the density of air (kg/m^3), k is the turbulent kinetic energy (m^2/s^2), and ε is the dissipation rate of turbulent kinetic energy (m^2/s^3).

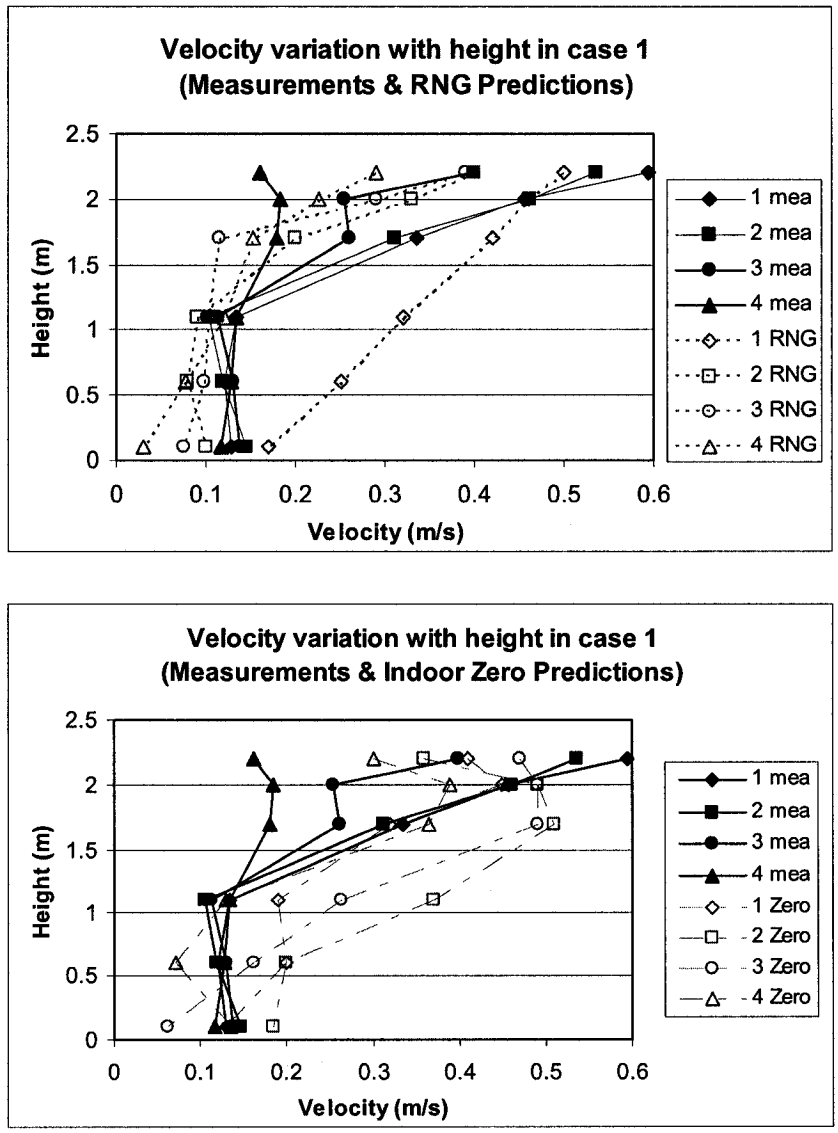

Figure 4.14: Velocity results (case1): measurements vs. predictions

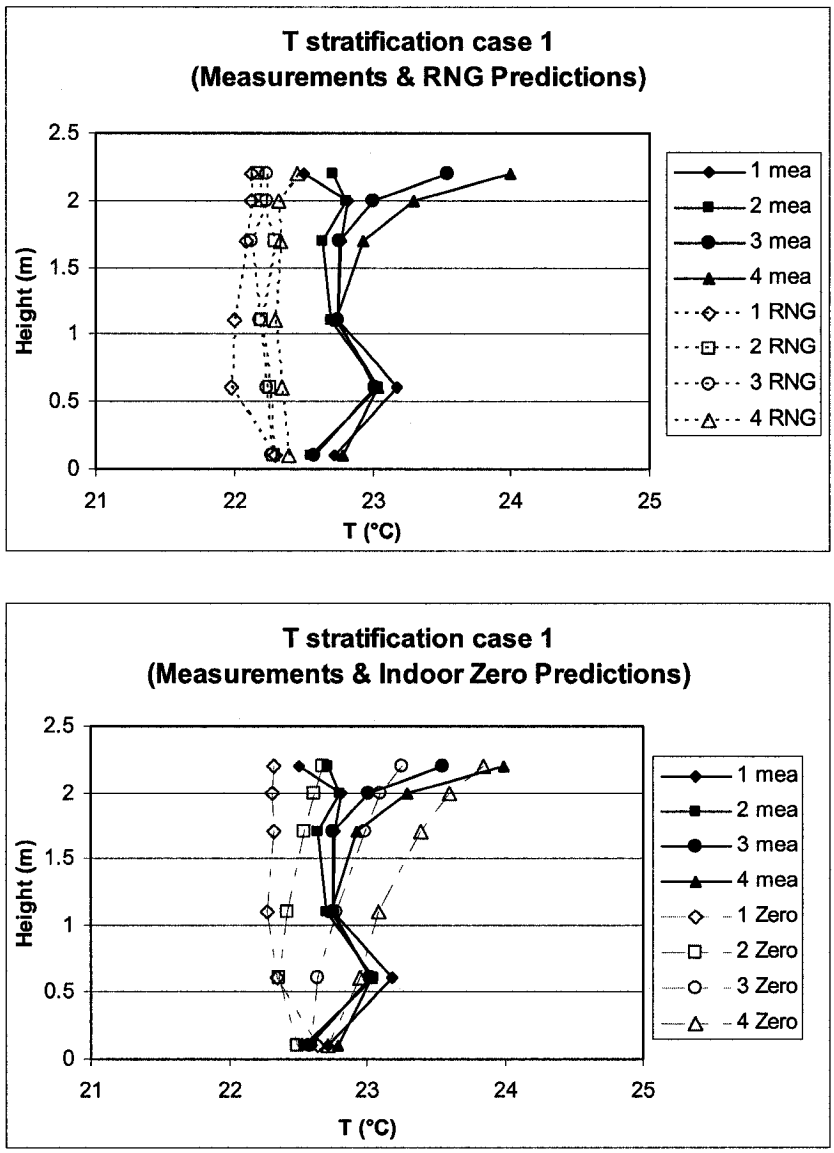

Figure 4.15: Temperature results (case1): measurements vs. predictions

From this equation, it can be seen that the low kinetic energy dissipation rate in the weakly turbulent regions may lead to over-prediction of the turbulent viscosity and thus result in low velocities. Therefore, the RNG k-ε model failed to predict the recirculation in some remote areas (Figure 4.12a). This contrasts with the situation with the indoor zero-equation model—local small recirculation was predicted in the upper right corner of

the room and near the right wall (as shown in Figure 4.12b). With the indoor zero-equation model, the turbulent viscosity is derived from,

$$\mu_t = 0.03974 \rho V l \tag{4-2}$$

where the local turbulent viscosity is related to the local mean air velocity V (m/s) and a length scale l (m). The length scale here was chosen as the distance from the nearest wall.

Here, the turbulent viscosity and thus the turbulent diffusion of momentum, is proportional to the local time mean velocity. It can thus deal with the weakly-turbulent regions better—the relatively low velocities would help to avoid the over estimations of μ_t. This also provides explanation of the observation that the indoor zero-equation model produced a faster decay of the air jet from the diffuser (shown in Figure 4.13), since the high local velocity in this region would result in large values of turbulent viscosity and amplify the decay tendency.

Regarding this, the μ_t/μ ratios (μ is the molecular viscosity) near the four side walls (where flow can be characterized as weakly turbulent or relaminarized) predicted by these two models were extracted from the simulation results, which are quite revealing: the RNG k-ε model estimated an average μ_t/μ ratio of 192, whereas a much lower number—about 57.5—was predicted by the indoor zero-equation model.

2. Log-law wall function with the RNG k-ε model

Another source of the potential modeling errors exists in the near wall treatment. It is worth mentioning that the log-law wall function was introduced to bridge the gap between the wall surface and the near-wall grids when implementing the RNG k-ε model (Launder and Spalding, 1974). Such a near wall treatment is based on the logarithmic profile approximation of the *zero-pressure-gradient flow* in the fully developed boundary

layer (see Appendix A for details).

However, Chen et al. (1990) claimed that the boundary layer in a room airflow field (driven by diffusers) might deviate from that of a *zero-pressure-gradient flow* and thus can not be perfectly characterized by the same profile approximation. Previous studies indicated that the log-law wall function might introduce significant errors in the estimates of convective heat transfer between room air and solid surfaces (Chen and Jiang, 1992; Niu and vander Kooi, 1992; Chen, 1995; Beausoleil-Morrison, 2000). Furthermore, the erroneous surface convection prediction would influence the airflow calculation due to the presence of the temperature term in the momentum equations. Previous studies also stated that the surface convection predictions from wall function were highly sensitive to the nature of room airflow (natural convection or forced convection) and the placement of the next-to-wall grids. Therefore, the log-law wall function may have caused errors in the predicted temperature and velocity in the current case, as seen in Figures 4.14 and 4.15.

In contrast with this, the indoor zero-equation model was applied to the near-wall regions directly, and the local convection coefficient h_c (adjacent to the wall) was calculated from the turbulent viscosity μ_t,

$$h_c = \frac{\mu_{eff}}{\mathrm{Pr}_{eff}} \frac{c_P}{y_{next-to-wall-node}} = \frac{\mu + \mu_t}{\mathrm{Pr}_{eff}} \frac{c_P}{y_{next-to-wall-node}} \tag{4-3}$$

where μ_{eff} is the effective viscosity (Pa·s), Pr_{eff} is the effective Prandtl number (Pr_{eff} = 0.9), c_P is the specific heat of air (J/kgK), $y_{next-to-wall-node}$ is the actual distance from the nearest wall/surface to the next-to-wall grid (m), and μ is the molecular viscosity (Pa·s).

It can be seen that h_c is proportional to viscosity (and thus proportional to local time mean air velocity). Previous research demonstrated that this approach was deficient at

representing the thermal boundary feature in the room air domain (Beausoleil-Morrison, 2000). This might be one of the reasons that the indoor zero-equation model could not predict the indoor thermal and airflow behavior here (as illustrated in Figures 4.14 and 4.15) with adequate accuracy.

Additional evidence was found in case 3 (shown in the subsequent section). Two extra heat sources (500 W each) were switched on in case 3, which increased the internal heat load density in the chamber from 30.3 W/m^2 (in case1) to 65 W/m^2. When comparing the predicted air velocity and temperature with measured data, the RNG k-ε model was found to have underestimated both the air velocity and temperature throughout the computation domain under the test conditions; while the indoor zero-equation model performed better than the RNG k-ε model, producing slightly higher air velocity and temperature than the measured values (that is, it overestimated the heat transfer and air movement when the heat load density was high).

Given the discrepancies associated with the RNG k-ε model (in conjunction with log-law wall function) and the indoor zero-equation model in this study, it is clear that further improvement regarding the turbulence modeling of room air is necessary. Though numerous alternative modeling approaches are available (e.g., low Reynolds number k-ε model), they have not proven to be universal replacements for the two models discussed above, due to stability issues and excessive computational requirements.

Consequently, the performance of the RNG k-ε and the indoor zero-equation models was found to be case specific (that is, sensitive to the nature of the flow and the heat load density in the domain), it can't be concluded that one model would always perform better than the other. When taking the CPU time consumed by these two models into

consideration, if the indoor zero-equation model generated reasonably good predictions, it would provide considerable benefits to the simulation-based optimization method under consideration. Accordingly, for the following cases with perforated grille type diffuser, the predicted results presented here were obtained from the indoor zero-equation model.

Results from cases 3 and 4

In Table 4.3, when taking case 1 as the reference case, it could be observed that:

1). All the other conditions in case 2 were almost identical to those in case 1, except that the supply air temperature in case 2 was 2 °C lower than that in case 1; therefore, comparison of the results obtained from cases 1 and 2 demonstrated the influence of supply air temperature on the room air.

2). Two hot plates (500 W each) were switched on in case 3, which increased the internal heat load density from 30.3 W/m^2 (in cases1, 2, and 4) to 65 W/m^2. The other operating conditions in case 3 were maintained close to those in case 1.

3). The operating states of case 4 and case 1 (e.g., wall surface temperatures, air delivery flow rate, and internal heat strength) were almost identical, except that in case 1 the conditioned air was supplied vertically up at 21 °C through floor grilles, while in case 4 air was delivered at 20 °C from the ceiling inlets (free openings) at an inclined angle of 30° to the side where the occupant was sitting.

The results obtained from cases 3 and 4 are presented next. The results for case 2 are not presented here due to the similarity of airflow pattern and temperature distribution observed from case 1 and case 2. Figures 4.16 and 4.17 present the measured and predicted velocity and temperature profiles at the four pole locations in cases 3 and 4, respectively.

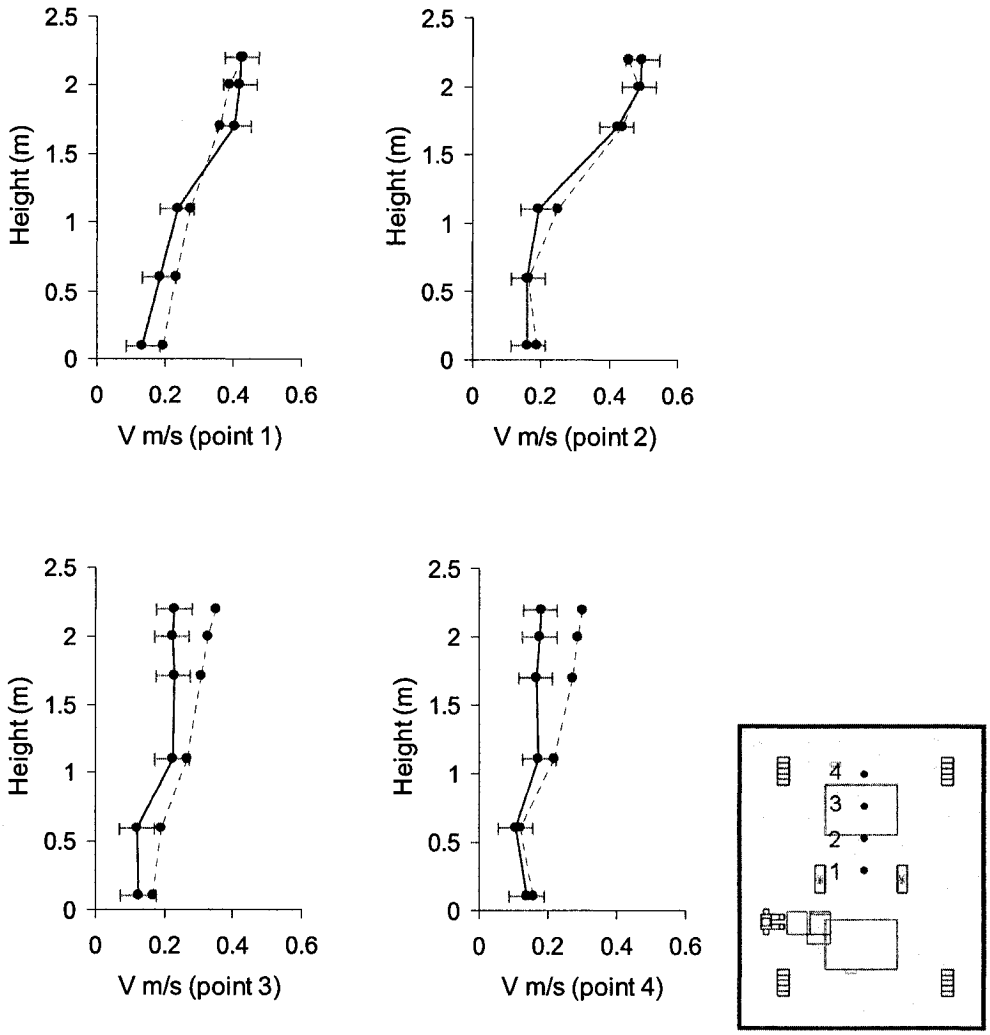

Figure 4.16: Velocity results (for case 3 with high heat load)

Solid line: measurements, dotted line: predictions

From Figure 4.16, it can be seen that for case 3 (with UFAD and high heat load), relatively low air velocities can be observed at elevations above 1.1 m near measurement points 3 and 4 (corresponding to areas close to the extra heat sources). The influence of extra heat sources on air velocities near points 1 and 2 was trivial. In case 3, the increased temperatures at all 4 measuring points (relative to the thermal states in case 1) proved that

the air was warmed up throughout the room by adding the heat sources.

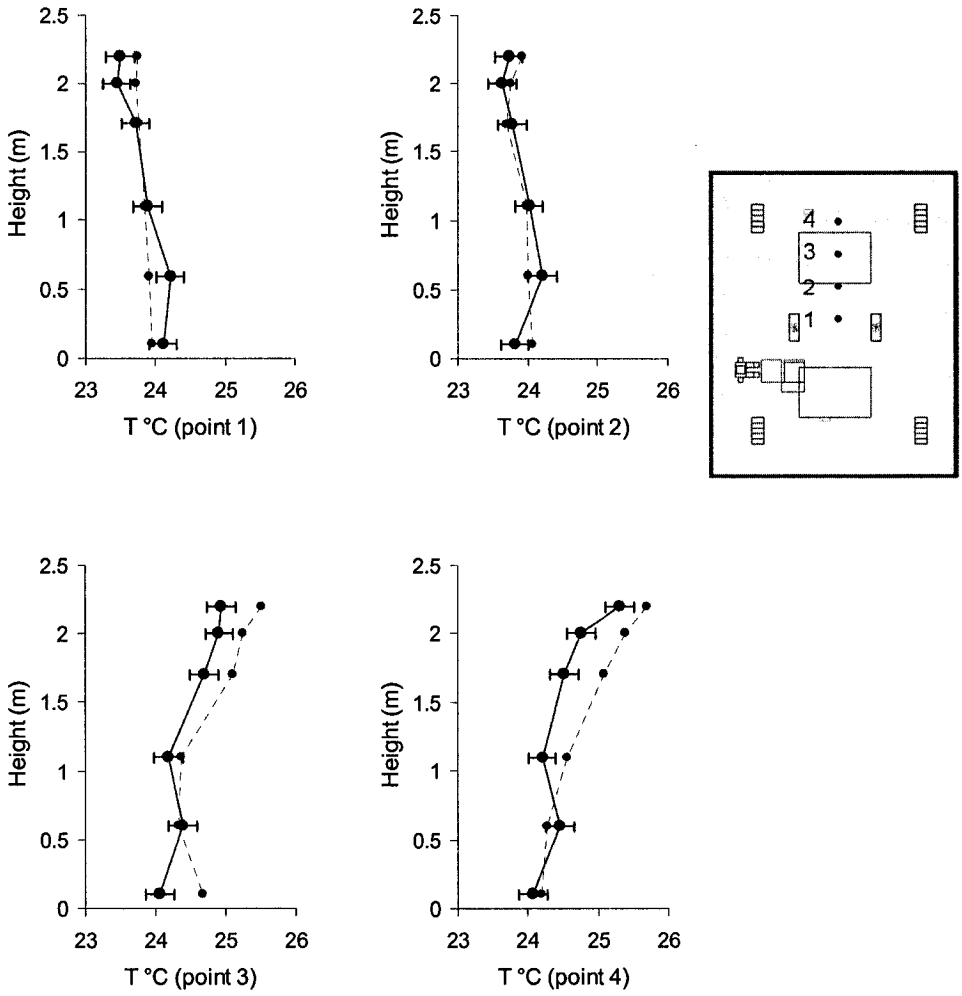

Figure 4.17: Temperature results (for case 3 with high heat load)

Solid line: measurements, dotted line: predictions

It also can be seen that numerical results do not perfectly agree well with the expected velocities and temperatures near the 3rd and 4th pole locations in case 3. Though the anemometers and thermal couples were not free from measurement errors (particularly at low velocity), the over-predictions of airflow and temperatures indicate that the CFD

calculations in this case may have amplified and overestimated the impact resulting from the hot plates (especially at point 4, which was the closest to the hot plates).

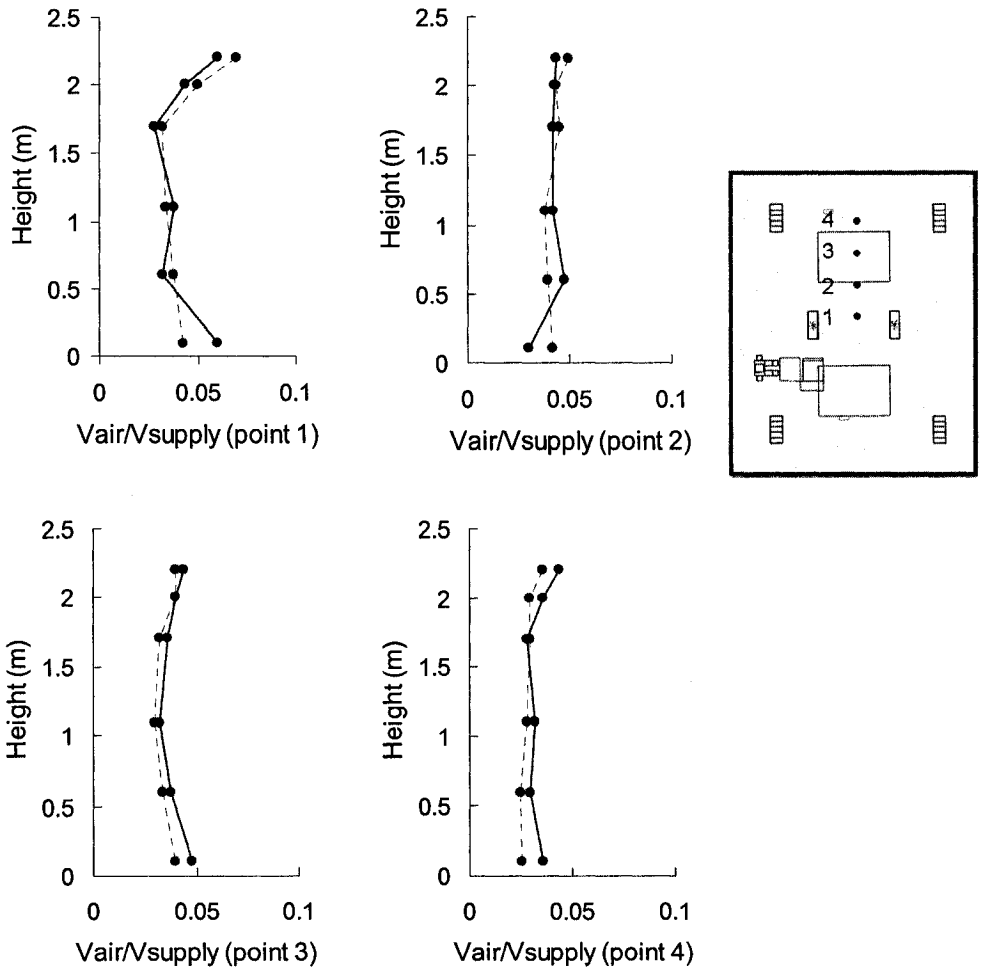

Figure 4.18: Normalized velocity results (for case 4 with MS)

Solid line: measurements, dotted line: predictions

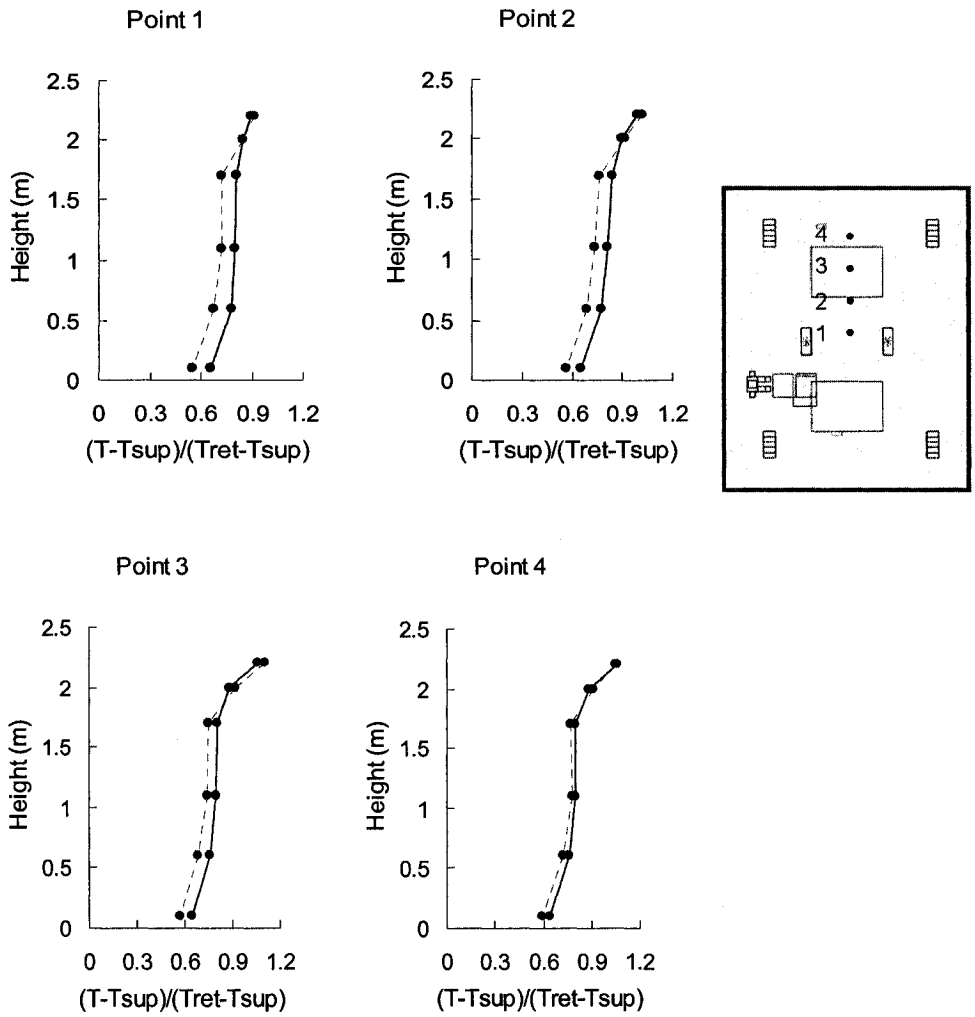

Figure 4.19: Normalized temperature results (for case 4 with MS)

Solid line: measurements, dotted line: predictions

Generally speaking, the simulated results agreed reasonably well with the experimental data for case 4 (with MS system), where the room air was well mixed. For all four measurements locations, the magnitudes of temperature and velocity readings were found to be close to each other (indicated by Figure 4.17).

It is worth noting that the air throw from the ceiling terminals is heading toward the

right side of the room, and the measurement points are located on the other side of the room, thus relatively high air temperatures and low air velocities were recorded at the four measurement points in case 4. It is very interesting that temperature stratification can be observed in case 4 with ceiling mounted MS. This might be due to the near-stagnant flow regime near the measurement points (demonstrated by the low velocities near all the four measurement points).

4.4.2 MS and UFAD with passive swirl diffusers

CFD simulations were also performed to examine the performance of passive swirl diffusers, with both MS and UFAD system. Elaborate measurements with regard to the airflow pattern near the diffusers and the vertical profile of temperature, air velocity, and tracer gas (CO_2) concentration in the space were provided by Cermak (2004), satisfying the desire for verification.

As illustrated in Figure 4.18, the mock-up office where the measurements were taken was equipped with a floor swirl diffuser at each of the four corners of the room, or alternatively, conditioned air could be delivered through one overhead round diffuser located at the center of the room.

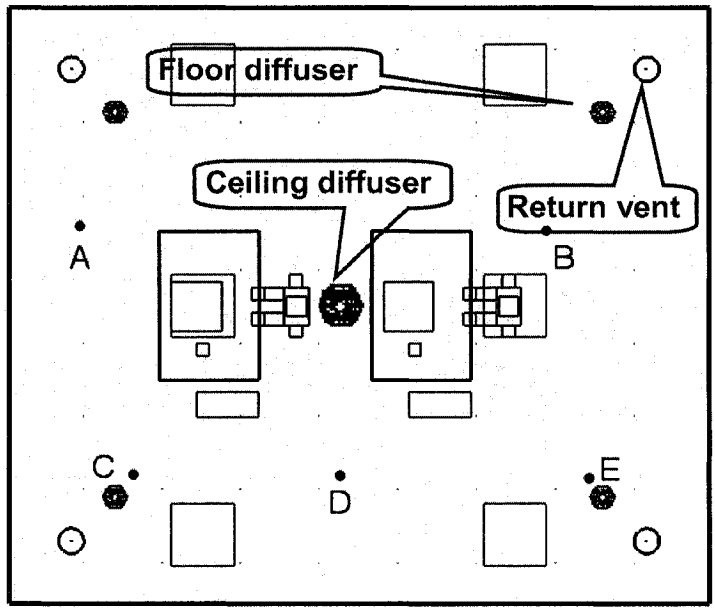

Figure 4.20: Measurement points and air terminals

In the case of UFAD system, data were collected at the 5 pole locations labeled as A, B, C, D and E throughout the room (as shown in Figure 4.18); whereas the measuring points were limited to A and B in the cases with MS. The measurements of temperature, velocity, and CO_2 concentration were taken using sensors installed along each pole at various heights. The experimental facilities and measurement design were thoroughly documented by Cermak (2004). As introduced earlier, prototype CFD models were built to mimic the actual geometry, the thermal/airflow boundary inputs, and the CO_2 dosing system as well.

Before exploring the temperature, velocity, and tracer gas concentration results, let us first take a look at the flow pattern of the discharged air jet in the vicinity of diffusers.

Airflow pattern created by swirl diffuser

As previously mentioned, special treatment and refinement were integrated into the modeling of the swirl diffuser. This modeling method could be credited with reliability

only when it can capture the feature of airflow pattern.

Figure 4.21: Air discharge from floor swirl diffusers: smoke visualization vs. predicted particle traces

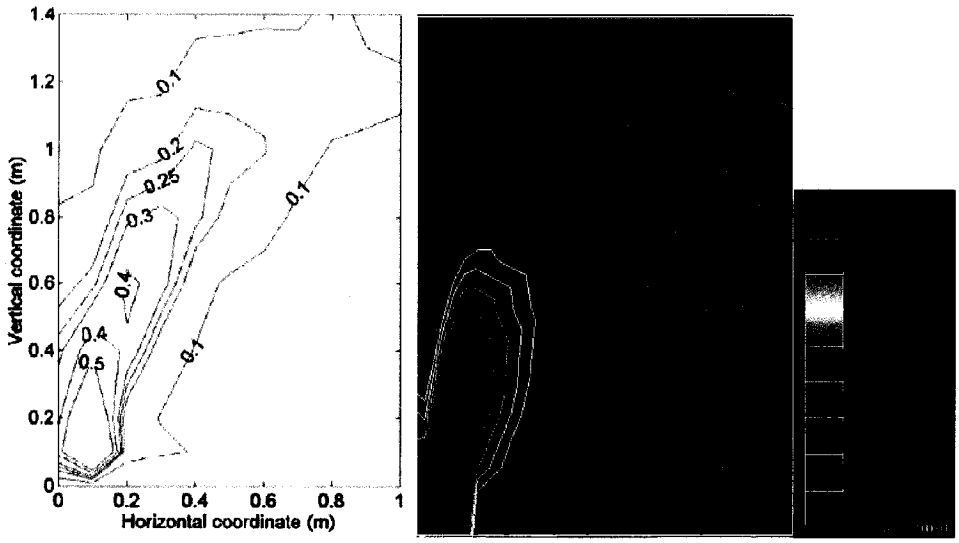

Figure 4.22: Air velocity contours: measurement (left) vs. prediction (right)

Figure 4.19 provides a comparison between the smoke visualization and predicted airflow pattern (described by particle traces), demonstrating close agreement between the numerical results and the expectations. In Figure 4.20, the distribution of air velocity (both predicted and measured) is plotted. In this circumstance, the diffuser delivered 20 L/s of conditioned air (T_{supply} = 20 °C) into the room. As can be seen from Figure 4.20, an

air throw height of ~1.0 m and a clear zone with diameter of ~0.4 m was produced. Air throw height and clear zone are defined as the vertical distance and the horizontal distance from the centre of the diffuser where the supply air terminal velocity degrades to 0.25 m/s, where the disturbance due to excessive airflow is considered to be negligible.

The discharge airflow pattern and velocity field demonstrated in Figures 4.19 and 4.20 are both predicted by the RNG k-ε model. Simulations with the indoor zero-equation model were also performed; however, it was found that the indoor zero-equation model was deficient at capturing the swirling behavior and the entrainment effect. Thereafter, the RNG k-ε was employed in the simulation cases with floor-mounted swirl diffusers.

Profiles of velocity, temperature, and CO_2 concentration (with UFAD)

When the UFAD system was in service, data were collected at poles from A to E. The predicted velocity and temperature profiles, obtained from the RNG k-ε model, are presented comparatively with those in-situ readings. Data was collected by a measurement station consisting of 16 omni-directional thermal anemometers. The low velocity anemometers had an accuracy of ±0.02 m/s within the measurement range of 0.05 m/s to 1 m/s; while the temperature measurement accuracy was ±0.3 °C.

The velocity, temperature, and normalized CO_2 concentration results are plotted in Figures 4.21, 4.22, and 4.23, respectively. The graphs also present experimental results for comparison purpose to demonstrate the accuracy of numerical predictions.

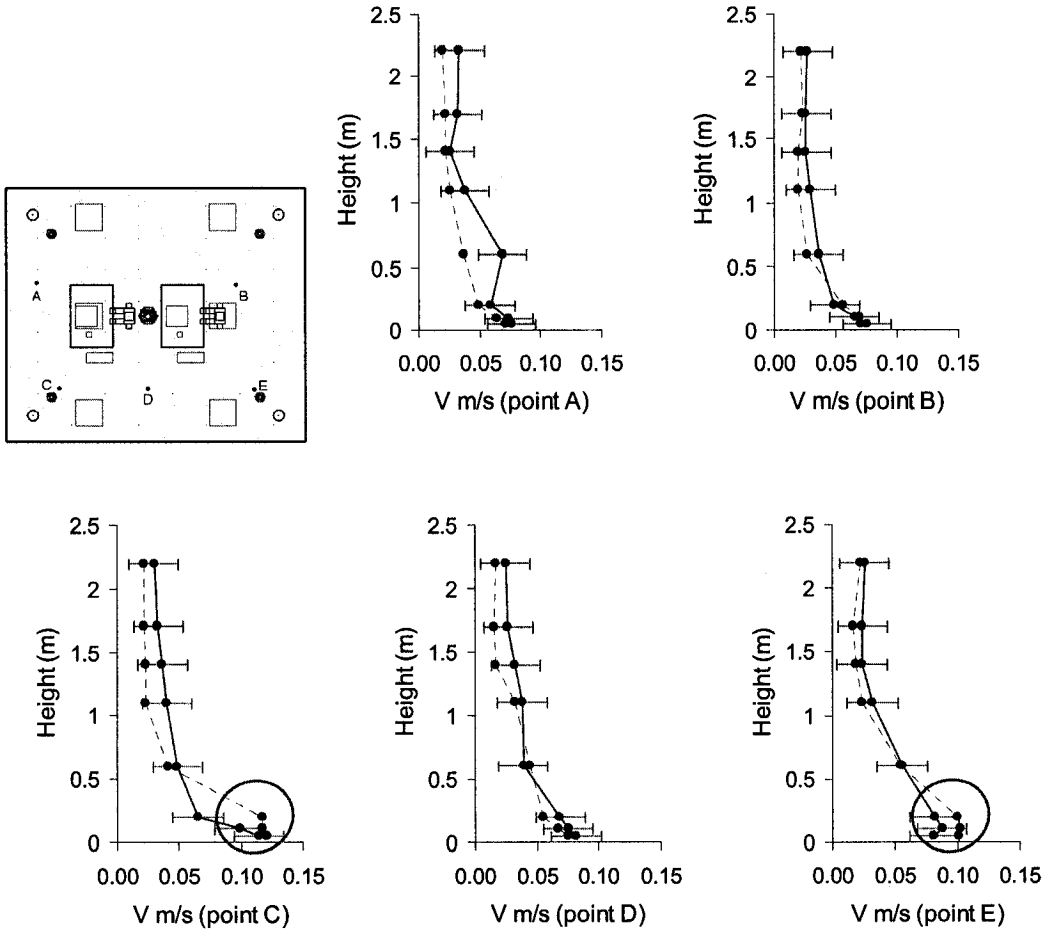

Figure 4.23: Velocity profiles (UFAD with swirl diffusers)

Solid line: measurements, dotted line: predictions

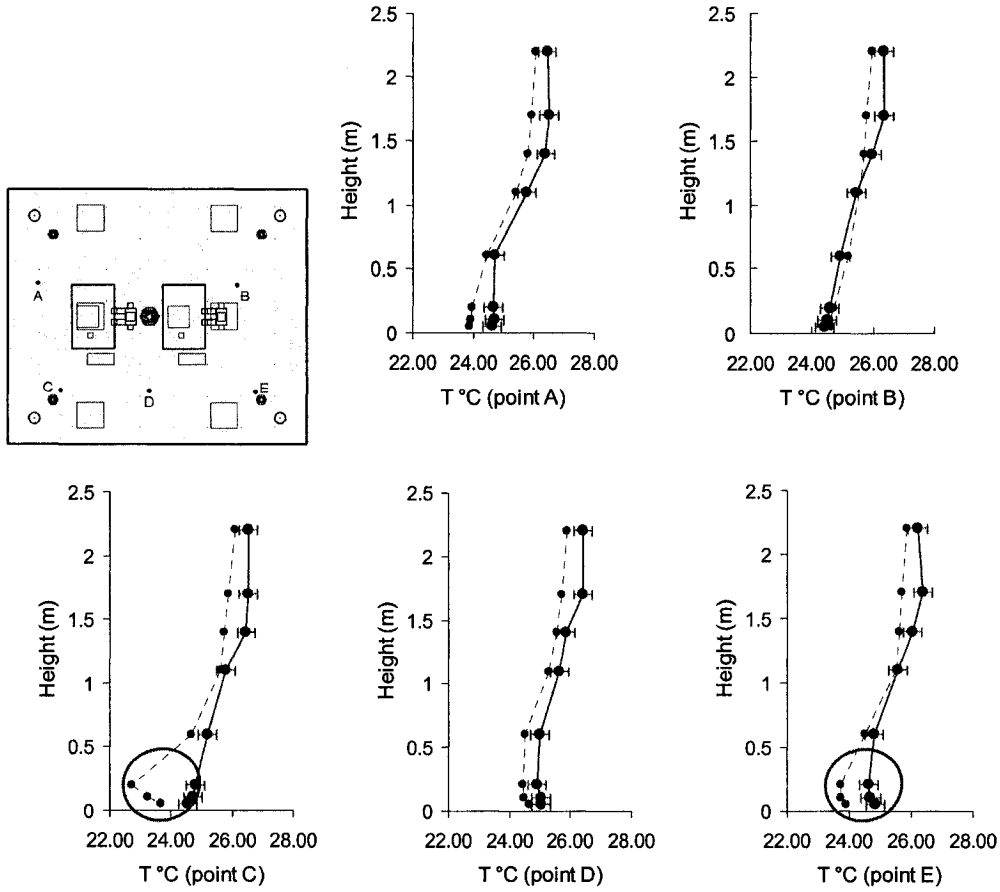

Figure 4.24: Temperature profiles (UFAD with swirl diffusers)

Solid line: measurements, dotted line: predictions

It is worth mentioning that the CO_2 concentration results was presented here in a non-dimensional form (the reciprocal of contaminant removal efficiency E_c), written as

$$c(-) = \frac{1}{E_c} = \frac{(c - c_{\sup ply})}{(c_{return} - c_{\sup ply})} \tag{4-4}$$

where c is the CO_2 concentration at points of interest, c_{supply} is the CO_2 concentration in the supply air, which was set to at 400 ppm during the measurement, c_{return} is the CO_2 concentration in the return air, which was to be determined from CFD calculation.

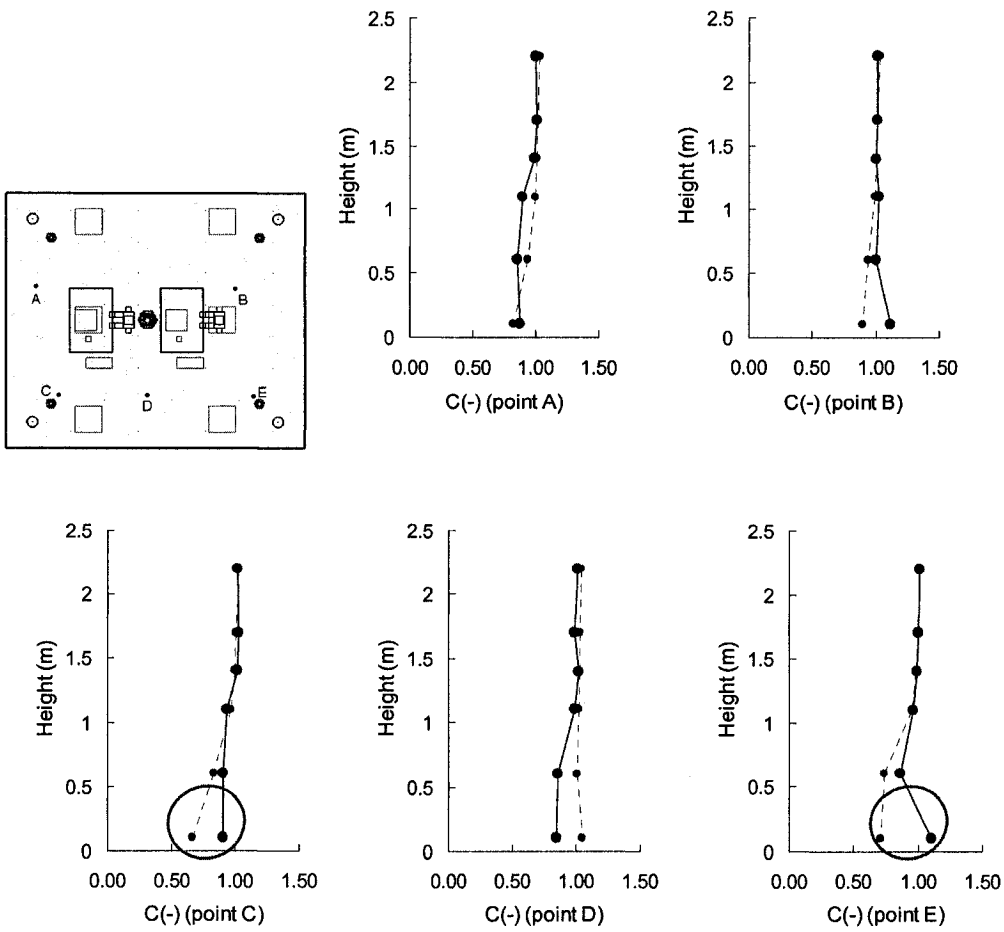

Figure 4.25: Normalized CO_2 concentrations (UFAD with swirl diffusers)

Solid line: measurements, dotted line: predictions

Generally speaking, the simulation matches the measurements reasonably well. Relatively large discrepancies can be found in the velocity results, which are still tolerable. It should be noted that, when the measured velocity goes below 0.05 m/s, inherent measurement uncertainties associated with the instrument could not easily be identified and thus no attempt is made here to explain these discrepancies.

Relative to the experimental data, CFD simulation predicted relatively high velocities

and lower temperatures and CO_2 concentrations at some spots in the lower part of the room (especially at measurement points C and E). However, the simulation results seemed to be logical, since it is understandable that high velocity, low temperature, and low CO_2 concentrations would occur in the vicinity of the floor diffusers. Taking measuring point D as an example, a high CO_2 concentration was predicted by CFD. The location of sampling point D may explain these numerical results: point D was located very close to a CO_2 injection spot and remote from the supply diffusers (the diffusers were located at the four corners of the room, whereas point D was placed in the center front); therefore, high CO_2 concentration at this point was inevitable but this could not be seen from experimental data for unknown reasons.

Under the test conditions, the characteristics of the airflow produced by the UFAD system with passive swirl diffusers can be summarized as: at the lower levels in the room (below the elevation of 1.4 m), relatively low temperatures and high air velocities were produced; while in the upper region of the room (above 1.4 m), trivial variations of air velocity and temperature with height indicated the existence of an upper uniformly-mixed zone. Temperature stratification with the magnitude of 1.5~2.0 °C can be observed within the space.

Profiles of velocity, temperature, and CO_2 concentration (with MS)

When the ceiling swirl diffuser was in operation, measurements were taken at sampling pole locations A and B. Numerical experiments were performed to determine the reliability of the indoor zero-equation model and the RNG k-ε model for airflow simulations with the swirl type MS. The predicted results obtained from both models are presented in Figures 4.24 and 4.25 respectively, and measured data are also presented for

comparison purposes.

As can be seen from these figures, both the indoor zero-equation model and the RNG k-ε model have produced encouraging results, except for the velocity prediction at pole B, where the air movement was overestimated by the indoor zero-equation model and underestimated by the RNG k-ε model. But the reason for the high velocity readings in the measured data alone pole B could not be determined, as pole A and pole B were located symmetrically with respect to the supply diffuser; however, it was surprising that the magnitude of velocities detected at pole B was 0.07 m/s higher than those at pole A. Since the discrepancies resulting from the two turbulence models were found to be comparable in this case, it would be reasonable to choose the indoor zero-equation model to analyze the flow field driven by a ceiling swirl diffuser in this test room. (It is worth mentioning that, in some other cases with multiple ceiling swirl diffusers (those cases designed for preparing ANN training data pairs), the indoor zero-equation model ended up with divergence and thus was replaced by the RNG k-ε model.)

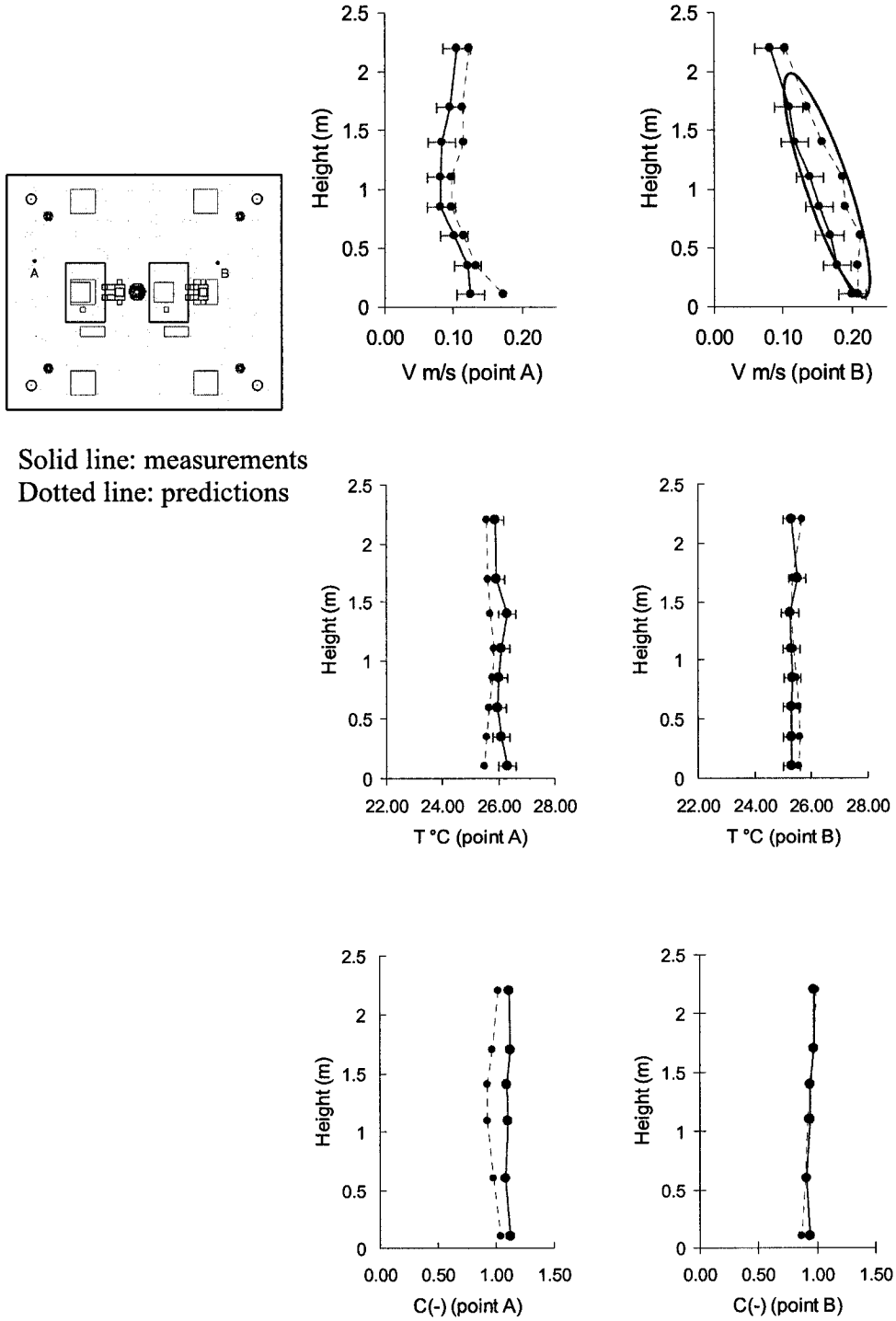

Figure 4.26 Predictions by the indoor zero-equation model (MS with a swirl diffuser)

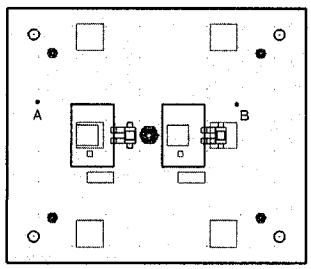

Solid line: measurements
Dotted line: predictions

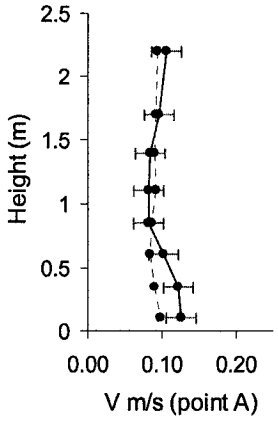

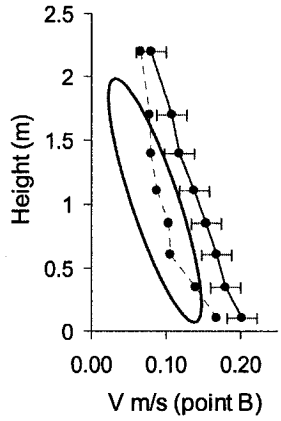

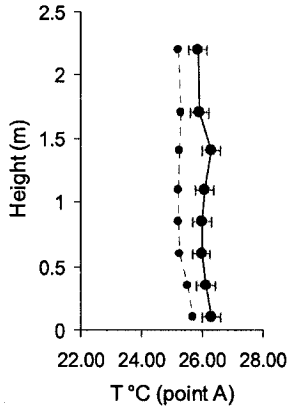

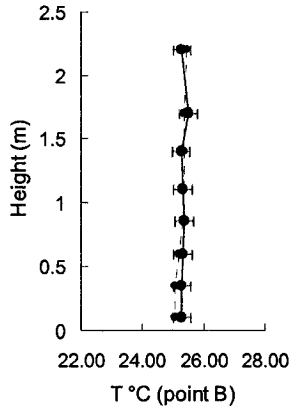

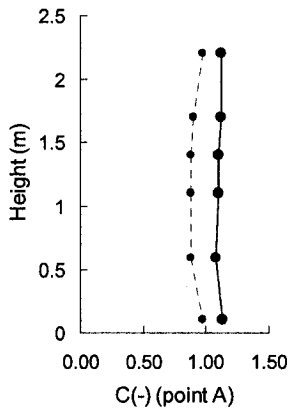

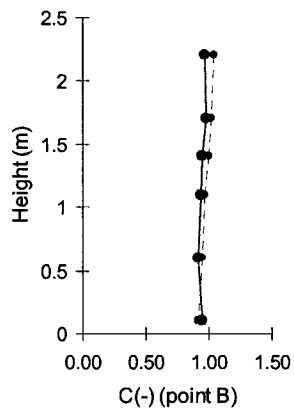

Figure 4.27: Predictions by the RNG k-ε model (MS with a swirl diffuser)

Relative to the results obtained in the case of UFAD with swirl diffusers, the characteristics of the flow field resulting from ceiling mounted swirl diffuser had the following features: with MS, the room air velocity, temperature, and CO_2 concentrations do not significantly vary with height; no temperature stratification could be observed in the flow field driven by the ceiling mounted swirl diffuser. The implication would be that the room air was well stirred and the physical quantities were uniformly distributed throughout the room. Regarding these observations, the experimental data were found to be consistent with CFD predictions.

4.5 Closing Remarks

As stated in the literature and in Appendix A, CFD simulation has inherent modeling and numerical errors. This necessitates comprehensive verification of CFD simulation results with field measured data. This chapter has described the verification treatment, which was based on experimental work carried out by the author and the data provided by another research group (Cermak and Melikov, 2005). Data collected from two full-size office type experimental chambers were used for verification, and both test chambers contained UFAD and MS systems. Grille-type and passive swirl diffusers, two types of diffusers commonly used in office spaces, were studied.

This chapter also proposed a simplified modeling approach to simulate the behavior of swirl diffuser. It was found that the predicted airflow pattern, the air throw height, the size of the clear zone, and the velocity distribution near the diffuser agreed closely with the smoke visualization and the expected velocity field. The validity of this modeling approach could thus be justified.

To assess the credibility of the CFD models created for the test rooms, data regarding

the vertical profiles of velocity, temperature, and tracer gas (CO_2) concentration (in the case with swirl diffusers) were employed as the objective quantities for verification. Comparisons between the experimental data and simulation results demonstrated satisfactory agreement, thus giving confidence in the modeling and numerical approaches adopted by the present CFD calculations.

Pilot CFD simulations were performed employing both the indoor zero-equation model and the RNG k-ε model. Aside from the case of UFAD system with multiple swirl diffusers, the indoor zero-equation model had produced comparable accuracy and saved substantial CPU time, in comparison with the RNG k-ε model. Given this, the indoor zero-equation model has been used hereafter to analyze the flow field resulting from UFAD and MS with grille-type diffusers and MS with one swirl diffuser; whereas, in the cases with multiple ceiling/floor mounted swirl diffusers, the RNG k-ε model was employed, since the indoor zero-equation model failed to produce encouraging results.

The validated cases presented in this chapter will serve as the baseline cases for the ANN training/testing data generation and optimization work hereafter.

CHAPTER 5

OPTIMIZATION OF VENTILATION SYSTEM DESIGN AND OPERATION IN OFFICE ENVIRONMENT: IMPLEMENTATION AND RESULTS

5.1 Introduction

Chapter 2 put forward a CFD simulation-based optimization scheme that was claimed to be suitable for the optimization of ventilation system design and operation in office environments. Such an optimizer is targeted at improving the occupant's sense of thermal satisfaction and IAQ with minimum energy inputs, and this objective can be realized by properly adapting the design measures and operational states of ventilation system in response to the variance in the office's thermal and airflow conditions.

Appendix A and Chapters 3 to 4 have addressed such topics as the theoretical basis of CFD, assessment of office indoor environments, and the applicability of CFD for simulating office indoor environments in some baseline cases. The current chapter builds on this foundation and sets out to demonstrate the implementation and application of the CFD simulation-based numerical optimization method.

Section 5.2 puts forward how to establish an ANN model—a relatively inexpensive model for *response surface approximation* (RSA), by using the data obtained from extensive CFD simulations. Such a low fidelity model could replace CFD to compute the objective function and constraints with sufficient accuracy when implementing GA optimization; as a result, the computational costs could be significantly decreased. The training data preparation and ANN model training and testing are also presented in detail

in this section. Following this, the development and implementation of ANN-embedded multi-variable GA are illustrated in Section 5.3. For the current problem, the objective function was constructed to aggregate and weight indicators such as PMV (for thermal comfort assessment), ε_v (for IAQ evaluation), and energy usage for cooling purpose and supply fan operation. Sensitivity analysis was performed in advance to determine the appropriate weighting factors in the objective function, and the results are presented in Section 5.3. Under various office thermal/airflow conditions, the optimization method was applied to adapt the design parameters and operational states of ventilation systems to realize the research objectives. The optimization results are presented in Section 5.3. Finally, closing remarks are made in Section 5.4.

It is worth mentioning that the validity and effectiveness of this ANN-based GA optimization method is also demonstrated through an example searching for the global minimum of a classic multi-modal optimization problem (Rosenbrock's function), as presented in Appendix B.

5.2 ANN Training and Testing

Recalling the statements in Chapter 2, it is clear that the validity and efficiency of ANN for RSA is critically dependent on the quality of training data sets, the network topology, and the training method. Issues other than the training data preparation have already been addressed in Chapter 2; therefore, how to generate representative and holistic data pairs by performing CFD simulations is put forward before the ANN training and testing are presented.

5.2.1 Data pairs preparation for ANN training

Inputs and outputs for ANN

Influential parameters summarized in Chapter 3 (see Table 3.2) were chosen as the simulation parameters for the CFD study and thus as input variables to the ANN model. These input variables span a broad range of thermal and airflow parameters, including inner surface temperature, internal heat load density, indoor contaminant emission rate, ventilation system type, diffuser type, number of diffusers in office, distance between diffuser and occupant, distance between return vent and contaminant source, as well as supply air temperature and flow rate. It is worth mentioning that the influence of outdoor air temperature on the indoor flow field is characterized by the inner surface temperature, thus the outdoor air temperature is excluded from the input matrix. Also, the outdoor air flow rate is controlled to maintain the CO_2 concentration in the supply air at a constant level (400 ppm).

Since there were limited options for the ventilation system type, diffuser type, and number of diffusers, these three parameters were not treated as individual input in the initial layer of the network. Instead, an input variable (referred to as "system configuration variable") was devised to represent a particular system configuration that could be characterized by a combination of these three parameters. For instance, when "system configuration variable" was set to one, it denoted the UFAD system with two grille-type diffusers; when this variable was set to 2, it represented the MS with 1 swirl diffuser, and so on. To sum up, this resulted in a neural network containing 8 input variables.

The outputs of ANN include those objective indices introduced in Chapter 3. Indices

such as PMV, *head-to-ankle temperature difference* ($\Delta T_{HeadToAnkle}$), *equivalent temperature* (ET) variation (between the left-hand side and right hand side of the occupant), and local air velocity were used to assess the thermal comfort level; CO_2-based *ventilation effectiveness* (ε_v) was used for IAQ evaluation; and fan power input (E_{fan}) and cooling energy requirement ($E_{cooling}$) are taken into consideration to account for energy consumed by ventilation. Accordingly, each ANN model contains seven output variables.

Problem associated with training data preparation

Quality of training data is one of the key issues affecting the learning ability of a network. In order to improve the generalization performance of the network, it was preferable to train the network with a large number of training data pairs that can cover the full ranges of design parameters. However, it was evident that the larger the volume of training data, the longer it would take for the training process. On top of this, it should be noted that the training data were prepared by performing CFD simulations, too large a volume of training data would thus result in excessively high computational costs. As a result, due consideration should be given to the issue regarding how to generate sufficient but limited training data points in order to ensure the quality of network training on one hand and avoid excessive CFD case studies on the other hand.

A common approach to design numerical experiments (for data generation in this case) is to vary one variable at a time and keep the other variables at constant values, repeating the process for each variable. This would create a case pool of size N^K, where N is the resolution of the variables and K is the total number of variables (here $K = 7$). It is clear that, as 7 inputs are under consideration, even a low level resolution would result in a

large number of case studies. Consequently, care was taken to improve the design of numerical experiment and shrink the number of cases to be studied.

The concept of factorial design (Montgomery, 1976) is often introduced to address such an issue. Originally, factorial design theory was applied to design the parameters of physical experiments. By using a minimum number of experiments, it enables the assessment of the effects of two or more parameters and their interactive effects on the objective variables. When performing factorial experiments to identify the influential parameters, it is typical to select only two values of each variable (that is, N is set to 2)—a representative high value and a typical low value over the full range. Then this is a so called 2^K factorial experiment. Therefore, if the principle of 2^K factorial design were adopted here, it would have resulted in $2^7 = 128$ cases to be studies. However, this was based on the idea that each of the input variables can be only set to two possible values, which would inevitably degrade the learning ability and generalization capability of the network, especially around the intermediate levels of the input variables. In this study, it was necessary to introduce a new approach for numerical experiment design into the context of the current study.

Latin hypercube sampling

The *Latin Hypercube sampling* (LHS) method was used to generate the distribution of simulation parameters in the numerical experiment. After the original paper (McKay et al., 1979) where LHS was proposed, it was used widely both in engineering and in risk analysis. LHS is sometimes referred to as a deterministic simulation of computational experimentation. This statistical method is targeted at generating collections of parameter values from an allowable multidimensional distribution.

Essentially, LHS selects random sampling points for each parameter over its entire range in a stratified manner. With this method, N sets of design points are generated by projecting individual variables onto N different levels. The points for each variable are determined randomly and independently. As a result, the finite samples produced can reasonably represent the overall uncertainty of the inputs. Taking a problem with two variables and 5 design points as an example, the square grid containing the sample points is a *Latin Square*, which is shown in Figure 5.1. It is worth noting that there is only one sample in each row and column.

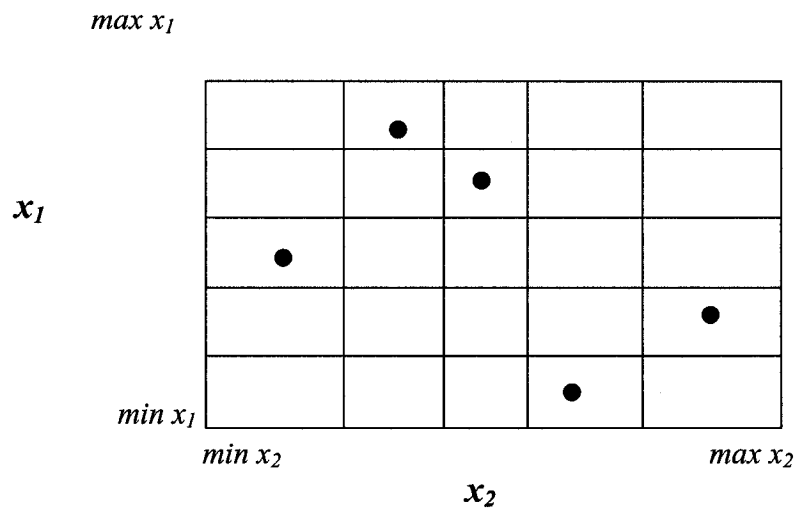

Figure 5.1: Latin square: 5 random pairings of 2 variables

A *Latin hypercube* is a plausible generalization of this concept to an arbitrary dimension, provided there is only one sample contained in each axis-aligned hyper-plane. The dimension of the hypercube, in other words, the number of sample points, is to be determined in advance from the user's needs. McKay (1988) suggested that more than $2n$ sampling data sets ($N \geq 2K$, N is also the total number of cases) should be generally sufficient to solve problems of practical interest.

As previously mentioned, K was equal to 7 in the present case; that is, we were trying to sample a function with 7 variables for each ventilation system scenario. Given this, N was set to 18 in the current case—the allowable range of each variable (as listed in Table 3.2) was partitioned into 18 intervals. The number 18 was chosen here, which was slightly higher than the recommended number of $2K = 14$. As a result, 18 suits of random sample points were then generated to satisfy the *Latin hypercube* requirements.

Simulation parameters / Ranges / Case No.	Heat gain	T_{supply}	V_{sup}	T_{surf}	DDO†	Emission	DRS‡
	25~45 (W/m^2)	15~22 (°C)	80~160 (L/s)	20~35 (°C)	0.5~2 (m)	0.3~1.5 (L/min)	0.5~2.5 (m)
1	41.722	19.118	80.683	30.708	1.263	0.558	1.108
2	30.299	21.652	95.444	31.085	1.203	0.633	2.429
3	37.659	18.477	119.099	20.518	1.719	1.107	1.366
4	32.238	20.696	134.791	34.283	0.525	1.087	2.013
5	35.121	17.795	85.164	32.622	1.871	1.213	1.191
6	27.487	20.441	133.246	28.672	1.630	0.989	2.313
7	38.937	15.335	99.194	26.253	0.859	1.281	1.893
8	29.424	15.699	127.202	29.250	0.782	0.735	0.881
9	44.087	18.812	120.748	24.315	0.934	1.429	0.745
10	31.173	16.710	153.321	23.629	1.004	0.367	0.716
11	40.983	19.561	156.847	20.985	0.706	0.928	0.544
12	34.120	17.645	91.427	31.950	1.343	0.872	1.828
13	36.198	17.327	105.313	22.215	1.152	1.466	2.121
14	26.402	15.876	141.379	27.259	1.918	0.678	1.577
15	43.693	21.438	114.696	33.882	1.477	1.338	1.403
16	40.105	20.860	143.635	25.388	1.812	0.485	2.276
17	32.849	16.374	109.765	22.727	1.510	0.795	0.970
18	25.092	19.893	148.704	28.076	0.605	0.316	1.614

† DDO: Distance from diffuser to occupant
‡ DRS: Distance from return grilles to contaminant source

Table 5.1: CFD case designed by LHS (for UFAD system with 4 swirl diffusers)

The sample points (by LHS) of the simulation parameters generated for the UFAD system with four swirl diffusers are listed in Table 5.1 for demonstration purpose. The

simulation cases designed for the UFAD system with one/two grille type diffusers, for the UFAD system with two swirl diffusers, for the MS with one/two grille type diffusers, and for the MS system with one/two swirl diffusers were generated in a similar way; no attempt was made to list all the sampling points for those scenarios.

By inserting the obtained sampling data points as the input parameters into the reference CFD program (validated in Chapter 4), extensive CFD simulations were performed to predict the corresponding outputs and to create the data base for ANN training. In conjunction with the baseline cases (in which the measurements were taken), around 150 training data sets were included into the database.

It is worth mentioning that the variations in the heat load density and in the CO_2 emission rate were realized by varying the heat power and CO_2 generation rate from two extra heat/contaminant sources added to the space, as shown in Figure 5.2. In addition, the placements of diffusers and return grilles were varied in the CFD model to adjust the distance from diffuser to occupant (DDO) and the distance from return grilles to contaminant source (DRS), while the locations of the occupants and the contaminant sources were kept unchanged. The displacement extremes of the diffusers and the return grilles are also illustrated in Figure 5.2 (taking the case of the UFAD system with 4 diffusers as an example).

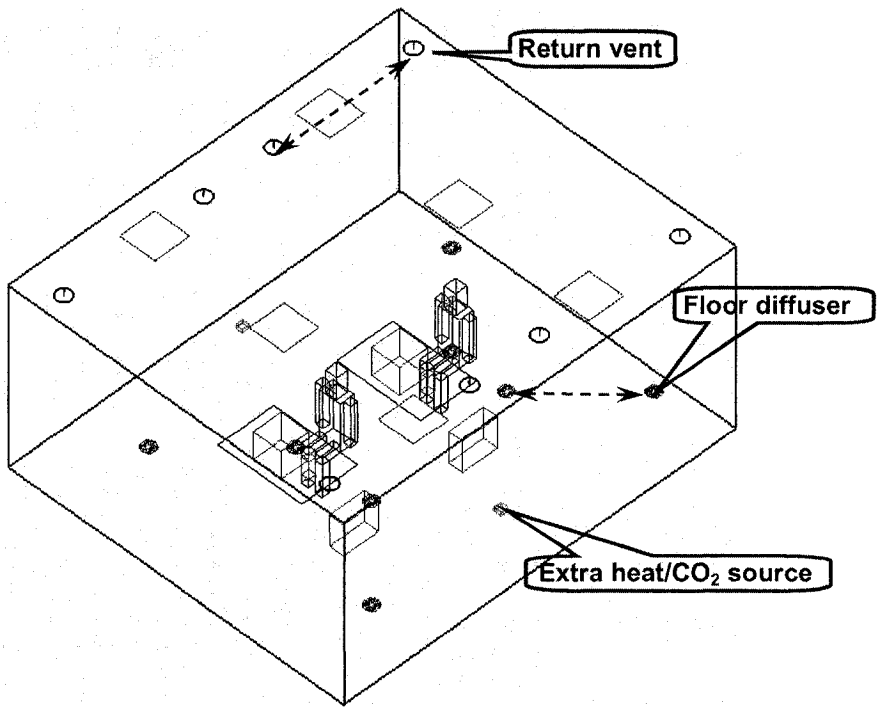

Figure 5.2: Extra heat/CO_2 sources and placement of air terminals

Data preprocessing and postprocessing

ANN training process can be made more efficient when certain preprocessing steps are applied to the raw data pairs. The networks in this study incorporated the hyperbolic tangent sigmoid function in the initial/hidden layers and a linear transfer function in the output layer, and Levenberg-Marquardt and Bayesian regularization were selected as the algorithms when implementing back-propagation training. Given this network structure and training scheme, it would be preferable to scale the input and target data into the range of -1 to 1. Prior to being fed into the network, the input data sets were normalized in this study by using the maximum and minimum values of respective variables.

$$Input(i,j)_{nor} = \frac{2[Input(i,j) - MinInput(i)]}{[MaxInput(i) - MinInput(i)]} - 1 \qquad (5\text{-}1)$$

where subscript *nor* stands for normalized value, i denotes the ith variable, j denotes the

*j*th data set (or, the *j*th observation), *MaxInput(i)* and *MinInput(i)* are the maximum and minimum values of the *i*th input variable found over all data sets, respectively.

After the training process, the outputs from the network corresponded to the normalized targets; accordingly, it would be necessary to perform de-normalization manipulations to scale the outputs back into the original ranges. Such an inverse operation is straightforward,

$$Output(i,j) = 0.5[Output_{nor}(i,j)+1]\times[MaxOutput(i)-MinOutput(i)]+MinOutput(i) \tag{5-2}$$

where *i* denotes the *i*th output variable, *MaxOutput(i)* and *MinOutput(i)* are the maximum and minimum values of the *i*th output variable found over all data sets, respectively.

5.2.2 ANN training and testing results

An ANN with 30 intermediate neurons in the hidden layer was created, trained, and tested by using the data sets generated from extensive CFD simulations. When adopting Bayesian regularization training algorithm to improve the generalization capability of the network, all the candidate data were used for training purpose. The training algorithm was considered to reach convergence if both the *sum of squared error* (SSE) and the *sum of squared weights* (SSW) stabilized over certain iterations (as shown in Figure 5.3).

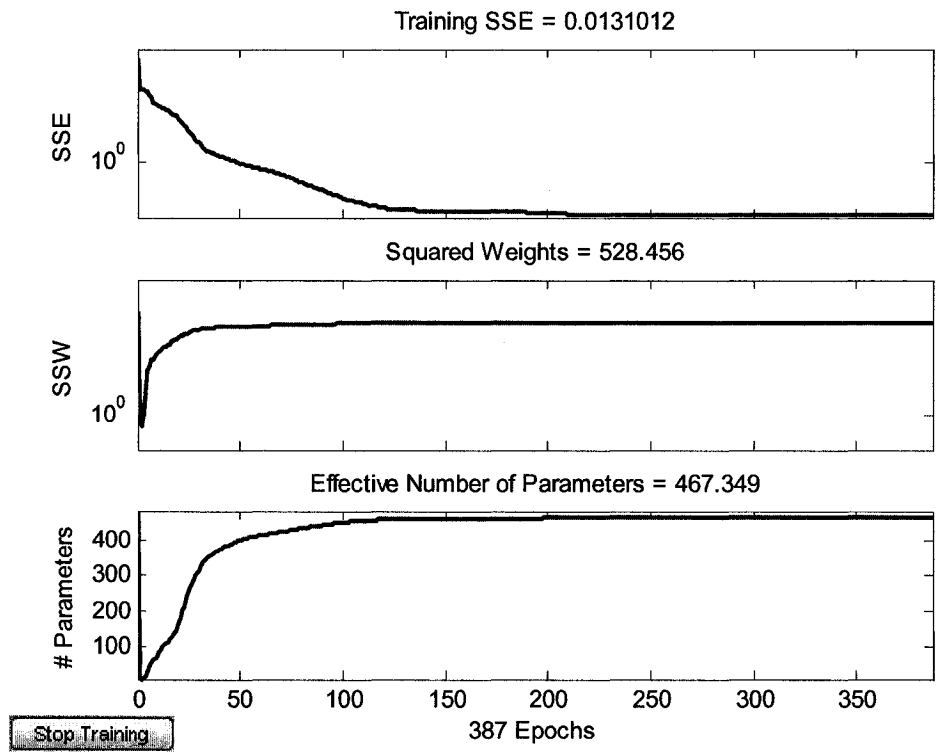

Figure 5.3: Convergence history of ANN training with Bayesian regularization

The training process with 387 epochs took about 15 minutes to reach the convergence on a dual-processor Pentium IV workstation (Dell Precision 670) with CPU speed at 3.4 GHz. The SSE at the final stage was found to be 0.0131, which could be translated to a *mean squared error* less than 1.9×10^{-3} (as the network contained 7 outputs). Out of the weights and bias assigned to all the neurons (the network contained 30 hidden neurons, 8 inputs, and 7 outputs and thus results in about $8\times30+30\times7 = 450$ weights; also, bias was assigned to some of the neurons), 467 parameters (indicated by "#Parameters" in the above figure) were active and behaved as effective linkage in the final trained network. In addition to the training error, another indicator can be also used to evaluate the learning capability of network based on "experience": the regression of the network outputs on the corresponding expected outputs (as shown in Figure 5.4).

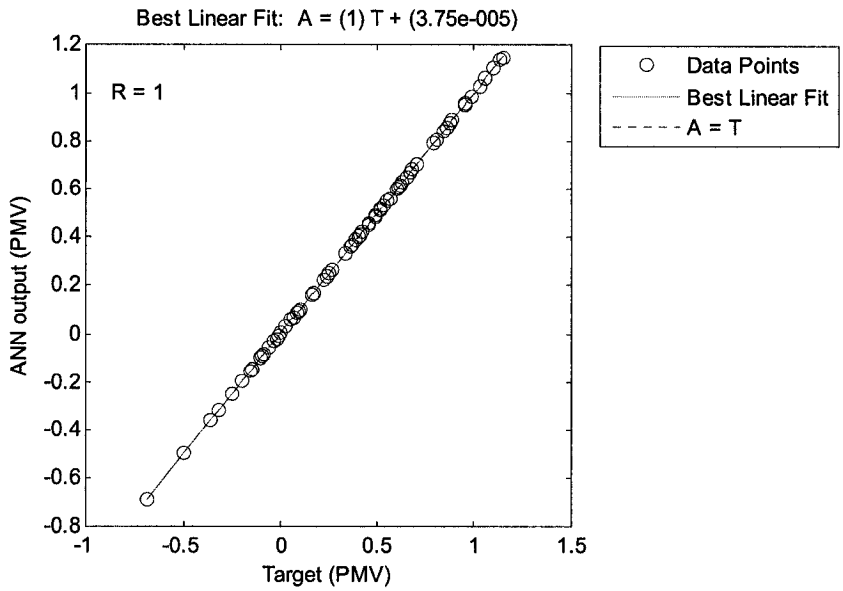

Figure 5.4 (a): The linear regressions of ANN predicted PMV on targets

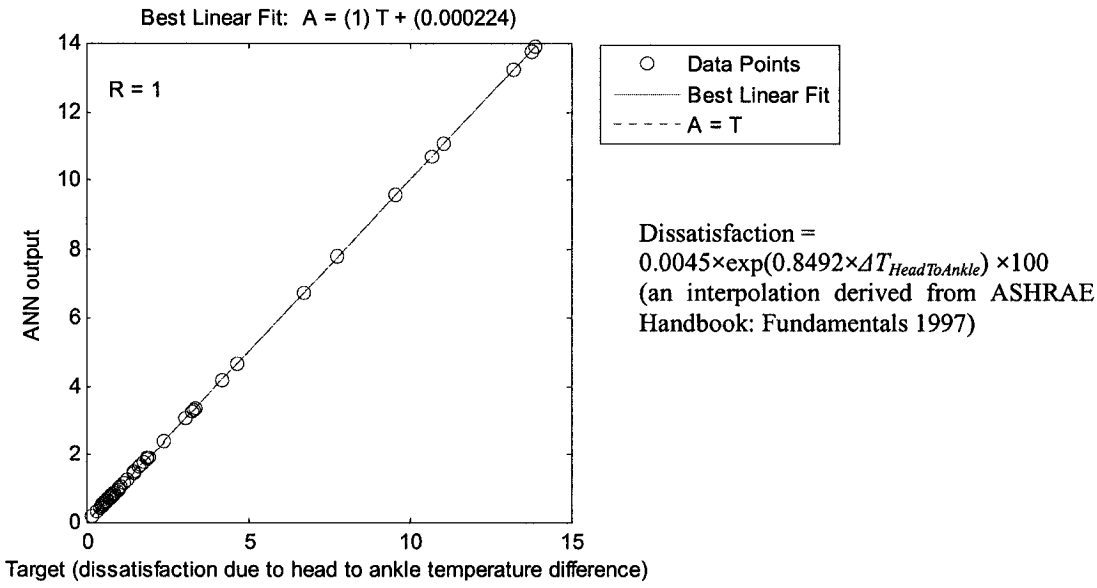

Figure 5.4 (b): The linear regressions of ANN predicted $\Delta T_{HeadToAnkle}$ on targets

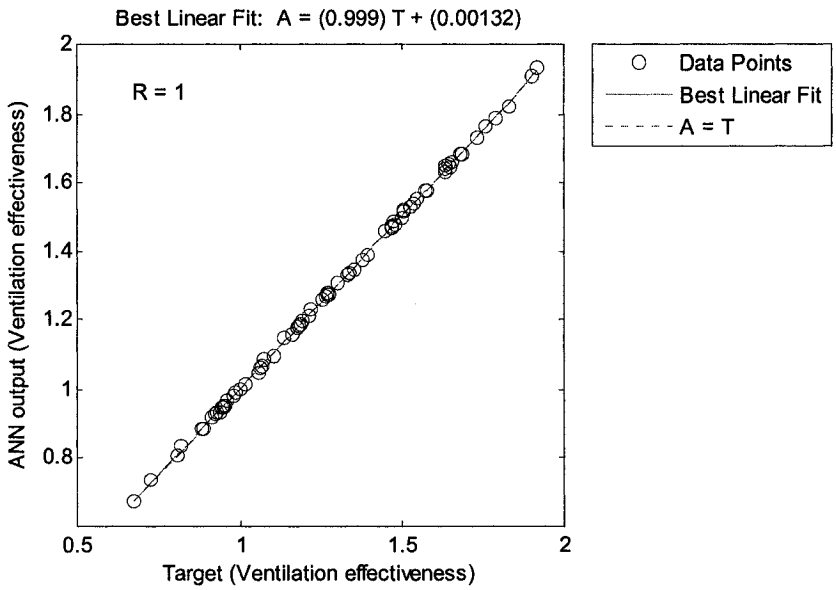

Figure 5.4 (c): The linear regressions of ANN predicted ε_v on targets

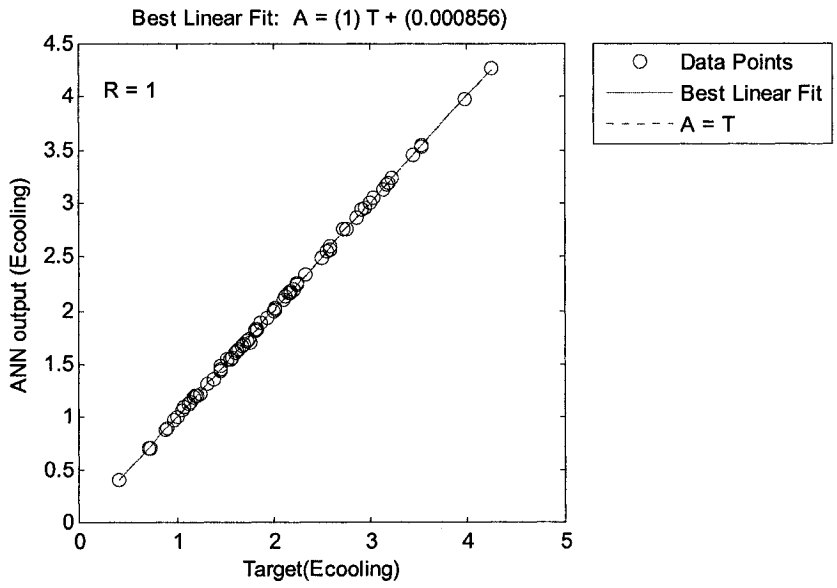

Figure 5.4 (d): The linear regressions of ANN predicted $E_{cooling}$ on targets

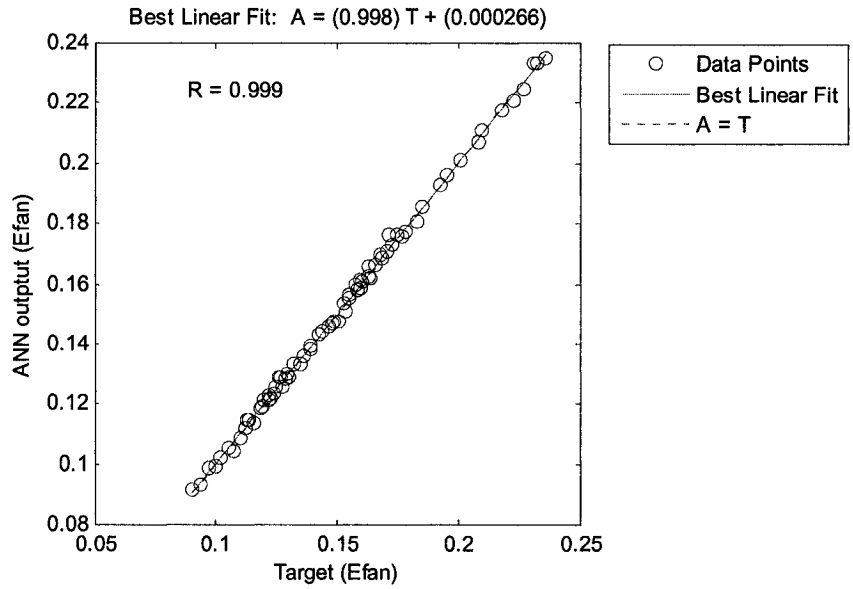

Figure 5.4 (e): The linear regressions of ANN predicted E_{fan} on targets

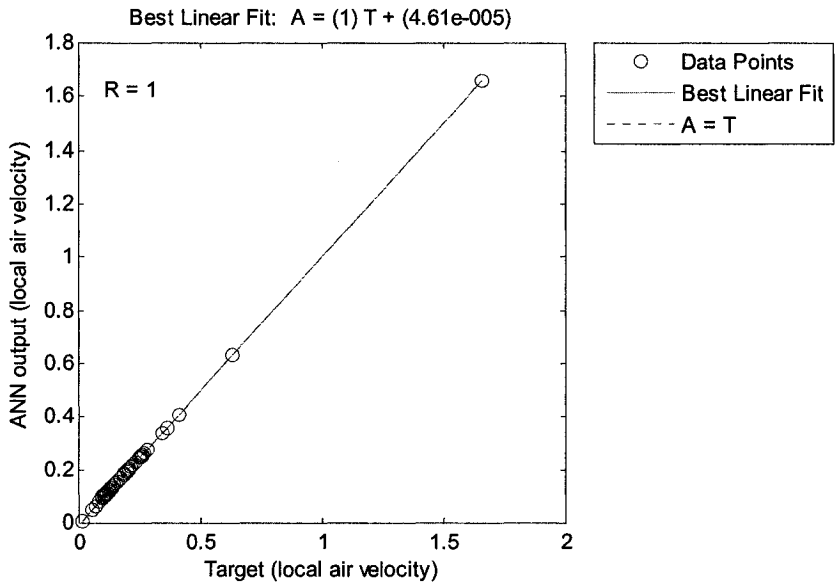

Figure 5.4 (f): The linear regressions of ANN predicted air velocities on targets

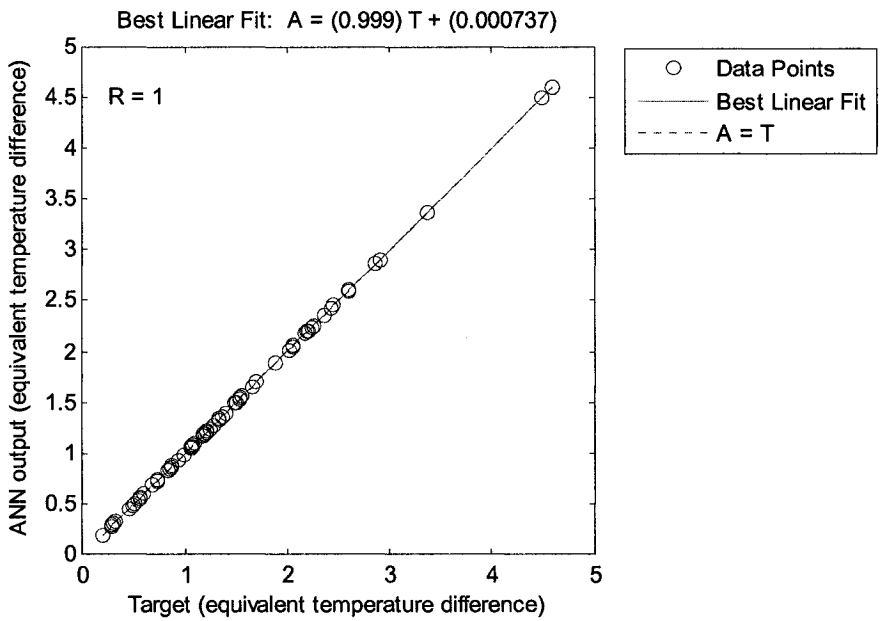

Figure 5.4 (g): The linear regressions of ANN predicted ΔET on targets

The linear regressions plotted above indicate that the final trained network predicted the desired outputs with adequate reliability. *R* stands for regression correlation coefficient in the above figures. For all 7 outputs from the network, it was found that the corresponding *R* values were very close to 1, demonstrating perfect correlations between the outputs and the target values.

Afterwards, 30 extra cases (the simulation parameters were also generated by LHS) that were not used for training were fed into the network to test generalization. Comparisons between the ANN outputs and target outputs for these 30 cases demonstrate how well the network can span the "unseen" scenarios. Figure 5.5 and Table 5.2 present the relative errors corresponding to the ANN predictions for these 30 test cases (PMV, ε_v, $E_{cooling}$, and E_{fan} are presented here for demonstration purpose), which indicate that the

average error of the network is less than ± 6%. For more than half of the 30 cases, the relative errors were less than 3.5%. Such a small magnitude of relative error demonstrates the current network's convincing capability for generalization and for system response prediction.

Relative error		≤ 3.5%	≤ 6.5%	≤ 8.5%	≤ 10.5%
No. of test cases when errors fall into the range	PMV	12	8	7	3
	ε_v	15	12	2	1
	$E_{cooling}$	20	4	3	3†
	E_{fan}	20	6	3	1

† For one testing case, the relative error associated with the ANN predicted $E_{cooling}$ was found to be 15%.

Table 5.2: Relative errors in the ANN test cases

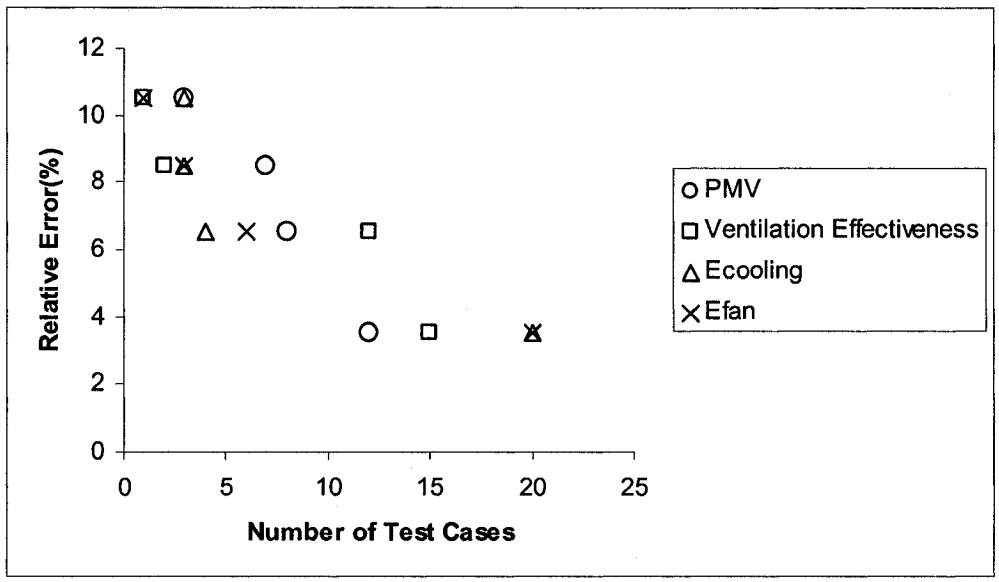

Figure 5.5: Relative errors of the ANN test cases

5.3 Results from ANN-based GA Multi-variable Optimization

5.3.1 Specification of the objective function

When implementing GA, fitness is evaluated inside the GA computation loops by

calculating the value of the objective function. The formulation of objective function (sometimes referred to as cost function) would thus have signification impact on both the search process and the final results.

The goal of current study was to lower the energy consumed for ventilation as much as possible and how to provide satisfactory comfort and IAQ in an office space. Given the thermal and airflow conditions and the contaminant level in the office, these objectives can possibly be achieved through appropriate selection of the ventilation system type, the diffuser type, and the number of diffusers, through proper placement of the supply and return terminals, and through moderating the supply air temperature and flow rate.

As previously mentioned, PMV, CO_2 concentration-based ε_v, and energy input for cooling load offset and fan operation were selected as the indices to measure comfort, IAQ and energy usage, respectively. Also, the thermal and airflow states of room air had to comply with the constraints imposed on the *head-to-ankle temperature difference* ($\Delta T_{HeadToAnkle}$), the variation of ET over the occupant's body, and the local air velocity. Accordingly, the objective function was prescribed by aggregating and weighting the above indices into one equation.

$$J(X) = Min\left[w_{tc}\left(\sum_i \left(\frac{ABS(PMV_i)}{PMV_{\max}} \right) \right) + w_{iaq} \frac{\varepsilon_{v\max}}{\varepsilon_v} + w_{fan}\left(\frac{E_{fan}}{E_{fan\max}} \right) + w_{cooling}\left(\frac{E_{cooling}}{E_{cooling\max}} \right) + PT \right] \tag{5-3}$$

where X is the input vector, consisting of all the controlled variables including the design parameters and operating settings of ventilation systems. Subscript i denotes the number of occupants, as PMV is evaluated separately for individual occupant. w_{tc}, w_{iaq}, w_{fan}, and

$w_{cooling}$ represent the weighting factors for thermal comfort index, IAQ index, fan power index, and cooling power index, respectively.

It should be mentioned that GA in the current case was attempting to minimize the cost function. Therefore, the first term in the cost function represents proximity of occupants' thermal sensation (represented by PMV index) to a neutral value; the second term reflects the removal of indoor contaminants; the third and fourth terms are targeted at minimizing the energy consumed by space cooling and supply fan; the last term of the cost function is a penalty term, which accounts for the aforementioned constraints imposed on the flow and thermal conditions. PMV_{max}, ε_{vmax}, E_{fanmax}, and $E_{coolingmax}$ are the maximum values of corresponding objective variables that can be observed from the training data, which were used to scale the objective variables into a usable range ([0, 1] in the current case).

The magnitude of the weighting factors are to be specified by the user according to personal preference and based on a sensitivity analysis. Different decision-makers will not have the same goals in system design. For example, when a user is more concerned about the overall comfort level than IAQ, w_{tc} would be set to a higher value relative to w_{iaq}; for maximum energy efficiency design, w_{fan} and $w_{cooling}$ can be set to 1, whereas w_{tc} and w_{iaq} can be set to 0; etc. Results from sensitivity analysis by varying the magnitude of individual weights are presented in the next section.

5.3.2 Sensitivity analysis—impact of weighting factors on optimization results

Trade-offs always exist between the attempts to improve air quality/comfort level and the attempt to reduce energy usage for ventilation. The relative magnitude of weighting

factors in the prescribed objective function represents user preference as mentioned in previous section. Appropriate values of such factors can be only determined by fine-tuning through investigative optimization searches.

Using sensitivity analysis, which is frequently used to identify the influence of input parameter variations on simulation or experimental results, the following work was carried out to diagnose the impact of various combinations of weighting factors on the optimization results.

A hypothetical case for an office equipped with a four-swirl-diffuser UFAD system was taken as the subject of the sensitivity analysis. In the reference case, the values of uncontrolled variables were given as: the internal heat load density was 30 W/m^2, the inner surface temperature was 35 °C, and the emission rate of CO_2 sources was 1.0 L/min; whereas the controlled variables were set to: supply air temperature was at 20 °C, the system delivered 80 L/s of conditioned air into the office, and the distance from the diffuser to the occupant and the distance from the return grille to the contaminant/heat sources were taken as 1.74 m and 2.3 m, respectively. The above office configurations and thermal/airflow conditions in the baseline case resulted in PMV value, ε_v, $E_{cooling}$, and E_{fan} as 0.98, 1.29, 1.83 kW, and 0.1628 kW, respectively.

To assess the sensitivity of optimization results to the variations of weighting factors, five exploratory GA optimization searches were launched with this base model. The convergence history of a typical GA search is plotted in Figure 5.6. In each GA search, the values of particular weighting factors were altered and entered into the objective function; accordingly, the GA engine was re-started to search for the optimal controlled variables to minimize the various versions of the objective function. The optimal

solutions guided by these five combinations of weighting factors were then compared with the objective indices obtained from the baseline case, demonstrating the relative improvement.

Table 5.3 illustrates the results obtained from the sensitivity analysis (in the table's *Improvement* column, the positive number represents saving in energy demand or improvement in comfort and IAQ with respect to the results of the baseline case, and vice versa). In Table 5.3, w_1, w_2, w_3, and w_4 stand for w_{tc}, w_{iaq}, $w_{cooling}$, and w_{fan}, respectively.

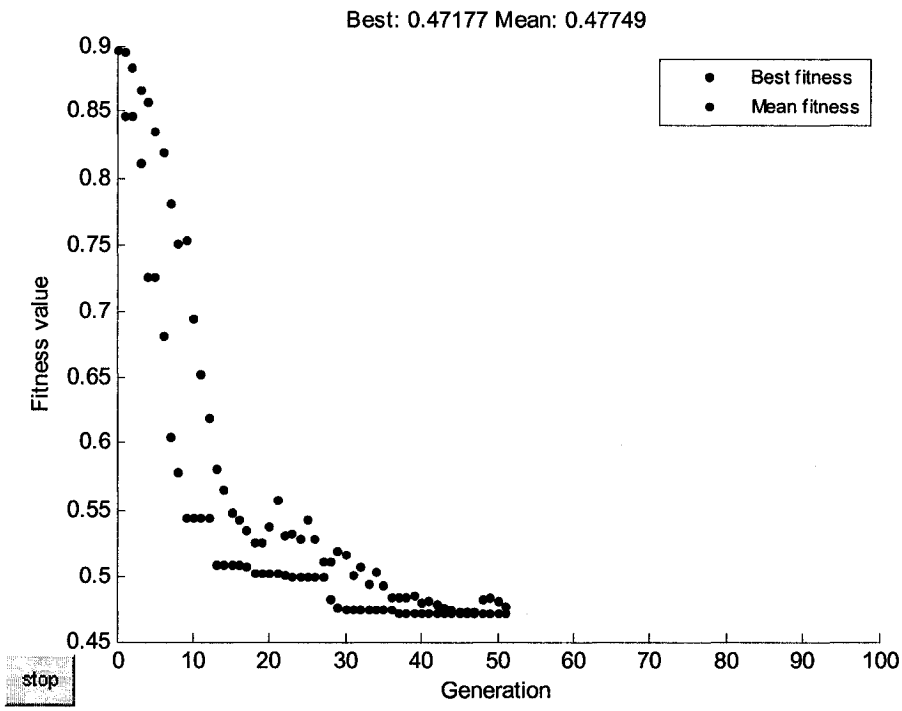

Figure 5.6: Convergence of a GA search

	Baseline case		Combination A				**Combination B**				**Combination C**				Combination D				Combination E			
			w_1	w_2	W_3	w_4	w_1	W_2	w_3	w_4	w_1	W_2	W_3	w_4	W_1	w_2	W_3	w_4	W_1	w_2	w_3	w_4
			0.5	0.25	1	1	**1**	**0.25**	**2**	**1**	**0.5**	**0.1**	**1**	**0.5**	1	0.1	0.8	0.5	1	0.05	0.5	0.25
			Optimal solution				**Optimal solution**				**Optimal solution**				Optimal solution				Optimal solution			
Control Variables	T_{supply} (°C)	20	15				**22**				**20.125**				17.563				15.063			
	V_{sup} (L/s)	80	80				**80**				**80**				80				156			
	DRS (m)	2.300	2.500				**0.500**				**1.914**				1.828				1.875			
	DDO (m)	1.740	0.817				**0.500**				**0.629**				0.547				0.772			
Objective variables			Best perf†		Improve-ment (%)		**Best perf**		**Improve-ment (%)**		**Best perf**		**Improve-ment (%)**		Best perf		Improve-ment (%)		Best perf		Improve-ment (%)	
	PMV	0.980	0.786		19.796		**0.802**		**18.160**		**0.618**		**36.983**		0.503		48.685		0.001		99.908	
	ε_v	1.290	3.088		139.059		**2.161**		**67.255**		**1.919**		**48.552**		1.794		38.870		1.648		27.540	
	$E_{cooling}$ (kW)	1.830	2.436		-33.185		**1.272**		**30.455**		**1.661**		**9.190**		2.056		-12.400		3.801		-107.745	
	E_{fan} (kW)	0.163	0.165		1.360		**0.162**		**0.417**		**0.162**		**0.281**		0.163		-0.295		0.267		-64.256	

† Best perf: the optimum values of objective indices produced by the near optimal solution

Table 5.3: Results from sensitivity analysis: impact of weighting factors on optimization results

As demonstrated by Table 5.3, the optimization results were highly sensitive to the choice of weighting factors. When the relative magnitude of a weighting factor is increased and thus the objective function places more emphasis on the corresponding target term, this target would be enhanced by the optimizer. For example, $w_{cooling}$ in Combination B ($w_3 = w_{cooling} = 2$) was higher than that in Combination A ($w_3 = w_{cooling} = 1$); not surprisingly, Combination B yielded an optimization solution with 30% saving in cooling energy demand (relative to the baseline case), whereas Combination A required 33% more cooling energy (also relative to the baseline case). The saving in cooling energy with Combination B was achieved by increasing the supply air temperature (T_{supply}) from 15 °C to 22 °C and by keeping the supply air flow rate (V_{sup}) unchanged. In addition, though the T_{supply} was increased and V_{sup} remained the same, the PMV and ε_v were not compromised in the case with Combination B; this was because the diffusers were relocated closer to the occupant (DDO = 0.5 m) and the return grilles were moved closer to the contaminant/heat source (DRS = 0.5 m).

Also, as can be clearly seen from the optimization results guided by weighting factors Combination A, D, and E, the improvements in PMV were usually achieved at the cost of increased cooling and fan energy requirements. If the relative magnitude of w_{tc} was strengthened, as with Combination D and E where w_1 (w_{tc}) was kept at 1 while w_2 (w_{iaq}) and w_3 ($w_{cooling}$) were weakened, the more than encouraging improvements in comfort level (demonstrated by PMV values close to neutral with Combinations D and E) came with the price of lower values of ε_v and greater cooling energy demands. The increases in $E_{cooling}$ with Combination D and E were due to the increase in overall V_{sup} (156 L/s with Combination E vs. 80 L/s in the baseline case) and the drop in T_{supply} (17.56 °C with

Combination D and 15.06 °C with Combination E vs. 20 °C in the baseline case).

Since the interests of current research span all the three issues—thermal comfort, IAQ, and energy usage, the implications from Table 5.3 are: Combinations B and C appear to be appropriate choices for weighting factors in the current study. This is because the optimal solutions guided by these two combinations produced improvements in all the objective targets, and the improvements in these three aspects are more or less balance.

It is worth noting that the choice of weighting factors is problem dependent, in some optimization cases with overhead MS, it was found that the combination of $w_{tc} = 0.5$, $w_{iaq} = 0.25$, $w_{cooling} = 1$, and $w_{fan} = 0.5$ produced reasonable results.

5.3.3 Optimization case studies

Once the values of weighting factors were determined in the aforementioned objective function, GA could be then applied for minimization search. When given the value of un-controlled variables (also included in the input matrix), such as the *inner surface temperature* (T_{surf}) at exterior walls, the internal head load density, and the indoor contaminant emission rate, GA will start searching for an near optimal set of control variables, containing superior system type and diffuser type, appropriate number of diffusers, better placement of supply and return air terminals, and optimal supply air temperature and flow rate, with the goal of achieving the research objectives. Typically, an ANN-based GA search takes 5 to 10 minutes to converge on a dual-processor Pentium IV workstation (Dell Precision 670) at 3.4 GHz speed.

First case study: varying the internal heat load density

The first set of results presented here demonstrate how the optimization engine adapts to the variations in the internal heat load density, with the goal of improving the comfort

level and IAQ and cutting down the energy usage at the same time. The internal heat load density explored here ranged from 25 W/m^2 to 45 W/m^2, which was realized by increasing the heat generation from the two extra heat sources (as shown in Figure 5.2).

When varying the heat load, the other uncontrolled variables, including the T_{surf} and contaminant emission rate, were kept at constant levels—the wall surface temperature was set to 25 °C and the overall CO_2 emission rate was fixed at 1.0 L/min. Results with both the UFAD system and the MS are presented here. The original UFAD system contained 4 swirl diffusers, and the supply diffusers were located 1.74 m away from the occupants and the return grilles were 2.3 m away from the extra contaminant/heat sources. For the original MS (with only 1 swirl diffuser), DDO and DRS were set to be at 0.5 m and 2.3 m, respectively. Both the original systems delivered 100 L/s of conditioned air at 18 °C. These design parameters and operating states were extracted from the test conditions in the original experimental chamber (Cermak, 2004), which was designed and operated by senior building professionals.

Under these conditions, the GA optimization search spanned the realistic ranges (as listed in Table 3.2) of the controlled variables. The optimizer was allowed to choose between the swirl-type and the grille-type diffuser and to decide where to place one or two diffusers in the office. The supply air temperature of UFAD was allowed to vary between 15 °C and 22 °C; while the supply air temperature of MS could vary between 13 °C and 20 °C. DDO may vary from 0.5 m to 2.0 m and DRS could vary from 0.5 m to 2.5 m.

In the case of UFAD, the weighting factors (w_{tc}, w_{iaq}, $w_{cooling}$, and w_{fan}) in the objective function were taken as 0.5, 0.1, 1, 0.5 (determined from the sensitivity analysis);

whereas 0.5, 0.25, 1, 0.5 were assigned to these weights in the case of MS. Table 5.4 illustrates how the optimized operational states and design parameters adapt in response to the variance in internal heat load density. Since the optimizer found UFAD with 4 swirl diffusers and MS with 2 swirl diffusers performed better than the original system configurations, the "*improved UFAD*" here denotes UFAD with 4 swirl diffusers in the office and the "*improved MS*" denotes MS with 2 swirl diffusers in the office.

Original UFAD (4 swirl diffusers)	T_{supply} (°C)	18				
	V_{sup} (L/s)	100				
	DDO (m)	1.74				
	DRS (m)	2.3				
Improved UFAD (4 swirl diffusers)	**Internal heat load density (W/m^2)**	**25**	**30**	**35**	**40**	**45**
	T_{supply} (°C)	20	18.641	18.203	18	16.844
	V_{sup} (L/s)	119.550	122.300	124.600	125.540	125.670
	DDO (m)	1.544	1.343	1.043	0.936	0.693
	DRS (m)	1.058	1.033	0.500	0.534	0.500
Original MS (1 swirl diffuser)	T_{supply} (°C)	18				
	V_{sup} (L/s)	100				
	DDO (m)	0.500				
	DRS (m)	2.300				
Improved MS (2 swirl diffusers)	**Internal heat load density (W/m^2)**	**25**	**30**	**35**	**40**	**45**
	T_{supply} (°C)	18.981	18.231	18.115	18.057	18.000
	V_{sup} (L/s)	120.962	120.672	120.076	120.264	120.072
	DDO (m)	0.631	0.711	0.813	0.922	1.077
	DRS (m)	1.850	1.505	1.500	0.504	0.500

Table 5.4: Optimized design measures/operational states vs. heat load density

(T_{surf} = 25 °C; overall CO_2 emission rate = 1 L/min)

It can be seen from the above table that the design parameters and operational states of the ventilation systems responded to the increasing internal heat load (realized by

increasing the heat generation from the two extra heat sources) in the following ways:

- The supply air temperature of the *improved UFAD* presented a descending trend as internal heat load increases.
- Both the *improved UFAD* and the *improved MS* delivered a larger amount of conditioned air (approximately 120 L/s) into the space in comparison with the original systems (100 L/s) to satisfy the cooling load.
- With both the *improved UFAD* and *improved MS*, the return grilles were relocated closer to the heat sources (as demonstrated by the decreasing DRSs as internal heat load increased), relative to the original systems.
- With the *improved UFAD*, DDO was reduced gradually as the heat load increased, which means the air is delivered in the vicinity of the occupant to offset the impact of surplus heat; however, this tendency can not be observed with the *improved MS*. This may be because, in the latter case, as the two ceiling mounted diffusers were moving away from the occupants (increase in DDO), they were approaching the heat sources and can thus act directly and efficiently on the heat sources.

The goal of the optimization is to pull PMV closer to a neutral value, to achieve maximum *ventilation effectiveness* (ε_v), and to minimize the energy requirements for cooling purpose and for fan operation. Figures 5.7 to 5.10 further illustrate the extent to which the optimal solution can improve the objective indices in these scenarios with optimal design configurations and operating parameters, by plotting the PMV, ε_v, $E_{ccoling}$, and E_{fan} (resulting from the optimized solution) against the internal heat load density.

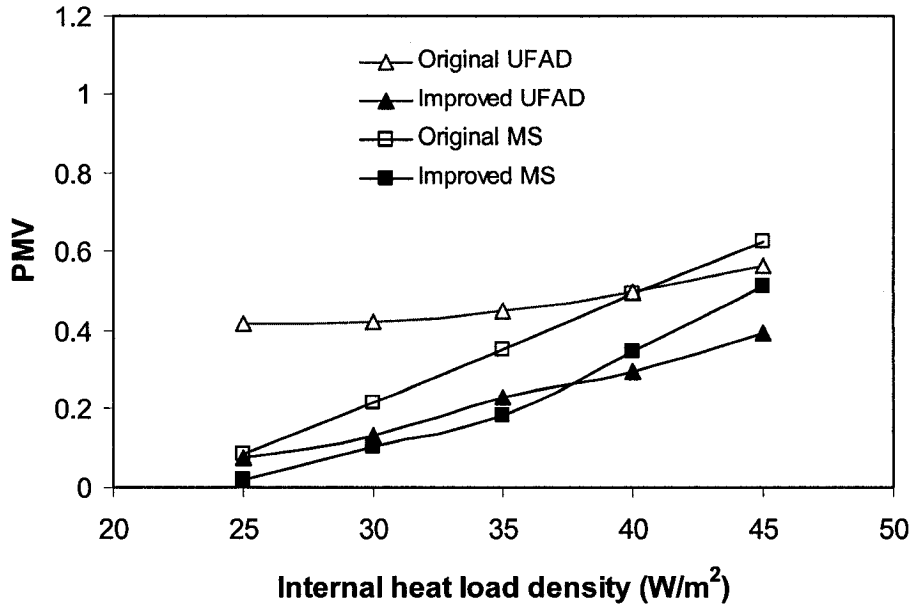

Figure 5.7: Optimization results: PMV vs. heat load density

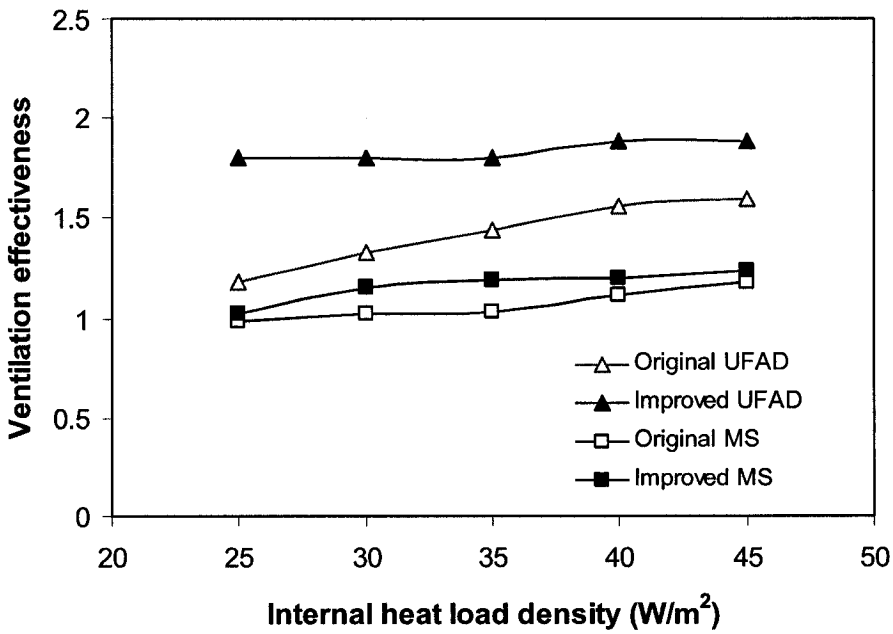

Figure 5.8: Optimization results: ε_v vs. heat load density

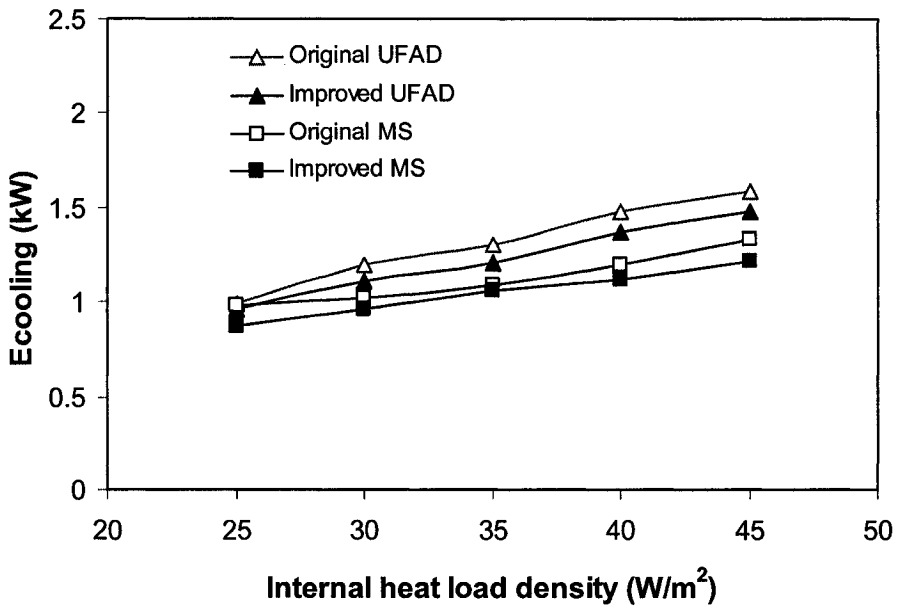

Figure 5.9: Optimization results: $E_{cooling}$ vs. heat load density

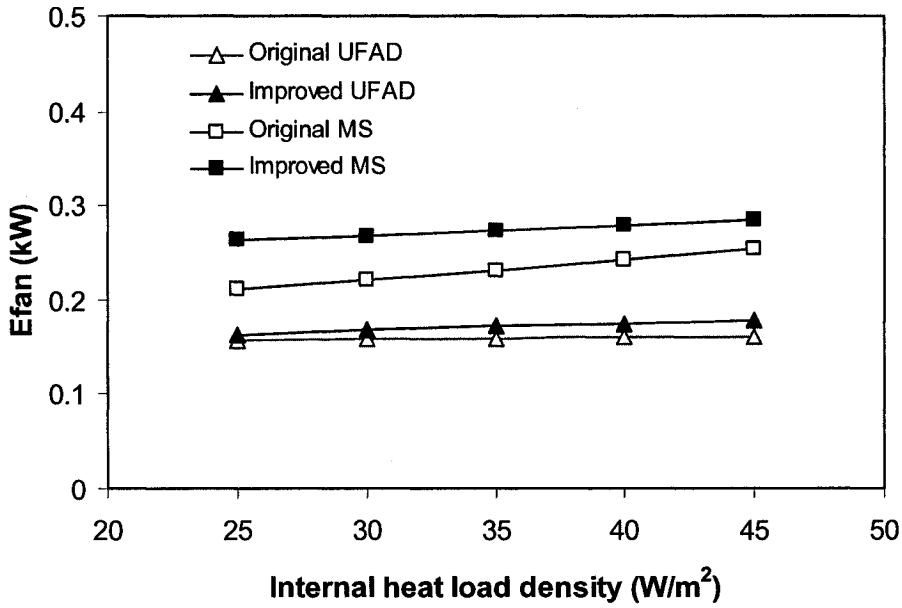

Figure 5.10: Optimization results: E_{fan} vs. heat load density

The above figures demonstrate that, in comparison with the *original UFAD* system, the *improved UFAD* system was able to improve the PMV and ε_v and cut down the $E_{cooling}$ by significant margins (average improvements at 54%, 30.4%, and 6.6%, respectively). Since the *improved UFAD* system is supplying 20 L/s more air into the office, it consumes ~10 % more energy at the supply fan, in comparison to the *original UFAD* system. It is worth noting that the magnitude of fan power input (typically at 0.2 kW under the tested conditions) was much smaller than the cooling energy requirement (which ranged from 1 kW to 1.5 kW in this case); therefore, the optimizer sacrificed the fan power to achieve the above improvements in PMV, ε_v, and $E_{cooling}$; meanwhile, the overall energy consumption ($E_{cooling}$+E_{fan}) was reduced.

Figures 5.7 to 5.10 also indicate that the *improved MS* also substantially enhanced thermal comfort and ventilation effectiveness (improvements at 45.7% and 8.7%, respectively), and reduced the cooling energy demand by 6.8%. As expected, the *improved MS* required 18.4% more energy to drive the supply due to the higher V_{sup} (approximately 120 L/s vs. 100 L/s in the *original MS*).

Second case study: varying the T_{surf}

Another series of optimization tasks were performed to demonstrate how the optimization engine adapted to the variations in the T_{surf}. The T_{surf} varied from 20 °C to 35 °C, at 5 °C intervals in these cases; meanwhile, the internal heat load density and the overall CO_2 emission rate were kept at 35 W/m^2 and 1.0 L/min, respectively. Results with both UFAD system and MS are presented next. The design parameters and operation states of the original systems and the improved systems are described in Table 5.5. It is worth noting that the UFAD with 2 swirl diffusers was shown to outperform the original

UFAD with 4 swirl diffusers.

Original UFAD (4 swirl diffusers)	T_{supply} (°C)	18			
	V_{sup} (L/s)	100			
	DDO (m)	1.74			
	DRS (m)	2.3			
Improved UFAD (2 swirl diffusers)	**T_{surf} (°C)**	**20**	**25**	**30**	**35**
	T_{supply} (°C)	20.670	18.125	17.484	16.540
	V_{sup} (L/s)	121.188	119.800	118.970	115.670
	DDO (m)	1.992	1.999	1.285	0.697
	DRS (m)	1.938	1.641	0.511	0.500
Original MS (1 swirl diffuser)	T_{supply} (°C)	18			
	V_{sup} (L/s)	120			
	DDO (m)	0.500			
	DRS (m)	2.300			
Improved MS (2 swirl diffusers)	**T_{surf} (°C)**	**20**	**25**	**30**	**35**
	T_{supply} (°C)	18.438	18.054	16.730	15.670
	V_{sup} (L/s)	120.145	120	120.016	120
	DDO (m)	1.861	0.832	0.889	0.621
	DRS (m)	2.250	1.750	1.550	0.650

Table 5.5: Optimized design parameters/operational states vs. T_{surf}

(Internal heat load density = 35 W/m^2; overall CO_2 emission rate = 1 L/min)

Also, the following figures (Figures 5.11 to 5.14) present how the optimal solution could improve the objective indices under these tested conditions. The PMV, ε_v, $E_{ccoling}$, and E_{fan} resulting from the optimized solution are plotted against T_{surf}. It can be observed that, relative to the *original MS*, the *improved MS* produced more pleasant thermal conditions (an average improvement in PMV at 50.9%) and better air quality (ε_v increases by 18% approximately) with a 11% deduction in $E_{cooling}$; while the E_{fan} into the *original MS* and the *improved MS* were almost identical.

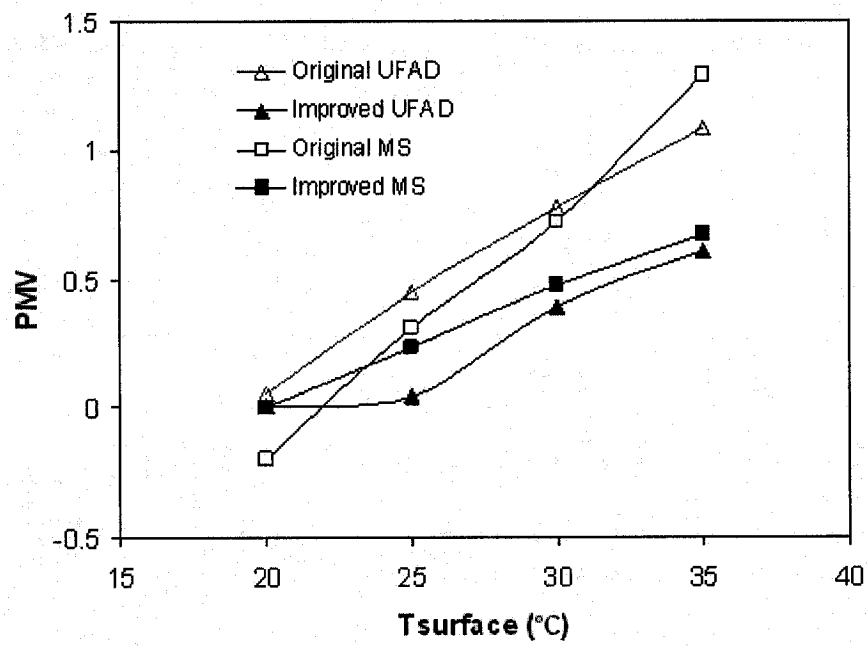

Figure 5.11: Optimization results: PMV vs. T_{surf}

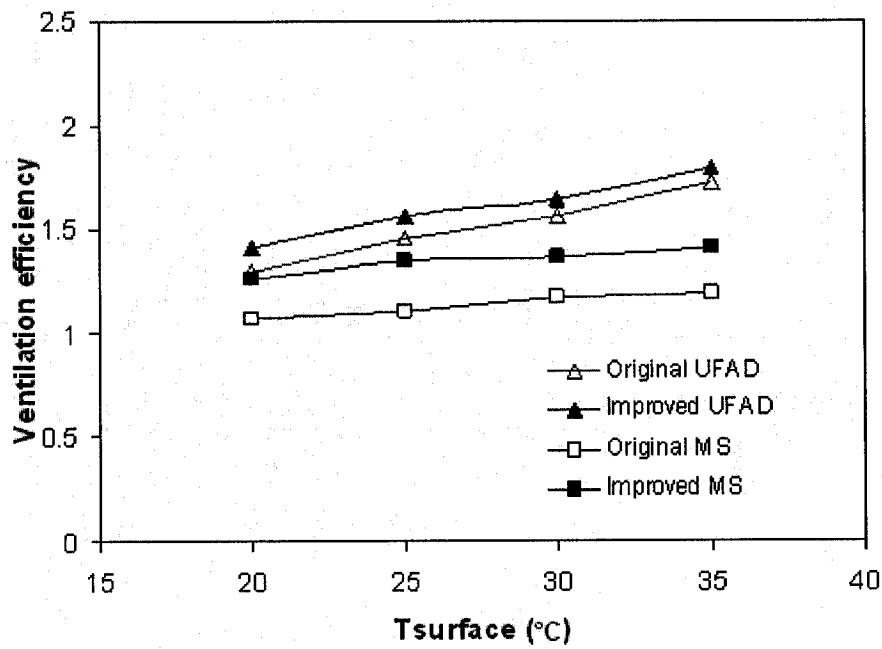

Figure 5.12: Optimization results: ε_v vs. T_{surf}

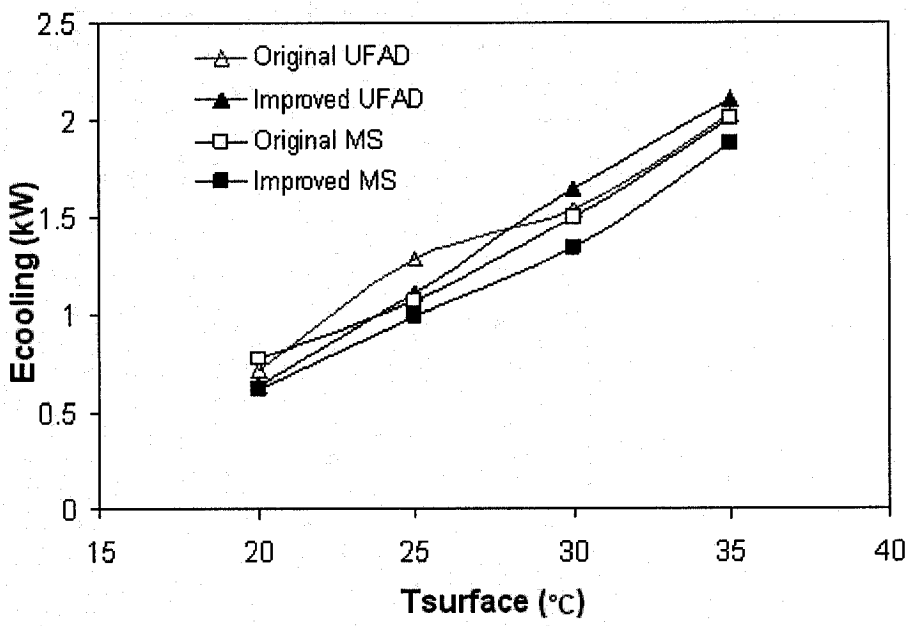

Figure 5.13: Optimization results: $E_{cooling}$ vs. T_{surf}

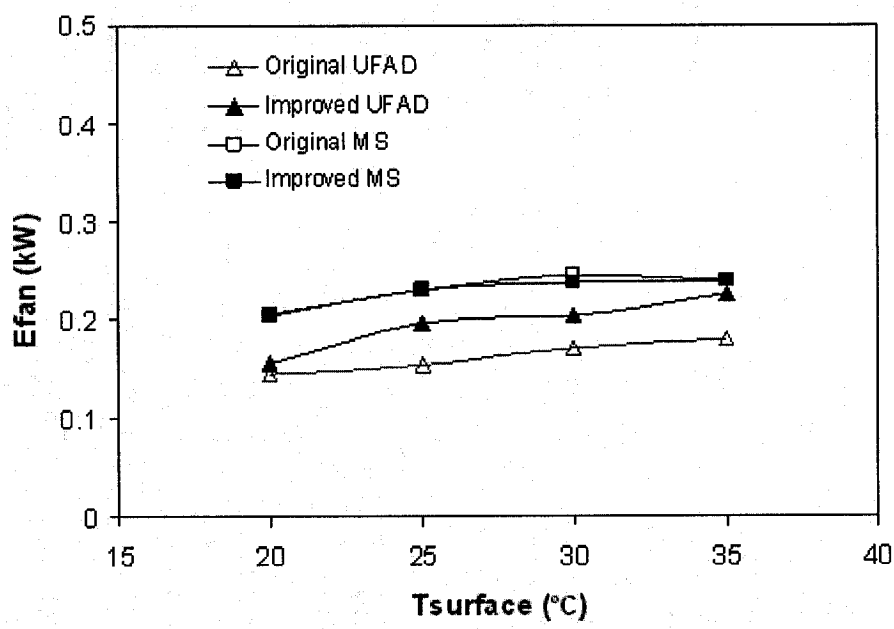

Figure 5.14: Optimization results: E_{fan} vs. T_{surf}

The *improved UFAD* also resulted in a more favorable PMV and ε_v (average

improvements in PMV and ε_v were at 69.3% and 6.27%, respectively), with respect to the *original UFAD* system; however, when the T_{surf} was raised above 30 °C, the *improved UFAD* had to consume slightly higher cooling energy (in comparison with the original UFAD) to satisfy the relatively high cooling requirement (given that the internal heat load density was set to 35 W/m^2 here). With both improved UFAD and MS, the improvements in overall performance were achieved through more appropriate placement of diffusers and return grilles (see Table 5.5).

5.3.4 Verification of the optimal solutions

Based on the above optimization work, CFD simulations were performed to verify the preponderance of the optimal solutions. Both the original systems and the improved systems were re-simulated by applying the working conditions listed in Tables 5.4 and 5.5. CFD simulation results at two operating points are presented next.

Operating point one (T_{surf} = 30 °C; Internal heat load density = 25 W/m^2; CO_2 emission rate = 1 L/min)

Figures 5.15 to 5.17 present the CFD simulation results obtained with both the *original UFAD* and the *improved UFAD* at a particular operating point (T_{surf} = 25 °C; Internal heat load density = 30 W/m^2; CO_2 emission = 1 L/min). The operating conditions of both the *original UFAD* and the *improved UFAD* are presented in Table 5.6 and the performance improvements are also summarized in Table 5.6. In the $E_{cooling}/E_{fan}$ column, the "improvement" corresponds to a reduction in overall power (combining $E_{cooling}$ and E_{fan} together).

System	Operation state	PMV	ε_v	$E_{cooling}$/ E_{fan} (kW)
Original UFAD (4 diffusers)	DRS = 2.3 m, DDO = 1.74 m T_{supply} = 18 °c, V_{sup} = 100 L/s	0.42	1.324	1.198/0.158
Improved UFAD (4 diffusers)	DRS = 1.03 m, DDO = 1.3 m T_{supply} = 18.64 °c, V_{sup} = 122.3 L/s	0.13	1.795	1.110/0.168
Improvement		**69.2%**	**36%**	**5.8%**

Table 5.6: Operating point 1: original UFAD vs. improved UFAD

The temperature and velocity distributions in the vicinity of the diffusers, the PMV contour at 1.1 m height, and the CO_2 concentration contour in a vertical plane near the occupant are plotted. These figures illustrate the performance improvements resulting from the optimal design and operating parameters. For example, the *improved UFAD* can cool down the space better (as shown in Figure 5.16) and can more efficiently drew the contaminant (CO_2) away from the occupant (as shown in Figure 5.17), and these improvements can be realized by relocating the diffusers closer to the occupants and moving the return grilles closer to the extra CO_2/heat sources (as highlighted in Figure 5.15).

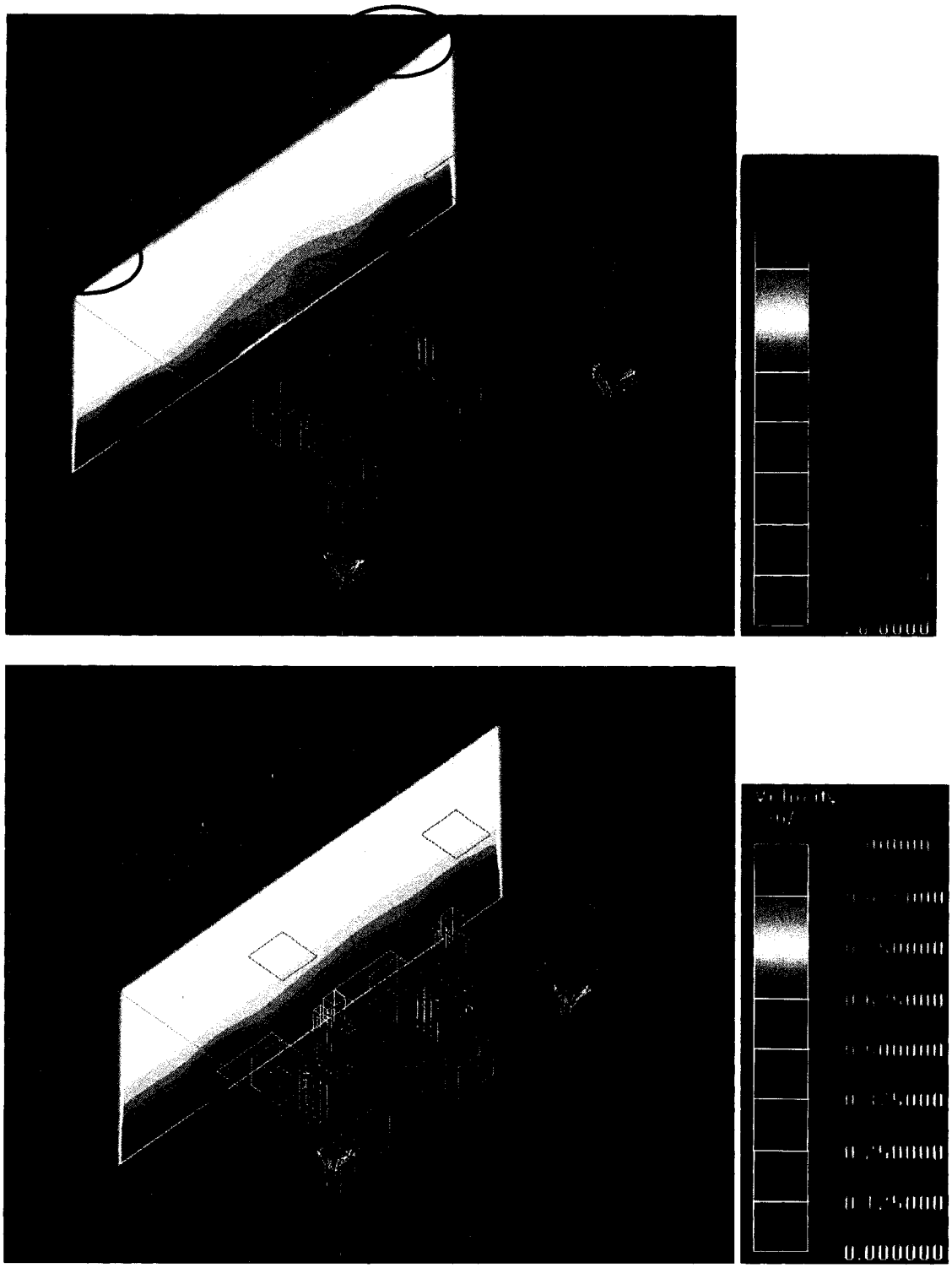

Figure 5.15: Temperature contour and discharge velocity: original UFAD (upper) vs. improved UFAD (lower)

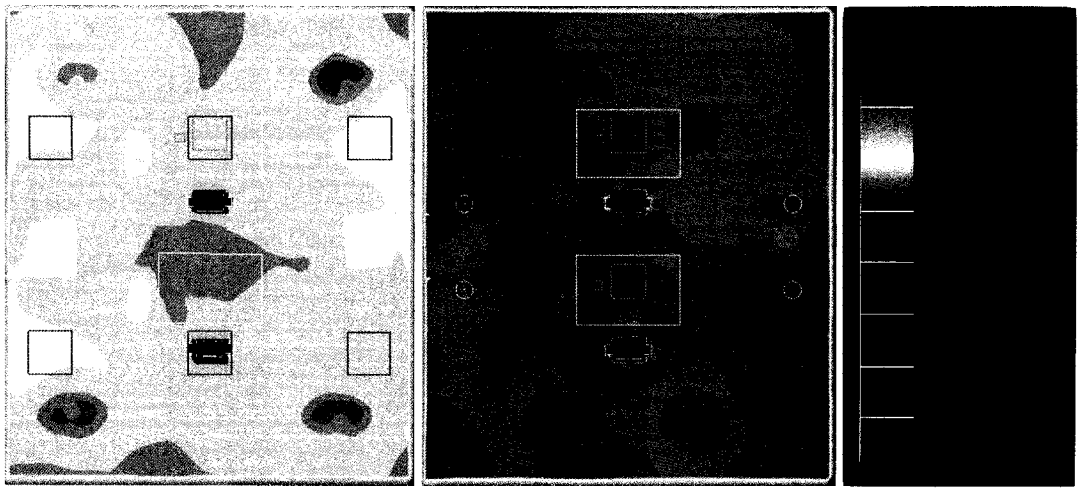

Figure 5.16: PMV contour: original UFAD (left) vs. improved UFAD (right)

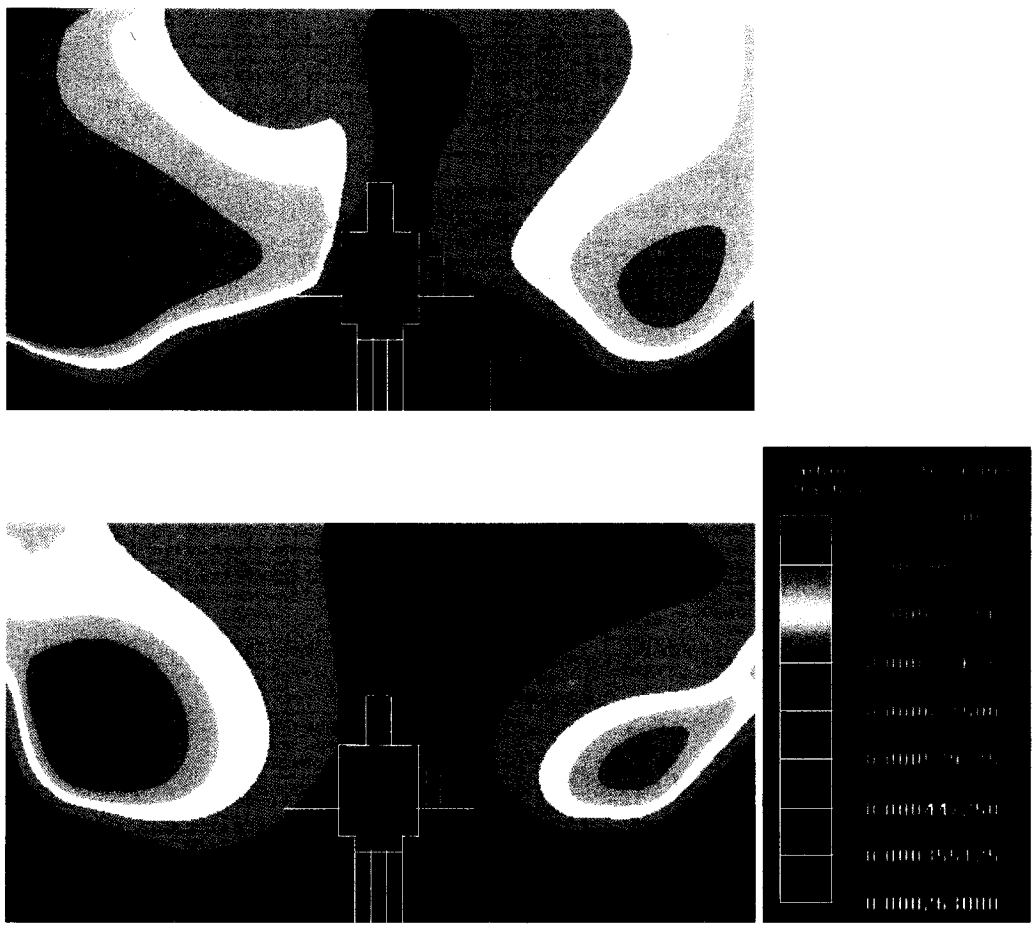

Figure 5.17: CO_2 concentration contour: original UFAD (upper) vs. improved UFAD (lower)

Operating point two (T_{surf} = 30 °C; internal heat load density = 35 W/m^2; CO_2 emission = 1 L/min)

Next, Figures 5.18 to 5.20 present the CFD simulation results obtained with the *original MS* and the *improved MS* at another operating point (T_{surf} = 30 °C; internal heat load density = 35 W/m^2; CO_2 emission = 1 L/min). The temperature distribution near the return grilles, the velocity vectors adjacent to the diffuser, the PMV contour at 1.1 m height, and the CO_2 concentration contour in a vertical plane near the contaminant source and return grilles are plotted. These figures clearly demonstrate the performance improvement resulting from the optimized design parameters and operating states with the *improved MS*. As demonstrated in the CFD simulations results, the adapted MS reduced the PMV value at the level of 1.1 m from 0.7 to 0.45, and it delivered fresh air in the vicinity of the occupants and resulted in low CO_2 concentrations in the breathing zone. The operating conditions of both the *original MS* and the *improved MS* are presented in Table 5.7, and the performance improvements are also summarized in Table 5.7. One thing worth of mentioning is that, in this case with such a high cooling load, the ceiling mounted swirl diffuser created non-uniform thermal/airflow conditions in the space and temperature stratification can be observed from Figure 5.18; however, this differs from the results demonstrated in Figures 4.26 and 4.27, where the temperature stratification was not noticeable (in that case, the heat load was much lower than in the current case).

System	Operation state	PMV	ε_v	$E_{cooling}$/ E_{fan} (kW)
Original MS (1 swirl diffusers)	DRS = 2.3 m, DDO = 0.5 m T_{supply} = 18 °C, V_{sup} = 120 L/s	0.72	1.173	1.496/0.246
Improved MS (2 swirl diffuser)	DRS = 0.9 m, DDO = 1.75 m T_{supply} = 16.73 °C, V_{sup} = 120 L/s	0.48	1.367	1.346/0.238
Improvement		**33.3%**	**16.5%**	**9%**

Table 5.7: Operating point 2: original MS vs. improved MS

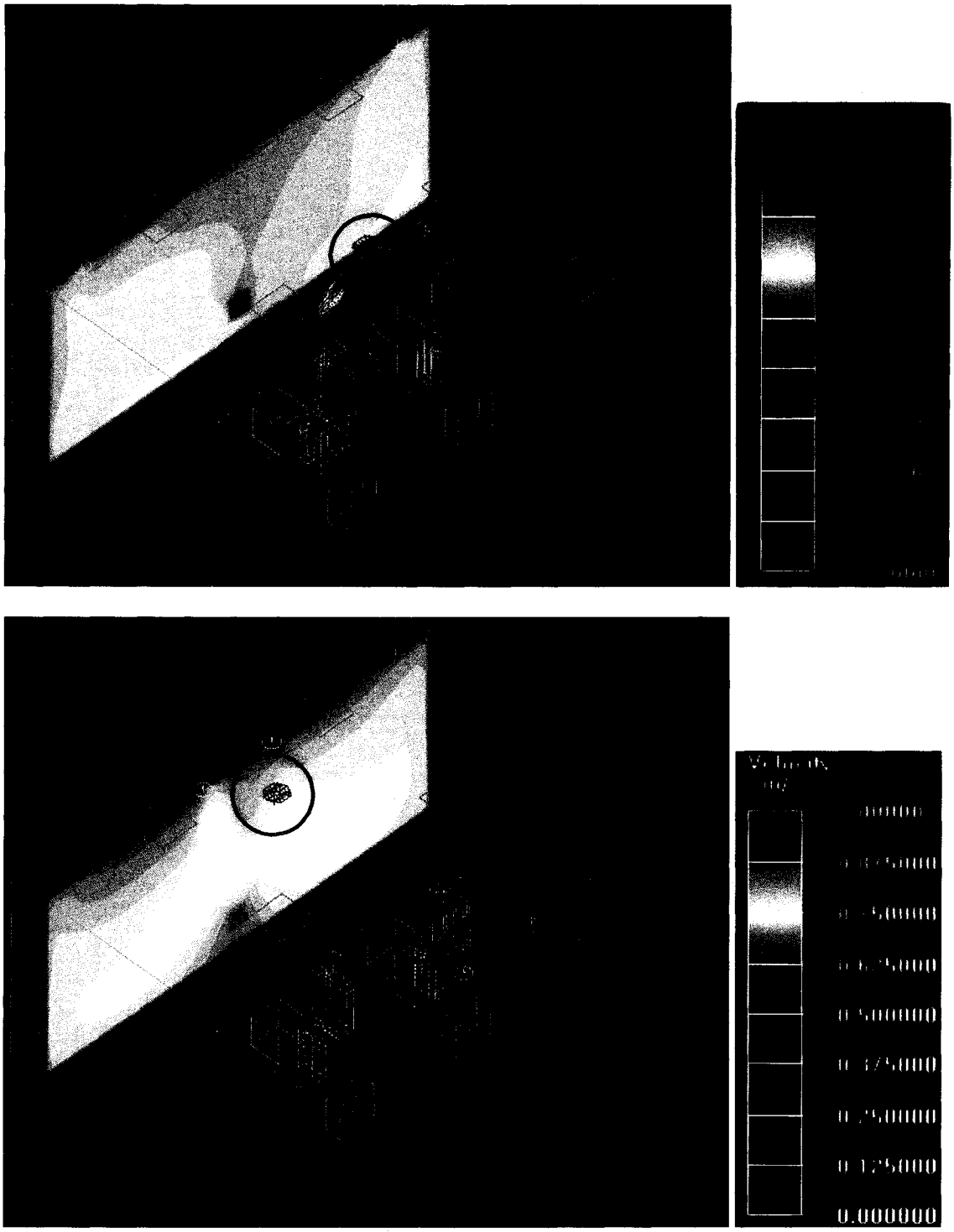

Figure 5.18: Temperature contour and discharge velocity: original MS (upper) vs. improved MS (lower)

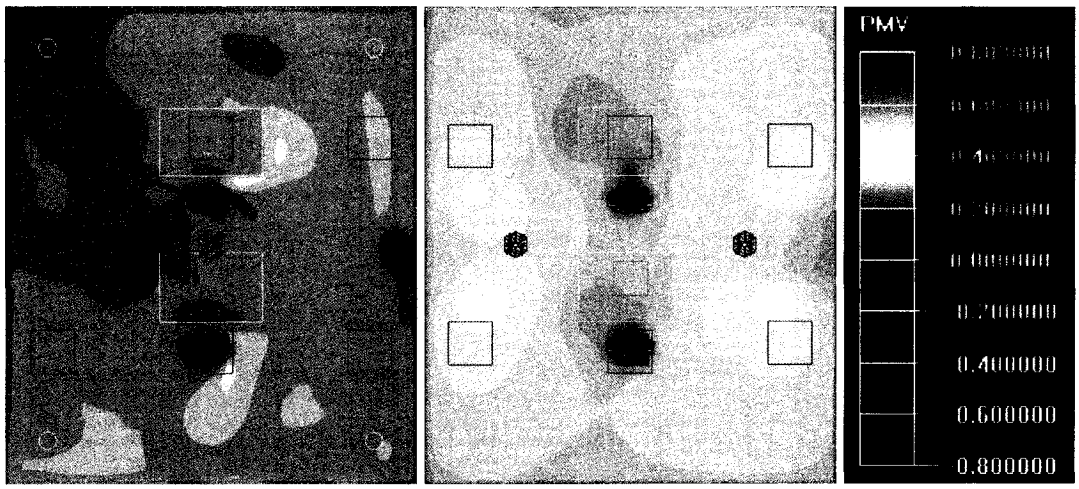

Figure 5.19: PMV contour: original MS (left) vs. improved MS (right)

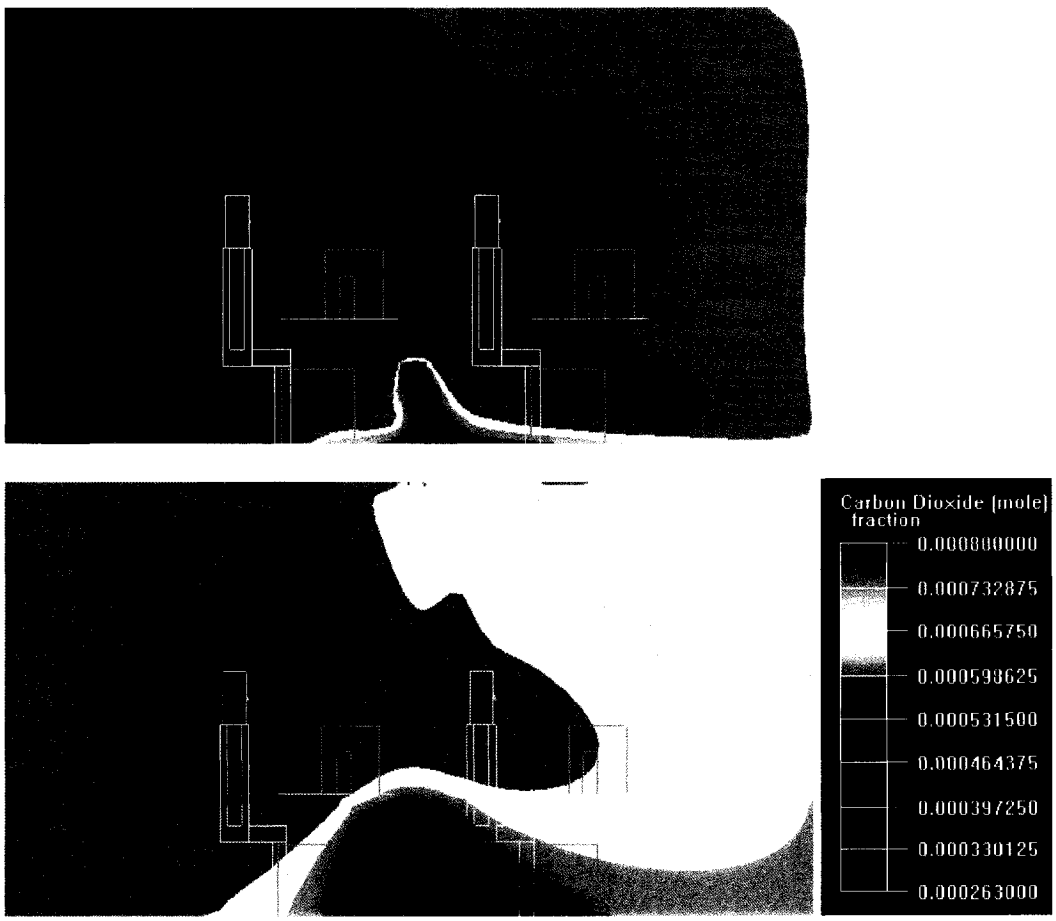

Figure 5.20: CO_2 concentration contour: original MS (upper) vs. improved MS (lower)

5.4 Closing Remarks

Chapter 2 built the theoretical basis of the ANN-based GA optimization approach, and this chapter has described the implementation and results of this optimization approach, with the goal of realizing the research objectives—improving the design and operation of ventilation systems in office environments.

This chapter first described the training and testing of ANN models. The performance of such a low fidelity model for RSA is critically dependent on the quantity and the quality of training data sets. Since the training data are to be generated by performing CFD simulations, it was necessary to design the numerical experiment to save computing time. The LHS method was incorporated to design sufficient but limited CFD cases (to generate training/testing data pairs), in an attempt to ensure the quality of network training and avoid tedious practice of CFD simulations. The simulation parameters obtained from LHS were presented, and the corresponding CFD simulation results (approximate 150 data pairs) were used for training the ANN models (with the topology of 8×30×7).

These 150 training data pairs were employed to train the ANN models, and the back-propagation training with either Levenberg-Marquardt training function or Bayesian regularization algorithm was implemented. It was found that such training methods led to smooth convergence of the training process in current case. Furthermore, 30 additional cases were designed by applying LHS method, and the CFD predictions from these 30 cases were used for the purpose of ANN model testing. By feeding these 30 data sets (not previously used for training) into the established ANN model, the effectiveness of the ANN model in responding to "unseen" information could be demonstrated. The perfect

regressions of ANN predictions on target outputs (training data sets) and the small errors found with the 30 test cases demonstrated the network's convincing learning and generalization ability.

The established ANN model was incorporated into the GA optimization search, which substantially sped up the fitness evaluation. Originally, one time fitness evaluation would take 17 hours by performing a CFD simulation (using RNG k-ε turbulence model), whereas the ANN-based GA optimizer was able to reach convergence in 5 to 10 minutes (one GA optimization search would typically invoke fitness evaluation 5000 times).

The optimization results obtained from two series of case studies demonstrated that the current formulation of objective function, the choice of weighting factors, and the optimization methodology developed could efficiently and substantially enhance the performance of ventilation systems in office environments. Relative to the original ventilation system configurations in the experimental chamber (Cermak, 2004), the improved ventilation systems (both UFAD and MS) produced favorable PMV values and higher CO_2-based ventilation effectiveness, with less power for cooling, under the tested conditions.

In response to the variations in the test conditions (e.g., internal heat load density and inner surface temperature), the adapted ventilation systems improved the overall performance by modulating the supply air temperature and flow rate, switching to different air distribution modes (changing the system type, diffuser type, and the number of diffusers), and relocating the supply and return air terminals to more appropriate locations.

The optimized controlled variables were inserted back into the CFD model to verify

whether or not they could result in improvement in the office environment and to illustrate the degree of improvement. The controlled variables (simulation parameters) were held unchanged for the *original systems*, whereas the *improved systems* were re-simulated by applying the optimized controlled variables. The more than encouraging CFD simulation results at two operating points demonstrated the validity of the optimal solutions and also verified the suitability and effectiveness of the present optimization method for advancing the design and operation of ventilation systems in office environment.

CHAPTER 6

CONCLUSIONS AND RECOMMENDATIONS FOR FUTURE WORK

6.1 Concluding Remarks

With growing concerns over the impact of the indoor environment on office workers' well-being and productivity, coupled with the concern over the rising energy costs for space heating and cooling in office buildings, building designers and researchers have turned to advanced ventilation systems that integrate flexible and responsive elements. Such advanced elements as UFAD, passive swirl diffusers, and demand-controlled ventilation (e.g., CO_2 concentration-based) pose challenges to system design and operation.

The stated objective of the present study was to develop a robust and efficient simulation-based optimization method that may aid ventilation system design and operation in office space, with the goal of achieving satisfactory thermal comfort and *indoor air quality* (IAQ) with minimum energy cost. Such an objective was deemed a sufficient challenge due to the complexity of design space and operational measures and the multidisciplinary performance evaluation.

This thesis has described the development and implementation of a simulation-based optimization process that integrated CFD for simulating the office indoor airflow field, ANN for computing the objective indices based upon the CFD solutions, and GA as the optimization engine driving the optimization search. Collectively, these elements have contributed to the development of a robust, flexible, and efficient optimization tool that

well suited the analysis of office indoor environment.

The major steps leading to these developments can be illustrated as follows.

Characterizing office built environment

Considering the current research objective, accurate quantitative evaluation of indoor environment can be only realized by selecting appropriate criteria to assess the issues of comfort level, IAQ, and ventilation energy costs. Based upon a literature survey and review of available CFD simulation results, Chapter 3 outlined what criteria are suitable for the evaluation of comfort and IAQ in ventilated office spaces. Specifically, PMV-PPD values, *equivalent temperature* (ET), *head-to-ankle temperature difference* ($\Delta T_{HeadToAnkle}$), local air velocity in the vicinity of the occupant, CO_2 concentration distribution, and CO_2-based ventilation effectiveness were extracted from the literature as the criteria for indoor environment assessment in this work.

Previously, it has been uncommon to calculate the ventilation energy usage using CFD-predicted data exclusively; therefore, Chapter 3 also put forward how to derive the *fan power input* (E_{fan}) and the *space cooling energy demand* ($E_{cooling}$) based on the supply air conditions, outdoor air conditions, and the return air states. The supply air conditions and outdoor air conditions are CFD simulation input variables, whereas the return air states are to be predicted by the CFD program.

The adoption of these performance assessment indices enabled the current study to provide a holistic evaluation of thermal comfort, IAQ, and ventilation system energy efficiency.

Application and verification of CFD simulations of ventilated office indoor environment

CFD has been widely employed to simulate indoor airflow and heat transfer for more than a quarter century. As with any other numerical and modeling approach, CFD does not necessarily generate accurate or even reasonable results. This necessitates the comprehensive verification of CFD simulation results against field measured data.

Chapter 4 demonstrated the reliability of CFD simulations conducted in the current research by comparing the CFD estimates with experimental data obtained from two full-size office-type test chambers. The experimental facilities enabled the comparative investigations of the performance of UFAD and *mixing ventilation system* (MS); furthermore, both grille-type and passive swirl diffusers have been studied.

In order to overcome the challenge of modeling swirl diffusers, Chapter 4 proposed and implemented a simplified approach to simulate the behavior of swirl diffusers. It was found that the predicted airflow pattern, the air throw height, the size of the clear zone, and the velocity distribution near the diffuser agreed closely with the smoke visualization and the experimental data. The validity of this modeling approach could thus be justified.

To assess the credibility of the CFD model created for the test rooms, data regarding the vertical profiles of velocity, temperature, and tracer gas (CO_2) concentration (in the case with swirl diffusers) were taken as objectives for comparison. Generally, the simulated results agreed satisfactorily with the expectations, thus giving confidence in the modeling and numerical approaches adopted by the present CFD calculations. The validated cases could then serve as the reference cases for further preparation of ANN training/testing data sets.

Exploratory CFD simulations were also performed (as introduced in Chapter 4), using both the indoor zero-equation model and the RNG k-ε model to account for turbulence.

Based on the CPU time required and the degree of accuracies resulting from these two models, it was found that the indoor zero-equation model was applicable to the cases of UFAD and MS with grille-type diffusers and the case of MS with one swirl diffuser, whereas the RNG k-ε model was more suitable for the cases with multiple ceiling/floor swirl diffusers.

Applying *Latin hypercube sampling* (LHS) method to construct design space

The performance of ANN for *response surface approximation* (RSA) is critically dependent on the quantity and the quality of training data sets. Prior to performing extensive CFD simulations to generate the data pairs for ANN training and testing, the LHS method was introduced to design the numerical experiment. The LHS method was incorporated to design sufficient but limited CFD cases (to generate training/testing data pairs), with the goal of ensuring the quality of network training and avoiding excessive CFD case studies.

Chapter 3 surveyed the literature for parameters that have been proved to significantly affect the office indoor environment and ventilation energy consumption. 10 parameters were extracted from the literature and selected as the independent variables in the CFD modeling and as the controlled states in optimization work, including *inner surface temperature at exterior walls* (T_{surf}), internal heat load density, contaminant emission rate, ventilation system type, diffuser type, number of diffusers per office room, supply air temperature and flow rate, *distance from diffuser to occupant* (DDO), and *distance from return grille to contaminant/heat source* (DRS). Three input variables, namely the ventilation system type, the diffuser type, and the number of diffusers per office room, were aggregated to a single input variable, which resulted in a neural network containing

8 inputs.

Essentially, the LHS selects random sampling points for each parameter over its entire range in a stratified manner. Given that there were 8 inputs into each ANN model, 18 (18 > 2×7) suits of random sample points were generated within the allowable ranges, by applying the LHS method. That is, 18 groups of sampling points were substituted into the reference CFD program and those results from the 18 CFD case studies were used to train an individual ANN model. In total, approximate 150 (8×18+6 baseline cases) CFD simulations were performed to prepare the data pairs for ANN training, and 30 extra simulations were conducted for the purpose of ANN testing. These sampling points were found to cover the allowable range of each input parameter reasonably well; as a result, the ANN model created by using these training data was shown to possess satisfactory learning and generalization capacity.

Incorporating ANN model for fitness evaluation in GA

Chapter 5 demonstrated the training and testing process involved in the creation of an ANN model for RSA. Given the training data, a back-propagation training scheme with either Levenberg-Marquardt training function or Bayesian regularization algorithm was implemented for ANN training. Such a training method led to smooth convergence of the training process in the current case. Also, the perfect regressions of ANN predictions on target outputs indicated the strong learning capacity of the network. Furthermore, 30 additional data sets (not previously used for training) were input into the established ANN model to test how well the model would respond to "unseen" information. The relatively small errors found with the 30 test cases demonstrated the network's convincing generalization capability.

Such a low fidelity model could replace CFD in computing the objective function and constraints with sufficient accuracy when implementing GA optimization, with the goal of cutting down the computational effort. Chapter 5 also illustrated the development and implementation of ANN-embedded multi-variable GA. The incorporation of the ANN model into the GA optimization search was found to be able to substantially speed up the fitness evaluation. Originally, one time fitness evaluation would take 17 hours by performing a CFD simulation (with the RNG k-ε model), which contrasted with the case of the ANN-based GA optimizer—the whole optimization searching process reached convergence within 5 to 10 minutes (one GA optimization search typically invoked 5000 fitness evaluations).

Implementing GA optimization: responding ventilation design and operation to the variances in office thermal conditions

In the current optimization work, the objective function was formulated to aggregate and weight indicators such as PMV, ε_v, E_{fan}, and $E_{cooling}$. The magnitude of the weighting factors could be specified by the user according to design goals and based on sensitivity analysis, as different decision-makers will not have the same goal. For example, when a user is more concerned with a specific performance index, he/she would set the weighting factor corresponding to that objective index to a relatively higher value.

The optimal combination of weighting factors in this study were determined through sensitivity analysis; accordingly, in the optimization case with UFAD, the weights (w_{tc}, w_{iaq}, $w_{cooling}$, and w_{fan}) in the objective function were found to be 0.5, 0.1, 1, 0.5, whereas 0.5, 0.25, 1, 0.5 were found to perform well in the case of MS.

A GA with real-value representation was implemented to search for the near optimal

design configurations and operating states of ventilation systems under particular conditions, so as to achieve the research objective. Two series of optimization cases were devised to illustrate how the optimizer would adapt the ventilation system to the changes in thermal conditions.

The substantial improvements associated with the optimization results demonstrated that the current formulation of objective function, the choice of weighting factors, and the simulation-based optimization methodology efficiently enhanced the performance of ventilation systems in office environments. Under the tested conditions, the improved ventilation systems (both UFAD and MS) produced more favorable PMV values (up to 60% improvements) and higher CO_2-based ventilation effectiveness (up to 30% improvement) with less power input (up to 10% reduction) for cooling.

In response to the variations in the tested conditions (internal heat load density and T_{surf} were the controlled thermal conditions), the adapted ventilation systems improved the overall performance through modulating the supply air temperature and flow rate, switching to different air distribution modes (changing the system type, diffuser type, and the number of diffusers), and relocating the supply and return air terminals to more appropriate locations. It is worth noting that the improvements were made based upon the original ventilation system configurations in the experimental chamber—which were designed and monitored by senior building professionals (Cermak, 2004).

6.2 Recommendations for Future Work

This study has identified some areas worthy of further investigation. Although the work elaborated in this thesis represents a contribution to the development of a simulation-based optimization approach that is applicable to the analysis of office indoor

environment, much work remains to extend and advance it to a practical tool for aiding decision making during building system design and operation. Some recommendations are:

- More and more modern office buildings are monitored continuously in terms of the ventilation air conditions, the energy usage, the IAQ related indices (e.g., CO_2 concentration), and the indoor thermal conditions. Provided that holistic and comprehensive data are collected and included in a database, the use of ANN can become even more economical and efficient.
- The office scenarios considered in this work have excluded the impact of solar radiation passing through exterior window (there was no exterior window in the test chambers) to the indoor domain. The reasons are twofold. Firstly, the majority of existing CFD programs can not efficiently capture the behavior of the solar radiation (though some methods are claimed to be available with Airpak, as stated in Appendix A). Secondly, the current office-type test chambers are usually unglazed; therefore, it is often infeasible to obtain reliable data to validate those cases with solar radiation imposed upon the room air. Consequently, further improvements in modeling solar radiation behavior within the context of CFD simulation are required, and such advancements should be transferred to practical use. Also, it would be beneficial to include exterior glazing into full-scale office-type test chamber, so as to facilitate reliable field study in this area.
- The CFD simulations performed in the current study have been confined to a single office with two occupants. In the next stage, a challenging task would be expanding the problem domain to a larger area of open-plan offices (with cubicles)

or even to a whole office building, provided that adequate computer resources become available.

- The current study has focused on the cooling season (which is the common case in the core zone of an office building); however, the heating energy requirement of an office building is much higher than the cooling energy requirements in Canada, due to the long heating season. Therefore, it would be necessary to include the heating season into the further research context, so as to provide a more realistic and holistic evaluation.
- CO_2 released from two boxes at fixed locations was taken as the only indoor contaminant; however, other types of gas phase pollutants and other possible placement of contaminant source (e.g., area-type sources as carpet or painted wall/surfaces) are commonly encountered in office spaces. In addition, the impact of internal partitioning (e.g., partition height and location as well as air gap underneath, etc.) has been excluded here due to the absence of data for the validation of the CFD simulations. It would be necessary to address these issues in further CFD simulations, with the hope to establish a more comprehensive database.
- For the optimization driving method, it would be interesting for further studies to extend the current single-objective GA to a multi-objective GA. The multi-objective GA search for a Pareto-optimal front consisting of a set of optimal solutions. A range of possible optimal solutions is presented to the decision makers. By searching for the Pareto-optimal front, this type of algorithms can also minimize cost and maximize energy performance separately and simultaneously.

- Aside from the CFD simulation, it would also be interesting to incorporate the building energy simulation into the devised numerical optimization method. As a project the author is working on, the building energy simulation based optimization approach is used to explore the topic of "how low we can go (in terms of energy usage) in office buildings?"

REFERENCES

Airpak (2002), *Documentation*, Version 2.1, Fluent Inc.

Akimoto, T., Nobe, T., Tanabe, S., and Kimura, K. (1999), *Floor-supply Displacement Air-conditioning: Laboratory Experiments*, ASHRAE Transactions, 105(2): 739-749.

U.S. Department of Energy (2004), *ANSI/ASHRAE-IESNA 90.1-2004*, Washington DC, USA.

ASHRAE (1990), *ANSI/ASHRAE Standard 113: Method of Testing for Room Air Diffusion*, Atlanta, GA, USA.

ASHRAE (1997), *ASHRAE Handbook: Fundamentals*, Atlanta, GA, USA.

ASHRAE (2004), *ANSI/ASHRAE Standard 55-2004: Thermal Environmental Conditions for Human Occupancy*, Atlanta, GA, USA.

ASHRAE (2004), *ANSI/ASHRAE Standard 62-2004: Ventilation for Acceptable Indoor Air Quality*, Atlanta, GA, USA.

Arens, E.A., Bauman, F.S., Johnston, L.P., and Zhang, H. (1991), *Testing of Localized Ventilation Systems in a New Controlled Environment Chamber*, Indoor Air, 3: 263-281.

Atthajariyakul, S. and Leephakpreeda, T. (2004), *Real-time Determination of Optimal Indoor-air Condition for Thermal Comfort, Air Quality and Efficient Energy Usage*, Energy and Buildings, 36: 720-733.

Awbi, H.B. (1998), *Calculation of Convective Heat Transfer Coefficients of Room Surfaces for Natural Convection*, Energy and Buildings, 28: 219-227.

Awbi, H.B. (2003), *Ventilation of Buildings*, Spon Press, London, UK.

Baker, A.J., Williams, P.T., and Kelso, R.M. (1994b), *Development of a Robust Finite Element CFD Procedure for Predicting Indoor Room Air Motion*, Building and Environment, 29: 261-273.

Bartak, M., Beausoleil-Morrison, I., Clarke, J.A., Denev, J., Drkal, F., Lain, M., Macdonald, I.A., Melikov, A.K., Popiolek, Z., and Stankov, P. (2002), *Integrating CFD and Building Simulation,* Building and Environment, 37: 865-871.

Bauman, F.S. (2003), *Underfloor Air Distribution (UFAD) Design Guide*, ASHRAE, Atlanta, GA, USA.

Bauman, F.S., Arens, E.A., Tanabe, S., Zhang, H., and Baharlo, A. (1995), *Testing and Optimizing the Performance of a Floor-based Task Conditioning System*, Energy and Buildings, 22:173-186.
Bauman, F.S., Inkarojrit, V., and Zhang, H. (2000), *Laboratory Test of the ARGON Personal Air-Conditioning System (APACS)*, Project report [online], available: http://www.argonair.com/pdf/Argon%20Test%20Report.pdf

Bauman, F.S. and Webster, T. (2001), *Outlook for Underfloor Air Distribution*, ASHRAE Journal, 43: 18-25.

Beausoleil-Morrison, I. (2000), *The Adaptive Coupling of Heat and Air Flow Modeling within Dynamic Whole-Building Simulation*, Ph.D. thesis, University of Strathclyde, Glasgow, UK.

Bloem, H., deGraaf, M., Kreider, J.F., and Norlen, U. (1998), *The First System Identification Competition*, Proceedings of the ASME ISEC, Albuquerque, NM.

Cermak, R. (2004), *Design Strategies for Personalized Ventilation*, Ph.D thesis, Technical University of Denmark, Copenhagen, Denmark.

Cermak, R. and Melikov, A.K. (2005), *Air Quality and Thermal Comfort in a Room with Underfloor Displacement and Mixing Ventilation*, Proceedings of Indoor Air 2005, 2566-2570, Beijing, China.

Charles, K., Reardo, J.T., and Magee, R.J (2005), *Indoor Air Quality and Thermal Comfort in Open-plan Offices*, Construction Technology Update No. 64 [online], available: http://irc.nrc-cnrc.gc.ca/pubs/ctus/64_e.html

Chen, Q. (1995), *Comparison of Different k−ε Models for Indoor Air Flow Computations*, Numerical Heat Transfer, Part B: Fundamentals, 28: 353-369.

Chen, Q. and Jiang, Z. (1992), *Significant Questions in Predicting Room Air Motion*, ASHRAE Transactions, 98(1): 929-939.

Chen, Q., and Jiang, Z. (1996), *Simulation of a Complex Air Diffuser with CFD Technique*, Proceedings of ROOMVENT 1996, 1: 227-234.

Chen, Q., Moser, A., and Huber, A. (1990), *Prediction of Buoyant, Turbulent Flow by a Low-Reynolds-Number k −ε Model*, ASHRAE Transactions, 96(1): 564-573.

Chen, Q. and Moser, A. (1991a), *Simulation of a Multiple-nozzle Diffuser*, IEA Annex 20 Subtask 1 Research Item 1.20, Proceedings of 12th AIVC conference, 2: 1-13, Ottawa, Canada.

Chen, Q. and Srebric, J. (2000), *Simplified Diffuser Boundary Conditions for Numerical Room Airflow Models*, Final Report for ASHRAE RP-1009, 181 pages, Massachusetts Institute of Technology, Cambridge, MA.

Chen, Q. and Xu, W. (1998), *A Zero-equation Turbulence Model for Indoor Airflow Simulation*, Energy and Buildings, 28:137-144.

Chen, Y.M. and Chen, Z.K. (2000), *A Neural-network-based Experimental Technique for Determining Z-transfer Function Coefficients of a Building Envelop*, Building and Environment, 35: 181-189.

Cheong, K.W. (1996), *Ventilation and Air Quality in an Office Building*, Building Services Engineering Research&Technology, 17 (4): 167–176.

Cheong, K.W.D., Djunaedy, E., Poh, T.K., Tham, K.W., Sekhar, S.C., Wong, N.H., and Ullah, M.B. (2003), *Measurements and Computations of Contaminant's Distribution in an Office Environment*, Building and Environment, 38: 135-145.

Chow, T.T., Zhang, G.Q., Lin, Z., and Song, C.L. (2002), *Global Optimization of Absorption Chiller System by Genetic Algorithm and Neural Network*, Energy and Buildings, 34: 103-109.

Clarke, J.A., Dempster, W.M., and Negrão, C.O.R. (1995), *The Implementation of a Computational Fluid Dynamics Algorithm within the ESP-r System*, Proceedings of Building Simulation'95, 166-175, Madison, USA.

Curtiss, P.S., Kreider, J.F., and Brandenmuehl, M.J. (1993), *Energy Management in Central HVAC Plants Using Neural Networks*, ASHRAE Transactions, 99(1): 476-493.

Deardorff, J.W. (1970), *A Numerical Study of Three-dimensional Turbulent Channel Flow at Large Reynolds Numbers*, Journal of Fluid Mechanics, 41: 453-480.

Di Tommaso, R.M., Nino, E., and Fracastoro, G.V. (1999), *Influences of the Boundary Thermal Conditions on the Air Change Efficiency Indexes*, Indoor Air, 9: 63-69.

EPA (2001), *Healthy Buildings, Healthy People: A Vision for the 21st Century*, EPA report #402-K-01-003, Environmental Protection Agency, Washington, USA.

Etheridge, D. and Sandberg, M. (1996), *Building and Ventilation: Theory and Measurement*, Wiley, New York, USA.

Fanger, P.O. (1970), *Thermal Comfort*, Danish Technical Press, Copenhagen, Denmark.

Fanger, P.O. (2000), *Provide Good Air Quality for People and Improve Their Productivity*, Proceedings of the 7th International Conference on Air Distribution in Rooms, Reading, UK.

Fanger, P.O., Melikov, A.K., Hanzawa, H., and Ring, J. (1989), *Turbulence and Draft*, ASHRAE Journal, 31(7):18–23.

Faulkner, D., Fisk, W.J., and Sullivan, D.P. (1995), *Indoor Airflow and Pollutant Removal in a Room with Floor-based Task Ventilation: Results of Additional Experiments*, Building and Environment, 30: 323-332.

Faulkner, D., Fisk, W.J., Sullivan, D.P., and Wyon, D.P. (1999), *Ventilation Efficiencies of Desk-mounted Task/Ambient Conditioning System*, Indoor Air, 9: 273-281.

Fisk, W.J. (2002), *Health and Productivity Gains from Better Indoor Environments and Their Relationship with Building Energy Efficiency*, Annual Review of Energy and the Environment, 25(1): 537-566.

Fukao, H., Oguro, M., Ichihara, M., and Tanabe, S. (2002), *Comparison of Underfloor vs. Overhead Air Distribution Systems in an Office Building*, ASHRAE Transaction, 108 (1): 64-76.

Goldberg, D.E. (1989), *Genetic Algorithms in Search, Optimization, and Machine Learning*, Madison-Wesley, Reading, UK.

Haghighat, F., Jiang, Z., and Wang, J.C.Y. (1989), *Natural Convection and Air Flow Pattern in a Partitioned Room with Turbulent Flow*, ASHRAE Transactions, 95(2a): 600-610.

Haghighat, F., Huo, Y., Zhang, J.S., and Shaw, C.Y. (1996), *The Influence of Office Furniture, Workstation Layouts, Diffuser Types and Location on Indoor Air Quality and Thermal Comfort Conditions at Workstations*, Indoor Air, 6: 188-203.

Hassoun, M.H. (1995), *Fundamentals of Artificial Neural Networks*, MIT Press, USA.

Haykin, S. (1994), *Neural Networks-A Comprehensive Foundation*, Macmillan, New York, USA.

Holland, J.H. (1975), *Adaptation in Natural and Artificial Systems: an Introductory Analysis with Applications to Biology, Control, and Artificial Intelligence*, University of Michigan Press, USA.

House, J.M. and Smith, T.F. (1995), *A System Approach to Optimal Control for HVAC and Building System*, ASHRAE Transactions, 101(2): 647-660.

Huang, W. and Lam, H.N. (1997), *Using Genetic Algorithms to Optimize Controller Parameters for HVAC Systems*, Energy and Buildings, 26: 277-282.

Huo, Y. (1997), *Ventilation Impact on Indoor Air Quality Problems in Partitioned Offices*, Ph.D thesis, Concordia University, Montreal, Canada.

Huo, Y., Zhang, J., Shaw, C., and Haghighat, F. (1996), *A New Method to Describe the Diffuser Boundary Conditions in CFD Simulation*, Proceedings of ROOMVENT 1996, 2: 233-240.

International Facility Management Association (2003), *"Too cold" and "Too hot" Rank at Top of Workplace Complaints* [online], available: http://www.ifma.org/tools/monthly_media/insider/2003/03_may_16.html.

ISO 7730 (1994), *Moderate Thermal Environments—Determination of the PMV and PPD Indices and Specification of the Conditions for the Thermal Comfort*, International Organization for Standardization.

Jones P.J. and Whittle G.E. (1992), *Computational Fluid Dynamics for Building Air Flow Prediction—Current Status and Capabilities*, Building and Environment, 27: 321-38.

Ke, Y.P. and Mumma, S.A. (1997), *Optimized Supply-air Temperature (SAT) in Variable-air-volume (VAV) Systems*, Energy, 22(6): 601-614.

King, R.E. (1999), *Computational Intelligence in Control Engineering*, New York, Marcel Dekker, Inc.

Kreider, J.F., Claridge, D.E., Curtiss, P., Dodier, R., Haberl, J.S., and Krati, M. (1995), *Building Energy Use Prediction and System Identification Using Recurrent Neural Networks*, Journal of Solar Energy Engineering, 117: 161-166.

Kreider, J.F. and Wang, X.A. (1991), *Artificial Neural Networks Demonstration for Automated Generation of Energy Use Predictors for Commercial Buildings*, ASHRAE Transactions, 97(2): 775-779.

Lau, J. (2005), *The Performance of Floor-supply Displacement Ventilation in Workshop Configurations with Measurements and Simulation Studies*, Master Thesis, Purdue University, USA.

Launder, B.E. and Spalding, D.B. (1974), *The Numerical Computation of Turbulent Flows*, Computer Methods in Applied Mechanics and Energy, 3: 268-289.

Lee, H. and Awbi, H.B. (2004), *Effect of Internal Partitioning on Indoor Air Quality of Rooms with Mixing Ventilation-basic Study*, Building and Environment, 39: 127-141.

Lehrer, D. and Bauman, F.S. (2003), *Hype vs. Reality: New Research Findings on Underfloor Air Distribution Systems*, Center for the Built Environment, University of California, Berkeley, USA.

Lin, Z., Chow, T.T., Fong, K.F., Tsang, C.F., and Wang, Q. (2005), *Comparison of Performances of Displacement and Mixing Ventilations, Part I: Thermal comfort*, International Journal of Refrigeration, 28(2): 276-287.

Lin, Z., Chow, T.T., Fong, K.F., Tsang, C.F., and Wang, Q. (2005), *Comparison of Performances of Displacement and Mixing Ventilations, Part II: Indoor air quality*, International Journal of Refrigeration, 28(2): 288-305.

Lin, Z., Chow, T.T., Tsang, C.F., Fong, K.F., and Chan, L.S. (2005), *CFD Study on Effect of the Air Supply Location on the Performance of the Displacement Ventilation System*, Building and environment, 40: 1051-1067.

Lu, L., Cai, W.J., Xie, L.H., Li, S.J., and Soh, Y.C. (2005), *HVAC System Optimization—in Building Section*, Energy and Buildings, 37: 11-22.

Loudermilk, K.J. (1999), *Underfloor Air Distribution Systems for Open Office Applications*, ASHRAE Transaction, 105 (1): 605–613.

MacKay, D. J. C. (1992), *Bayesian Interpolation*, Neural Computation, 4(3): 415-447.

McKay, M.D., Conover, W.J., and Beckman, R.J. (1979), *A Comparison of Three Methods for Selecting Values of Input Variables in the Analysis of Output from a Computer Code*, Technometrics, 21: 239-245.

McKay, M.D. (1988), *Sensitivity Arid Uncertainty Analysis Using a Statistical Sample of Input Values*, Uncertainty Analysis, Y. Ronen, ed., CRC Press, 145-186.

Massie, D.D., Kreider, J.F., and Curtiss, P.S. (2004), *Neural Network Optimal Controller for Commercial Ice Thermal Storage Systems*, ASHRAE Transactions, 110(2): 361-369.

Matlab (2006), *Documentation*, Version 7.1, MathWorks Inc.

Matsunawa, K., Lizuka, H., and Tanabe, S. (1995), *Development and Application of an Underfloor Air-conditioning System with Improved Outlets for a 'Smart' Building in Tokyo*, ASHRAE Transactions, 101(2): 887-901.

Mei, L. and Levermore, G.J. (2002), *Simulation and Validation of a VAV System with an ANN Model and a Non-linear VAV Box Model*, Building and Environment, 37: 277-284.

Melikov, A.K., Cermak, R., and Majer, M. (2002), *Personalized Ventilation: Evaluation of Different Air Terminal Devices*, Energy and Buildings, 34: 829-836.

Melikov, A.K., Kaczmarczyk, J., and Cygan, L. (2000), *Indoor Air Quality Assessment by a "Breathing" Thermal Manikin*, Proceedings of ROOMVENT 2000, 101-106.

Mengistu, T. (2005), *Aerodynamic Design and Optimization of Turbomachinery Blading*, Ph.D thesis, Concordia University, Montreal, Canada.

Mihalakakou, G., Santamouris, M., and Tsangrassoulis, A. (2002), *On the Energy Consumption in Residential Buildings*, Energy and Buildings, 34: 727-736.

Milton, D.K., Glencross, P.M., and Walters, M.D. (2000), *Risk of Sick Leave Associated with Outdoor Air Supply Rate, Humidification, and Occupant Complaints*, Indoor Air, 10: 212-222.

Montgomery, D.C. (1976), *Design and Analysis of Experiments*, John Wiley & Sons, New York, USA.

Murakami, S. and Kato, S. (1989), *Numerical and Experimental Study on Room Airflow - 3-D Predictions Using the k-ε Model*, Building and Environment, 24: 85-97.

Nathanson, T. (1995), *Indoor Air Quality in Office Buildings: A Technical Guide*, Health Canada, Ottawa, Canada.

Natural Resources Canada (2005), *Energy Use Data Handbook Tables (Canada): Table 2&3* [online], available: http://oee.nrcan.gc.ca/corporate/statistics/neud/dpa/handbook_totalsectors_ca.cfm?attr=0.

Negrão, C.O.R. (1995), *Conflation of Computational Fluid Dynamics and Building Thermal Simulation*, Ph.D. thesis, University of Strathclyde, Glasgow, UK.

Nielsen, P.V. (1974), *Flow in Air Conditioned Rooms*, Ph.D. Thesis, Technical University of Denmark, Copenhagen, Denmark.

Nielsen, P.V. (1989), *Airflow Simulation Techniques —Progress and Trends*, Proceedings of 10th AIVC Conference, 1: 203-223.

Nielsen, P.V. (1992), *Description of Supply Openings in Numerical Models for Room Air Distribution*, ASHRAE Transactions, 98(1): 963–71.

Nielsen, P.V. (1997), *The Box Method—a Practical Procedure for Introduction of an Air Terminal Device in CFD Calculation*, Institute for Bygningsteknik, Aalborg University, Denmark.

Nilsson, H.O. and Holmér, I. (2003), *Comfort Climate Evaluation with Thermal Manikin Methods and Computer Simulation Models*, Indoor Air, 13: 28-37.

Niu, J. and van der Kooi, J. (1992), *Grid-Optimization for k −ε Turbulence Model Simulation of Natural Convection in Rooms*, Proceedings of ROOMVENT 1992, 1: 207-223.

Nizet, J.L, Lecomte, L., and Litt, F.X. (1984), *Optimal Control Applied to Air Conditioning in Building*, ASHRAE Transactions, 90(1b): 587-600.

Olesen, B.W., Koganei, M., Holbrook G.T., and Woods, J.E. (1994), *Evaluation of a Vertical Displacement Ventilation System*, Building and Environment, 29: 303-310.

Olofsson, T. and Andersson, S. (2002), *Overall Heat Loss Coefficient and Domestic Energy Gain Factors for Single-family Buildings*, Building and Environment, 37: 1019-1026.

Olofsson, T., Andersson, S., and Östin, R. (1998), *A Method for Predicting the Annual Building Heating Demand Based on Limited Performance Data*, Energy and Buildings, 28: 101-108.

Patankar, S.V. (1980), *Numerical Heat Transfer and Fluid Flow*, McGraw-Hill, USA.

Pejtersen, J., Brohus, H., and Hyldaard, C.E. (1999), *The Effect of Renovating an Office Building on Occupants' Comfort and Health*, Proceedings of Indoor Air 1999, Edinburgh, (2): 160-165.

Persily, A. (1997), *Evaluating Building IAQ and Ventilation with Indoor Carbon Dioxide*, ASHRAE Transactions, 103 (2): 193–204.

Rey, F.J. and Velasco, E. (2000), *Experimental Study of Indoor Air Quality, Energy Saving and Analysis of Ventilation Norms in Climatized Areas*, Energy and Buildings, 33: 57-67.

Rosenblatt, F. (1961), *Principles of Neurodynamics*, Spartan Press, Washington, USA.

Rumelhart, D. E., Hinton, G. E., and Williams, R. J. (1986), *Learning Representations by Back-propagating Errors*, Nature, 323: 533-536.

Sakamoto, Y., Nagaiwa, A., Kobayasi, S., and Shinozaki, T. (1999), *An Optimization Method of District Heating and Cooling Plant Operation Based on Genetic Algorithm*, ASHRAE Transactions, 105(2): 104-115.

Sekhar, S.C., Tham, K.W., and Cheong, K.W. (2003), *Indoor Air Quality and Energy Performance of Air-conditioned Office Building in Singapore*, Indoor Air, 13: 315-331.

Seppänen, O.A., Fisk,W.J. and Mendell, M.J. (1999), *Association of Ventilation Rates and CO_2 Concentrations with Health and Other Responses in Commercial and Institutional Buildings*, Indoor Air, 9: 226–252.

Shaw, C.Y., Zhang, J.S., Said, M.N., Vaculik, F., and Magee, C.J. (1993), *Effect of Air Diffuser Layout on the Ventilation Conditions of a Workstation: Part I-Air Distribution Patterns*, ASHRAE Transaction, 99(2): 125-132.

Shaw, C.Y., Zhang, J.S., Said, M.N., Vaculik, F., and Magee, C.J. (1993), *Effect of Air Diffuser Layout on the Ventilation Conditions of a Workstation: Part II-Air Change Efficiency and Ventilation Efficiency*, ASHRAE Transaction, 99(2): 133-142.

Shirai, R., Bauman, F.S., and Zagreus, L. (2003), *First Post-occupancy Evaluation (POE) of Block 225: Capitol Area East End Complex*, Interim report to California State Department of General Services and California Energy Commission, Center for the Built Environment, University of California, Berkeley, USA.

Shute, R.W. (1995), *Integrated Raised Floor HVAC: Lesson Learned*, ASHRAE Transaction, 101: 877-886.

So, A.T.P., Chow, T.T., Chan, W.L., and Tse, W.L. (1995), *A Neural Network-based Identifier/Controller for Modeling HVAC Control*, AHRAE Transactions, 101(2): 14-31.

Sodec, F. and Craig, R. (1990), *Underfloor Air Supply System—the European Experience*, ASHRAE Transaction, 96 (2): 690–695.

Sørensen, D.N. and Nielsen, P.V. (2003), *Guest Editorial: CFD in Indoor Air*, Indoor Air, 13:1.

Srebric, J., Chen, Q., and Glicksman, L.R. (1999), *Validation of a Zero-equation Turbulence Model for Complex Indoor Airflow Simulation*, ASHRAE Transactions, 105(2): 414-427.

Srebric, J. and Chen, Q. (2001), *A Method of Test to Obtain Diffuser Data for CFD Modeling of Room Airflow*, ASHRAE Transactions, 107(2): 108-116.

Srebric, J. and Chen, Q. (2002), *Simplified Numerical Models for Complex Air Supply Diffusers*, International Journal of HVAC&R Research, 8(3): 277-294.

Stonier, R. (1995), *CO_2: Powerful IAQ Diagnostic Tool*, Heat, Piping, and Air Conditioning, 67 (3): 88-90.

Sun, J. and Reddy, A. (2005), *Optimal Control of Building HVAC&R Systems Using Complete Simulation-based Sequential Quadratic Programming (CSB-SQP)*, Building and Environment, 40: 657-669.

Sutcliffe, H. (1990), *A Guide to Air Change Efficiency*, Technical Note AIVC 28, Air Infiltration and Ventilation Centre Warwick, UK.

Versteeg, H.K. and Malalasekera, W. (1995), *An Introduction to Computational Fluid Dynamics: the Finite Volume Method*, Longman Group.

Waldemark, J., Wiklund, H., Andersson, S., and Sandberg, O. (1992), *Neural Network Modeling of the Heat Load in District Heating System*, Fernwarme Int., 21(9):424-437.

Wan, M.P. and Chao, C.Y. (2005), *Numerical and Experimental Study of Velocity and Temperature Characteristics in a Ventilated Enclosure with Underfloor Ventilation Systems*, Indoor Air, 15: 342-355.

Wang, S.W. and Jin, X.Q. (2000), *Model-based Optimal Control of VAV Air-conditioning System Using Genetic Algorithm*, Building and Environment, 35: 471-478.

Wang, W.M., Zmeureanu, R., and Rivard, H. (2005), *Applying Multi-objective Genetic Algorithms in Green Building Design Optimization*, Building and Environment, 40: 1512-1525.

Wargocki, P., Wyon, D.P., Sundell, J., Clausen, G., and Fanger, P.O. (2000), *The Effects of Outdoor Air Supply Rate in an Office on Perceived Air Quality, Sick Building Syndrome (SBS) Symptoms and Productivity*, Indoor Air, 10: 222-237.

Webster, T., Bannon, R., and Lehrer, D. (2002), *Teledesic Broadband Center*, Center for the Built Environment, University of California, Berkeley, USA.

Webster, T., Bauman, F.S., and Ring, F. (2000), *Supply Fan Energy Use in Pressurized Underfloor Air Distribution Systems*, Center for the Built Environment, University of California, Berkeley, USA.

Wetter, M. (2004), *GenOpt Generic Optimization Program User Manual*, Version 2.0.0, Lawrence Berkeley National Laboratory, Berkeley, CA, USA.

Wetter, M. and Wright, J. (2003), *Comparison of a Generalized Pattern Search and a Genetic Algorithm Optimization Method*, Proceedings of Building Simulation'03, Eindhoven, the Netherlands.

Wright, J.A., Loosemore, H.A., and Farmani, R. (2002), *Optimization of Building Thermal Design and Control by Multi-criterion Genetic Algorithm*, Energy and Buildings, 43: 959-972.

Wyon, D.P. (1989) *Standard Procedures for Assessing Vehicle Climate with a Thermal Manikin*, SAE Technical Paper Series.

Wyon, D.P., and Sandberg, M. (1990), *Thermal Manikin Prediction of Discomfort due to Displacement Ventilation*, ASHRAE Transactions, 96 (1): 67–75.

Xing, H., Hatton, A., and Awbi, H.B. (2001), *A Study of the Air Quality in the Breathing Zone in a Room with Displacement Ventilation*, Building and Environment, 36: 809-820.

Xu, W. and Chen, Q. (1998), *Numerical Simulation of Air Flow in a Room with Differentially Heated Vertical Walls*, ASHRAE Transactions, 104 (1): 168-175.

Xu, H.T. and Niu, J.L. (2006), *Numerical Procedure for Predicting Annual Energy Consumption of the Under-floor Air Distribution System*, Energy and Buildings, 38: 641-647.

Yakhot, V. and Orszag, S.A. (1986), *Renormalization Group Analysis of Turbulence I, Basic Theory*, Journal of Scientific Computing, 1: 3-51.

Yuan, X., Chen, Q., Glicksman, L.R., Hu, Y.Q., and Yang, X.D. (1999), *Measurements and Computations of Room Airflow with Displacement Ventilation*, ASHRAE Transaction, 105 (1): 340-352.

Zhai, Z.Q., and Chen, Q. (2003), *Solution Characters of Iterative Coupling Between Energy Simulation and CFD Programs*, Energy and Buildings, 35: 493–505.

Zhai, Z.Q. and Chen, Q. (2005), *Performance of Coupled Building Energy and CFD Simulations*, Energy and Buildings, 37: 333-344.

Zhai, Z.Q., Chen, Q., Haves, P., and Klems, J.H. (2002), *On Approaches to Couple Energy Simulation and Computational Fluid Dynamics Programs*, Building and Environment, 37: 857-864.

Zhao, B., Li, X., Chen, X., and Huang, D. (2004), *Determining Ventilation Strategy to Defend Indoor Environment against Contamination by Integrated Accessibility of Contaminant Source (IACS)*, Building and Environment, 39: 1035-1042.

Zhou, L., Huang, H.Y., Shakeri, A., Rastan, S., Stach, B., Pero, K., Morofsky, E., and Haghighat, F. (2005), *Indoor Environment in an Office Floor with Nozzle Diffusers: a CFD Simulation*, Proceedings of Building Simulation'05, 1433-1440, Montreal, Canada.

Zhou, L., Wan, M.P., Chao, C.Y.H., and Haghighat, F. (2006), *A Comparison of an Underfloor Air Distribution System and a Mixing System: Measurements and CFD simulations*, Proceedings of Healthy Buildings 2006, 4: 299-304, Lisbon, Portugal.

APPENDIX A

MODELING INDOOR AIRFLOW AND HEAT TRANSFER WITH CFD

A.1 Introduction

Chapter 1 alluded to some issues regarding the applicability of experimental method for office environment investigations and thus argued for the adoption of CFD techniques in the present study. From Chapter 2, it can be seen that the numerical optimization method should be built upon CFD simulations with convincing accuracy. A brief introduction to the theoretical basis of CFD techniques (especially for indoor airflow and heat transfer modeling) is presented here. Accordingly, the important factors—important in that they have great influences on the computation time and simulation accuracy—can be better understood.

As previously mentioned, factors that may significantly affect the precision of CFD calculations include the turbulence modeling method employed, the thermal and airflow boundary conditions prescribed, the differencing scheme used to treat the terms in the governing equations, the quality of mesh (size and topology of computational grid), and the reliability of the solution algorithm. These pertinent elements of CFD are described in subsequent sections.

A.2 Nature of Room Airflow and Turbulence Models

Although the airflow can be laminar or weakly turbulent in some regions of a room, room airflow is generally considered to be turbulent. For example, Baker et al. (1994b)

observed that turbulence was weak in the regions remote from the supply diffusers or blocked by obstacles, but the room air motion was turbulent in most of the flow field.

For turbulence modeling, high resolution techniques such as *direct numerical simulation* (DNS) and *large eddy simulation* (LES) are the most accurate approaches. DNS depicts the turbulence characteristics by directly solving the Navier-Stokes equations and thus requires sufficiently small time and length scales (e.g., a length scale typical less then 0.1 mm for indoor airflow simulation (Murakami and Kato, 1989)); with LES, small eddies are first filtered from the flow, and Navier-Stokes equations are solved to represent the remaining large eddies. The identified small eddies are then simulated by a sub-grid model (Deardorff, 1970). Despite the attractive accuracy, the extremely strict requirements on computer capacity associated with these two models have impeded their broad applicability.

In order to reduce the computation time, turbulence transport models have been introduced into CFD, which allow the use of coarser grids and larger time scales. These models simplify the treatment of turbulent terms in the Navier-Stokes equations, by decomposing the turbulent movements to time-mean motions and high-frequency fluctuations. It is then necessary to introduce empirical correlations or additional transportation equations to account for the unknown high-frequency fluctuation terms. *Reynolds-stress models*, *algebraic-stress models*, and *zero/one/two-equation eddy-viscosity models* belong to this category, among which, the class of k-ε turbulence models have gained the greatest popularity in modeling room airflow and heat transfer. With k-ε models, the turbulent viscosity can be calculated by solving two additional equations treating the *turbulent kinetic energy* (k) and the *dissipation rate of turbulent kinetic*

energy (ε) as the independent variables. Numerous applications of the standard k-ε model in the indoor domain can be seen in the literature (Haghighat et al., 1989; Nielsen, 1989; Chen and Jiang, 1992; Jones and Whittle 1992; Haghighat et al., 1996; etc.), and no attempt is made to list all of them here. Furthermore, much effort has been put into examining the performance of existing k-ε models in room air simulation. Chen (1995) compared the simulation results obtained from the standard k-ε model to that of four other modified k-ε models by implementing all of them to simulate four different types of room airflow. Though the performances of alternative models may vary from case to case, depending on the flow characteristics, his studies revealed that the *renormalization group* (RNG) k-ε model (Yakhot and Orszag, 1986) generally performed better than other k-ε models studied (e.g., for airflow with mixed convection and for airflow induced by impinging jet). Based on that, the RNG k-ε model was recommended for indoor air simulation. Many CFD studies of the indoor domain have made use of the RNG k-ε model and provided evidence of its preponderance in this area.

The RNG k-ε model was devised to overcome an issue associated with the standard k-ε model—the latter is found to be too dissipative. In the results predicted by the standard k-ε model, very often the turbulent viscosity in recirculation area appears to be too high and vortices are damped out. Yakhot and Orszag (1986) integrated a mathematical technique called the "renormalization group" method into the standard k-ε model. This technique is implemented by choosing a group of slightly different constants and adding a source term.

Aside from two-equation models, zero-equation models have also shown some promise in room air simulation, due to the further reduction in computing effort and CPU

time. Instead of solving the transport equations for k and ε, zero-equation models relate turbulent viscosity to local mean air velocity using various empirical coefficients. Chen and Xu (1998) proposed the indoor zero-equation model, which was specifically developed for room airflow modeling. They applied both the indoor zero-equation model and the standard k-ε model to simulation room airflow driven by natural convection, forced convection, mixed convection, and displacement ventilation. The results indicated that the indoor zero-equation model can converge 10 times faster and produce a comparable level of accuracy (Chen and Xu, 1998); particularly, in the case with forced convection, the indoor zero-equation model outperformed the standard k-ε model in terms of capturing the secondary recirculation in the weakly turbulent region (this may be due to the over-prediction of the turbulent viscosity in this region when using the standard k- ε model, as previously discussed). Srebric et al. (1999) reported that the indoor zero-equation model was more applicable to stable flows than unstable swirling flows.

Since the optimization methodology for this study involved a large number of CFD simulations, it was worth the effort to comparatively examine the applicability and CPU time requirement of alternate turbulent models. The RNG k-ε model and the indoor zero-equation model were selected and implemented in this study to perform pilot case studies. The simulation results presented in Chapter 4 presume general familiarity with these models; therefore, a brief introduction to the pertinent numerical details cannot be skipped. The Reynolds-averaged governing equations representing the conservation laws of mass, momentum, and energy, as well as other equations pertaining to steady state incompressible flow are introduced next. The governing equations with both models are

presented in a simplified format in three-dimensional Cartesian coordinates.

A.2.1 Governing equations

The RNG k-ε model

Conservation of mass (Continuity)

$$\frac{\partial \rho u_i}{\partial x_i} = 0 \tag{A-1}$$

where ρ is the air density (kg/m^3), u_i is the mean velocity component in x_i direction (m/s), and x_i represents the three Cartesian coordinates, i = 1, 2, 3 corresponding to x, y, z axis.

Conservation of momentum

$$\frac{\partial \rho u_i u_j}{\partial x_j} = -\frac{\partial p}{\partial x_i} + \frac{\partial}{\partial x_j}\left[(\mu_t + \mu)\left(\frac{\partial u_i}{\partial x_j} + \frac{\partial u_j}{\partial x_i}\right)\right] + \rho\beta(T_{ref} - T)g_i \tag{A-2}$$

where u_j is the mean velocity component in x_j direction (m/s), p is the pressure (Pa), μ is the dynamic viscosity (Pa·s), μ_t is the turbulent viscosity (Pa·s), β is the thermal expansion coefficient of air (K^{-1}), T_{ref} is the reference temperature (K), T is the local temperature (K), and g_i is the gravity acceleration in i- direction (m/s^2) ($g_i = 0$ for $i \neq 2$).

Since the temperature variation in room air is relatively small compared to the absolute temperature value, Boussinesq approximation is employed to relate local air density to the local air temperature, which allows faster convergence.

Conservation of energy

$$\frac{\partial \rho c_p u_i T}{\partial x_i} = \frac{\partial}{\partial x_i}\left[c_p \sigma(\mu + \mu_t)\frac{\partial T}{\partial x_i}\right] + S_q''' \tag{A-3}$$

where c_p is the specific heat of air (J/kgK), σ is the inverse effective Prandtl number, and S_q''' is the thermal source term (W/m^3). The inverse effective Prandtl number is

calculated by applying RNG theory (Airpak, 2002):

$$\left|\frac{\sigma-1.3929}{\sigma_0-1.3929}\right|^{0.6321}\left|\frac{\sigma+2.3929}{\sigma_0+2.3929}\right|^{0.3679}=\frac{\mu}{\mu+\mu_t} \tag{A-4}$$

with $\sigma_0 = 1/\mathrm{Pr}$ is the inverse molecular Prandtl number,

$$\mathrm{Pr}=c_p\mu/K \tag{A-5}$$

where K is the thermal conductivity (W/mK).

Species transport equation

$$\frac{\partial}{\partial x_i}(\rho u_i C)=\frac{\partial}{\partial x_i}\left(\Gamma_{C,eff}\frac{\partial C}{\partial x_i}\right)+S_C \tag{A-6}$$

where C is the mass fraction of a chemical species (μg/kg), $\Gamma_{C,eff}$ is the effective turbulent diffusion coefficient for C (kg/ms), S_C is the source term for C (μg/m^{3}s).

The effective turbulent diffusion coefficient is given by,

$$\Gamma_{C,eff}=\frac{\mu_{eff}}{Sc_{eff}}=\frac{\mu+\mu_t}{Sc_{eff}} \tag{A-7}$$

with effective Schmidt number = 1.0.

Calculating turbulent viscosity

$$\mu_t=\frac{C_\mu\rho k^2}{\varepsilon} \tag{A-8}$$

where C_μ = 0.085 is an empirical constant, k is turbulent kinetic energy (m^2/s^2), and ε is the dissipation rate of turbulent kinetic energy (m^2/s^3).

The turbulent kinetic energy k is defined as

$$k=\frac{1}{2}\sum_{i=1}^{3}(u_i')^2 \tag{A-9}$$

where u_i' is the fluctuating component of the velocity in x_i direction.

Transport equation for turbulent kinetic energy (k)

$$\frac{\partial \rho u_i k}{\partial x_i} = \rho \tau_{ij} \frac{\partial u_i}{\partial x_j} - \rho \varepsilon + \frac{\partial}{\partial x_j}\left[\left(\mu + \mu_t / \sigma_k\right)\frac{\partial k}{\partial x_j}\right] \tag{A-10}$$

where τ_{ij} is the Reynolds stress tensor and $\sigma_k = 0.72$ is an empirical constant.

And τ_{ij} can be written as

$$\rho \tau_{ij} = 2\mu_t S_{ij} - \rho(2/3)k\delta_{ij} \tag{A-11}$$

S_{ij} is the mean-strain-rate tensor and is defined by

$$S_{ij} = \frac{1}{2}\left(\frac{\partial u_i}{\partial x_j} + \frac{\partial u_j}{\partial x_i}\right) \tag{A-12}$$

δ_{ij} is the Kronecher delta, $\delta_{ij} = 1$ for i = j and $\delta_{ij} = 0$ for i $\neq$ j.

Transport equation for dissipation rate of turbulent kinetic energy (ε)

$$\frac{\partial \rho u_i \varepsilon}{\partial x_i} = \rho C\varepsilon_1 \frac{\varepsilon}{k}\tau_{ij}\frac{\partial u_i}{\partial x_j} - C\varepsilon_2 \rho \frac{\varepsilon^2}{k} + \frac{\partial}{\partial x_j}\left[\left(\mu + \mu_t / \sigma_\varepsilon\right)\frac{\partial \varepsilon}{\partial x_j}\right] \tag{A-13}$$

where $C\varepsilon_1 = 1.42$,

$$C\varepsilon_2 = 1.68 + \frac{C_\mu \lambda^3 (1 - \lambda/\lambda_0)}{1 + \beta\lambda^3} \tag{A-14}$$

$$\lambda \equiv \left(\frac{k}{\varepsilon}\right)\sqrt{2S_{ij}S_{ji}} \tag{A-15}$$

$\lambda_0 = 4.38$, $\beta = 0.012$, $\sigma_\varepsilon = 0.72$ are empirical constants.

The indoor zero-equation model

Conservation equations of mass, momentum, energy, and species concentration with the indoor zero-equation model are the same as those with the RNG k-ε model; however, the method used to calculate the effective turbulent heat diffusion coefficient with the indoor zero-equation model deviates from that with the RNG k-ε model.

The effective turbulent heat diffusion coefficient $\Gamma_{t,eff}$ here is defined by

$$\Gamma_{t,eff} = \frac{\mu_{eff}}{\mathrm{Pr}_{eff}} = \frac{\mu + \mu_t}{\mathrm{Pr}_{eff}} \tag{A-16}$$

and the effective Prandtl number $Pr_{eff} = 0.9$.

Calculating turbulent viscosity

$$\mu_t = 0.03974 \rho V l \tag{A-17}$$

where the local turbulent viscosity is related to the local mean air velocity V (m/s) and a length scale l (m). The length scale is chosen as the distance from the nearest wall here.

The above equations fully characterize the turbulent air motion, the heat transfer, and the chemical species transportation in the flow field. The distribution of the unknowns (pressure, temperature, three velocity components, chemical species' concentration, and k and ε with RNG k-ε model) can be determined by solving these equations.

A.2.2 Near wall treatment

Strictly speaking, the RNG k-ε can only apply to the fully turbulent regions characterized by high Reynolds number. When it comes to the viscous sub-layer near the solid surfaces/walls, where the viscous diffusion dominates the turbulent diffusion by far and Reynolds number is relatively low, making use of such a model may yield results with major discrepancies. One common approach to overcome this limitation is to introduce a damping function near the wall, which in essence, assumes the form of velocity and temperature profiles in the boundary layer. Of the many constructions of wall functions, the widely used "*Law of the wall*" function (Launder and Spalding, 1974) is employed in this study.

With this method, the y^+ values corresponding to the next-to-wall node is controlled

to ensure that this node is located in the fully turbulent region. Between this node and the wall, which is considered as a weakly turbulent or even re-laminarized sub-domain in the boundary layer, the wall function does not solve for the velocity field; instead, it assumes the profile of velocity to be logarithmic. This is based on the logarithmic profile approximation of the *zero-pressure-gradient flow* in the fully developed boundary layer. The equations are given as follows:

Velocity profile in near wall region

$$\frac{u}{u^*} = \frac{1}{K}\ln\left[Ey^+\right] \tag{A-18}$$

where $u^* = \sqrt{\tau_w/\rho}$ is the friction velocity (m/s), with τ_w being the wall shear stress (N/m^2), K = 0.399 is an empirical constant, and E reflects the wall roughness (E = 9.0 here).

The value of y^+ can be determined based on

$$y^+ = \left(\frac{u^*\rho}{\mu}\right)y \tag{A-19}$$

where y is the actually distance from the nearest wall/surface (m).

At the next-to-wall node, the wall function calculates the values of T, k and ε using the following equations:

Temperature at next-to-wall node

$$T = T_{wall} - {}^{q}\!/_{h_c} \tag{A-20}$$

with q is the heat flux (W/m^2), T_{wall} is the wall temperature (K), h_c is the convective heat transfer coefficient (W/m^2K).

Turbulent kinetic energy at next-to-wall node

$$k = \frac{(u^*)^2}{(C_\mu)^{1/2}} \tag{A-21}$$

where $C_\mu = 0.085$ is an empirical constant.

Dissipation rate of turbulent kinetic energy at next-to-wall node

$$\varepsilon = \frac{(u^*)^3}{Ky_{next-to-wall-node}} = \frac{(C_\mu)^{3/4} k^{3/2}}{Ky_{next-to-wall-node}} \tag{A-22}$$

Where $y_{next\text{-}to\text{-}wall\text{-}node}$ is the actually distance from the nearest wall/surface to the next-to-wall grid (m).

It is worth mentioning that, in the case of the indoor zero-equation model, the equations introduced in Section A.2.1 can be applied throughout the flow field and directly to the near wall area; if necessary, the convective heat transfer coefficient h_c on the boundary surfaces can be determined by

$$h_c = \frac{\mu_{eff}}{\mathrm{Pr}_{eff}} \frac{c_P}{y_{next-to-wall-node}} \tag{A-23}$$

A.3 Discretization Scheme

The governing partial differential equations introduced in subsection A.2.1 are highly non-linear and inter-coupled, for example, all the three velocity components appear in each of the momentum equations, the energy equation, and the transport equation of species; also, temperature is integrated into the momentum equation in the vertical direction to determine the local air density. Consequently, the analytical solution of these equations is often infeasible in most problems of practical interest.

With the CFD technique, discretization strategy is utilized to approximate the governing partial differential equations by a group of algebraic equations. It is the

algebraic equations that CFD is attempting to solve. The accuracy of solution is highly dependent on the discretization scheme applied to each term in the governing equations, especially to the more challenging convective term (though the diffusion and source terms also have to be treated).

In Airpak, a control-volume based technique is used for governing-equation spatial discretization (though other methods are also cited in the literature, such as the finite element technique). With the control-volume method, the discretization of governing equations could be only achieved by subdividing the computational domain into small cells using a system of grid elements. Instead of continuously solving the governing equations throughout the computational domain, the control-volume method estimates the values of independent variables (such as velocity components, pressure, temperature, and species mass fraction) only at those points located at the centers of the cells.

When treating the convection term, both first-order and second-order upwind-difference schemes are available in Airpak. With the first-order upwind scheme, the value of a variable at the interface of a control-volume is set equal to the cell-center value in the upstream control volume; whereas with the second-order upwind scheme, higher-order accuracy is achieved at cell faces through a second-order Taylor series expansion around the cell center point. In this study, the first-order scheme was used when performing investigative CFD simulations to test the applicability of turbulent models and boundary conditions; while second-order upwind scheme was used when calculating the final solutions.

A.4 Mesh Topology and Size

When generating the grid system (also referred to as meshes) for equation

discretization, the main concern is the accuracy of the numerical solution in terms of characterizing the temperature, velocity, and species concentration profiles in the problem domain. The numerical solver applies the solution procedure iteratively (moving from one cell to the neighbor cells and from one line to the next) to the discretized governing equations (algebraic equations); therefore, the topology and the size of the mesh plays a significant role in determining the calculation accuracy and computing speed.

According to the geometrical feature of the room and air terminals, the hexahedral mesh was used in this study; it is worth mentioning that for cases with more complicated geometry, the tetrahedral mesh (unstructured) is more applicable than the hexahedral mesh (Airpak, 2002).

After a grid dependency check (three levels of grid density were comparatively studied), the meshes in the final simulations were generated by specifying the maximum spacing interval in x, y, and z direction as 0.05 m, 0.04 m, and 0.05 m, respectively. The grids are designed to be coarser in those open regions where the variations of temperature, velocity, and species concentration are trivial. In the areas adjacent to the supply diffusers, return grilles, and other objects (e.g., heat sources), the meshes are locally refined by increasing the grid count number according to the actual sizes and aspect ratios of the objects and the local temperature gradient, heat power output, and flow rate, etc.).

Prior to commencing the solution procedure, it was necessary to check the aspect ratio, face alignment, and element volume in the mesh (grid quality control), in order to prevent excessively distorted elements and extremely small mesh sizes (10^{-12} m or smaller). For the current office environment simulation cases, the total number of cells

generated in the computation domain was within the range of 0.6 to 1.0 million.

Previously, the issue of near wall treatment was introduced; it is obvious that the location of the next-to-wall nodes (usually represented and measured by y^+ values associated with these grids) would have a major impact on the flow description and the convective heat transfer calculation in the near wall region. The optimal placements of these nodes are case dependent. In the present CFD studies, the y^+ values corresponding to the next-to-wall nodes (at solid surfaces or human body surfaces) are controlled to be between 30 and 100, which fall in the commonly recommended range of 30 to 120 for k-ε models with log-law wall function. y^+ values at and above 70 appear at the ceiling or floor surfaces adjacent to the supply diffusers, with a peak value detected to be around 108.

A.5 Specification of Boundary Conditions

The accuracy of CFD prediction is highly sensitive to the boundary conditions assumed and supplied (Awbi, 1998; Xu and Chen, 1998). Versteeg and Malalasekera (1995) even described a CFD solution exclusively as the extrapolation of thermal and airflow boundary conditions into the flow field. In this section, how to treat and define the boundary conditions at diffusers and at solid surfaces are introduced.

Since the room airflow in an office space is primarily driven by inlet diffusers, it is important for CFD simulations to accurately characterize the air throw coming from the diffuser as well as the penetration and spread of the air jet to other parts of the room.

Boundary conditions for modeling diffusers

Due to the large scale differences between the room and the diffuser sizes, it is often infeasible to copy the detailed geometric feature of a diffuser into a CFD model.

Modeling the diffuser with simplified boundary conditions is the common approach when performing room air simulation with CFD. Such simplified diffuser models allow the geometrical details to be neglected, while capturing the velocity field and jet penetration (Srebric and Chen, 2001).

Though many studies conducted elsewhere attempted to define the diffuser boundary conditions for modeling purpose (Nielsen, 1997; Chen and Jiang, 1996; Huo et al., 1996), two primary methods have been widely accepted and applied, namely, the box method (Nielsen, 1992) and the momentum method (Chen and Moser, 1991a). These two methods have been identified as the most appropriate approaches for CFD simulations of indoor airflow (Chen and Srebric, 2000), though the box method was found not suitable for scenarios where the buoyancy force plays a major role in air jet development (Srebric and Chen, 2002).

1. Box method

The box method does not explicitly model the jet behavior in the immediate vicinity of the supply diffuser; instead, it specifies flow boundary conditions at the surfaces of an imaginary box around the diffuser, while the flow within the box is ignored. At the surface parallel to the supply opening, the boundary conditions are described using measured data; that is, it is necessary to specify the distributions of the independent variables (such as velocity, temperature, species concentrations, turbulent kinetic energy, and dissipation rate of turbulent kinetic energy) at the box surfaces through which the flow is discharged. At the box surfaces that are perpendicular to the supply opening, the gradients of these variables crossing the box surfaces are considered to be zero. Obviously, the size of the box as well as the profiles of these variables around the diffuser

should be correctly determined to ensure the accuracy of this method.

2. Momentum method

With the momentum method, the supply diffuser is considered a free opening. Accordingly, the actual discharge velocity (u_0) is determined based on the airflow rate and the effective face area. This discharge velocity (u_0) is usually larger than the velocity value (u) obtained by simply dividing the volumetric flow rate by the face area of the diffuser. The difference between these two values (u_0 - u) can be used to calculate a momentum source term, which can be applied as a supplementary momentum boundary condition for the diffuser. In this way, the momentum method decouples the momentum and mass boundary conditions, in order to introduce an accurate amount of air into the room.

When the air jet leaves the diffuser, the momentum method describes the air throw by using the isothermal axisymmetric jet formula.

$$\frac{u_m}{u_0} = k_1 \frac{\sqrt{A_0}}{y} \qquad \text{(A-24)}$$

where u_m is the centerline jet velocity at a distance y from the diffuser (m/s), u_0 is the initial jet velocity (m/s), A_0 is the effective area (m^2), and k_1 is an user defined constant characterizing the decay of centerline velocity.

k_1 may be a function of many factors, such as the diffuser type, Reynolds number at inlet, jet confinement, and possibility of deflections (ASHRAE handbook, 1997).

With Airpak, both box method and momentum method are available. Based on the available performance data associated with the diffuser, the momentum method was selected in this study to define boundary conditions near the diffusers. It was also necessary to specify the species concentration, the temperature, the pressure, and the

turbulent intensity at the air inlets. The modeling of the diffusers under consideration (grille type perforated panel and swirl diffuser) was introduced in detail in Chapter 4.

Thermal and airflow boundary conditions at solid surface

When modeling room airflow with CFD, the domain boundary is placed at the internal surfaces of the building envelop assemblies (walls, windows, etc.), thus the solid masses of the fabrics are excluded from the computational domain. Thermal and airflow boundary conditions on such solid surfaces as well as on other internal surfaces (partitions, furniture, occupants' body surface, etc.) are required to solve the governing equations in the flow domain. Generally, there are three types of boundary conditions prescribed for practical problems (taking temperature as the independent variable): (1) T is given on the boundary surface (referred to as the Dirichlet condition); (2) the temperature gradient $\partial T/\partial x_i$ is specified on the boundary surface (referred to as the Neumann condition), x_i is the coordinate normal to the surface and; (3) $q = h(T - T_{ref})$, where the heat flux q, the reference temperature, and the convective heat transfer coefficient are provided (convective boundary condition, sometimes called the Robin condition). The following table summarizes the type of boundary conditions supplied to the solid surfaces encountered in this study.

Surface	Type of boundary condition	Specification
Exterior window/wall	First type	$T = T_{innersur}$, $u = 0$, $C = 0$
Internal wall/ceiling/floor	Second type (symmetry surface)	$\partial T/\partial x_i = 0$, $\partial u/\partial x_i = 0$, $\partial C/\partial x_i = 0$, $u = 0$
Surface of partitions/furniture		
Computer/light/other heat source	Third type	$q = h(T - T_{ambient}), q = q_{tatol}/A_{surface}$
Occupant	Third type	$q = h(T - T_{ambient}), q = 75/A_{surface}$

- **T_{surf} is the temperature on the inner surface of exterior wall or window.**
- **C is the species mass fraction.**
- **$T_{ambient}$ is the room ambient temperature adjacent to the objects under consideration.**
- **q_{total} is the total power of heat generated by a heat source.**
- **$A_{surface}$ is the surface areas of a heat source.**

Table A.1: Summary of boundary conditions at solid surfaces

The thermal conditions at the two surfaces of an internal wall were taken as identical, that is, the internal surfaces (e.g., on partitions and furniture surface) have symmetric boundary condition with no heat flux. Though the fabrics of exterior walls/windows are excluded from the computation domain, the heat flux passing through would significantly affect the temperature distribution and the overall airflow pattern in the indoor space. The exterior walls and windows are not considered as adiabatic, and the thermal boundary condition is defined by supplying the actual inner surface temperature. There are no operable windows (or other openings) and the building envelop assemblies are considered tightly sealed; therefore, zero air leakage (infiltration and exfiltration) is assumed (no mass transfer through the building envelope).

It is worth addressing the issue of how to treat radiation in CFD simulation. With

Airpak, the *surface to surface model* is utilized to model the radiation where temperature differences exist between two solid surfaces. In addition, the *solar load model* provides the possibility of including the effects of direct incident and diffusion solar radiation. Given the terrestrial location (latitude and longitude), the geometry, the date, the local time, and the thermal-optical features of boundary surfaces (absorptivity and transmissivity, for example), the solar load model can estimate the solar radiation imposed on the building envelope and indoor domain.

A.6 Sequential Solution Procedure

From the governing equations listed in subsection A.2.1, it can be seen that the velocity components, the temperature, and species mass fraction can be determined by solving the conservation equations. However, there is no equation for solving pressure. Airpak uses SIMPLE (*Semi-Implicit Method for Pressure-Linked Equations*) (Patankar, 1980)—a pressure-correction solution strategy—to bridge the gap. This method subdivides the solution procedure into five sequential steps.

In each iteration, SIMPLE starts with guessing a pressure field (P^*) and solves the momentum equations to get a tentative velocity field (u_i^*), accordingly. The estimated velocity field is inevitably erroneous due to the discrepancies in the hypothetical pressure values; therefore, in the second step, a velocity-correction adjustment is established by correlating the velocity-correction term (u_i') with a pressure-correction term (P'). The velocity-correction formula is then substituted into the continuity equation so that the pressure-correction terms can be solved in the third step. Next, the velocity-correction terms are determined and both the velocity and pressure field could be updated. Based on this, other variables of concern such as temperature and mass fraction of a species can be

solved in the last step, which ends the iteration loop. After this, the updated pressure (P^*) values are imposed on the momentum equations, and SIMPLE returns to the first step and moves to the next iteration. This five-step process is repeated until convergence is reached. Convergence criteria are generally set as follows: residuals of pressure, velocity, mass, specie concentration, k and ε should be less than 10^{-3}, and residual for temperature should be less than 10^{-6}.

The above pressure-velocity linkage solution procedure generates a series of linear algebraic equations over each iteration. Thus, an efficient equation solver is required to handle the large-size sparse matrices. The most common method is the *Tri-Diagonal Matrix Algorithm* (TDMA) iterative solution procedure, which was employed in this study.

For the problem under consideration, more than one target variables are to be solved simultaneously; however, the convergence pace of one variable differs from that of another. It is necessary to assign different under-relaxation factors to individual variables, so as to adjust the convergence rates and make them compatible. The optimal values of under-relaxation factors are case dependent. After tentative calculations, the under-relaxation factors for pressure, velocity, temperature, species concentration, k, and ε are specified as 0.7, 0.3, 1.0, 1.0, 1.0, and 1.0 in the cases with the RNG k- ε model; while in the case with the indoor zero-equation model, the under-relaxation factors for pressure, velocity, temperature, and species concentration are specified as 0.3, 0.2, 1.0, and 1.0.

A.7 Closing Remarks

Chapter 1 placed CFD in the context of the optimization scheme for this study. Chapter 2 indicated that the numerical optimization required a large number of CFD

simulations with convincing accuracy. It was thus necessary to provide an overview of CFD simulation methodology, explaining the factors that may significantly affect the CPU time and prediction accuracy with CFD modeling.

Although the coverage of this part has been limited and many other alternate approaches are available, the techniques introduced here were fond be efficient for room airflow and thermal behavior simulation in previous CFD studies in this area. Therefore, these are the methods and techniques being used in CFD simulations in the present study. To sum up, Table A.2 puts forward a brief description of important numerical details involved in current CFD simulations, which are implemented in Airpak.

Numerical aspects	**Model/method**
Turbulence model	Indoor zero-equation model or RNG k-ε model
Diffuser modeling	Momentum method
Discretization scheme	Control-volume based technique
Differencing the convection term	Second order up-wind scheme
Grid type/meshed cell number	Hexahedral/0.6~1.0 million
Solution algorithm	SIMPLE
Convergence criteria	Residue < 10^{-3} for mass, velocity, species concentration, pressure, k, ε; residue < 10^{-6} for energy
Under-relaxation factors with RNG k-ε	0.7 for pressure, 0.3 for velocity, 1.0 for temperature, species concentration, k, and ε
Under-relaxation factors with indoor zero-equation	0.3 for pressure, 0.2 for velocity, 1.0 for temperature and species concentration

Table A.2: Summary of numerical details in the current CFD simulations

APPENDIX B

OPTIMIZATION SCHEME VALIDATION

B.1 Introduction

A classic optimization problem, the Rosenbrock function, was selected to test the validity of the ANN-based GA optimization scheme. Such a banana function has a global minimum that is hidden among many local minima; therefore, it has been widely used to substantiate the validity and proficiency of the optimization algorithm under consideration. The problem description, the searching range, the ANN training, and the optimization results are presented in the subsequent sections.

B.2 The Rosenbrock Function

The Rosenbrock's function is defined as,

$$f(X) = \sum_{i=1}^{n-1} \left[100 \times \left(x_i^2 - x_{i+1}{}^2 \right) + \left(x_i - 1 \right)^2 \right] \qquad \text{(B-1)}$$

It is used here to demonstrate how to implement ANN and GA in Matlab. This banana function has a global minimum value of 0 at the point x_i = 1 (for all i). Such a global minimum is located in a parabolic shaped flat valley.

B.3 ANN-based Optimization Scheme Validation

As shown in Figure B.1, GA can be applied directly to the Rosenbrock's function to search for the global minimum; alternatively, an ANN model can be established to approximate the Rosenbrock's function and then GA can be applied to search for the

minimum using the low fidelity ANN model to evaluate fitness.

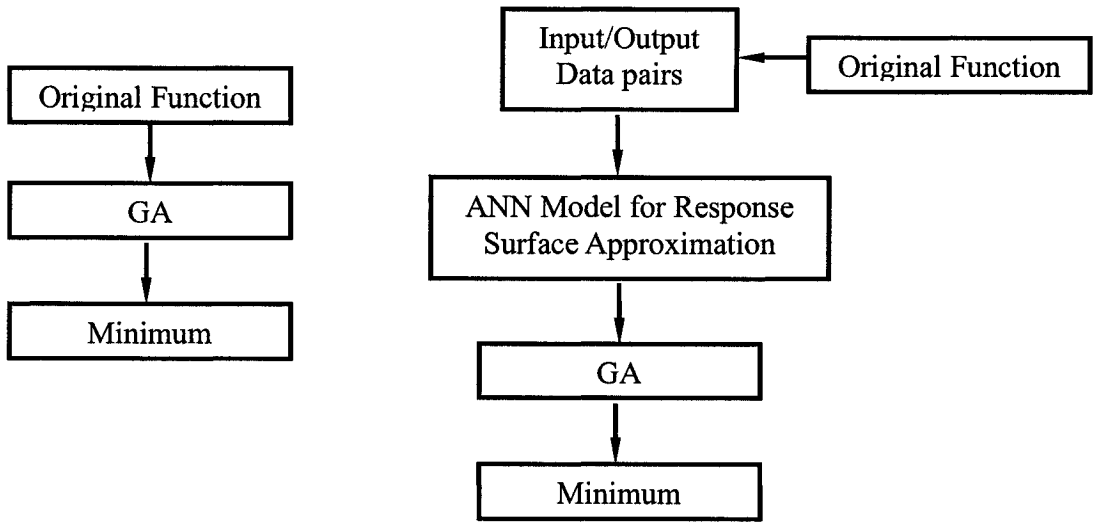

Figure B.1: Test the optimization scheme—flow chart

The ANN constructed here consisted of 1 hidden layer and 6 hidden neurons. 100 input/output data pairs were generated for ANN training purpose, and the ranges of the input variables were set to [-3, 3]. The 100 input/output data sets are divided to three groups for training, validating, and testing, respectively (which is referred to as the early stopping strategy). By doing so, the over-fitting of the training process could be effectively avoided and the generalization of the network can be improved. Figure B.2 shows the convergence history of the ANN training, validation, and testing. For comparison, the function surface is plotted based on the original function (Figure B.3) and the ANN approximation (Figure B.4), good agreement can be observed. In addition, Table B.1 presents the ANN predicted outputs and the exact output values for the 24 test data pairs and relatively small errors are observed between the approximations and the targets, which gives confidence in the network's generalization ability. It can be concluded that using 100 data sets for building the ANN model for response

approximation in the current case can provide satisfactory accuracy.

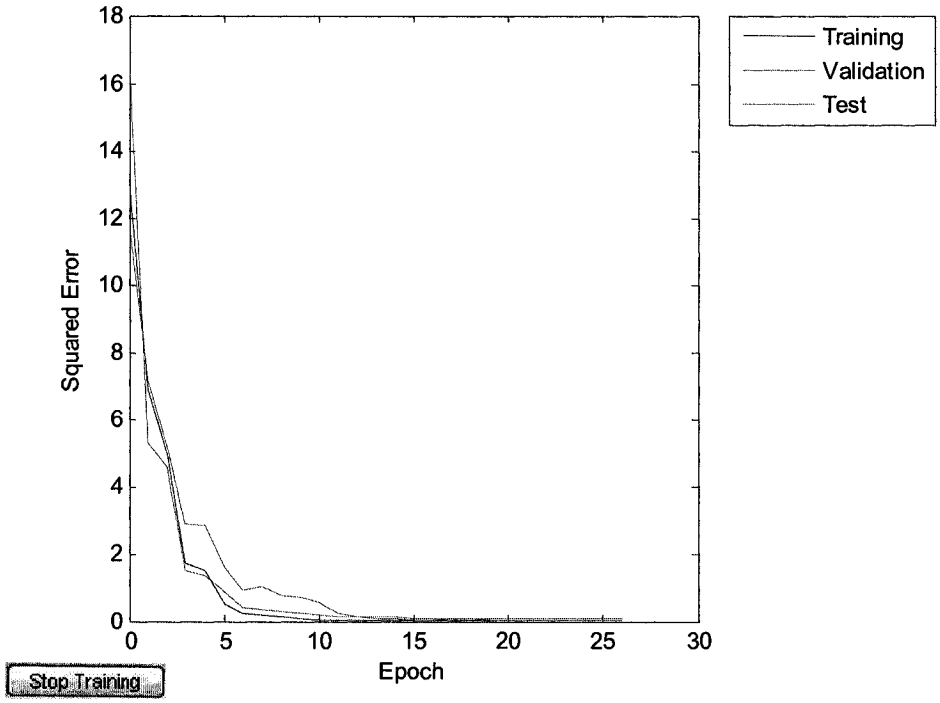

Figure B.2: Convergence of ANN training, validation, and testing with early stopping technique

Case No.	ANN prediction	Target value	Relative error (%)
1	882.8535	852.6664	3.540327
2	1260.888	1274.255	1.048992
3	1291.704	1296.574	0.375562
4	197.9195	174.2537	13.58121
5	6248.535	6434.944	2.896827
6	257.3227	246.6945	4.308242
7	242.7786	176.0115	37.93336
8	1118.432	1078.751	3.678375
9	2350.24	2376.465	1.103515
10	139.3358	132.505	5.155072
11	8952.897	8957.844	0.055233
12	338.77	270.1738	25.38967
13	1068.437	1011.017	5.679412
14	139.3531	166.4613	16.28502
15	3970.742	3963.458	0.183782
16	5842.293	5916.05	1.246741
17	577.4952	625.7107	7.705716
18	43.04786	50.75771	15.18951
19	122.991	137.174	10.33941
20	420.6196	399.2133	5.362134
21	5788.898	5948.055	2.675772
22	7502.094	7590.475	1.164367
23	21.75358	15.68107	38.7251
24	2327.6	2453.279	5.122899

Table B.1: ANN predicted and expected outputs for the 24 test data points

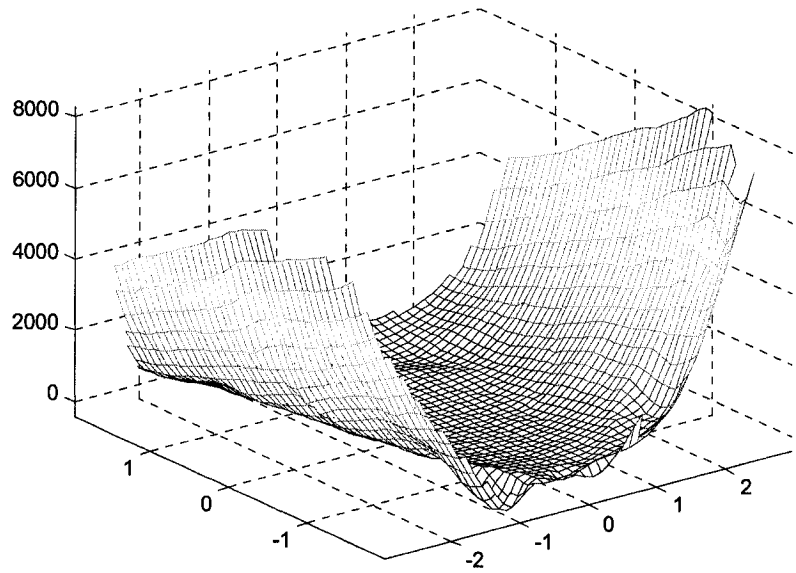

Figure B.3: Surface plotted: the original Rosenbrock function

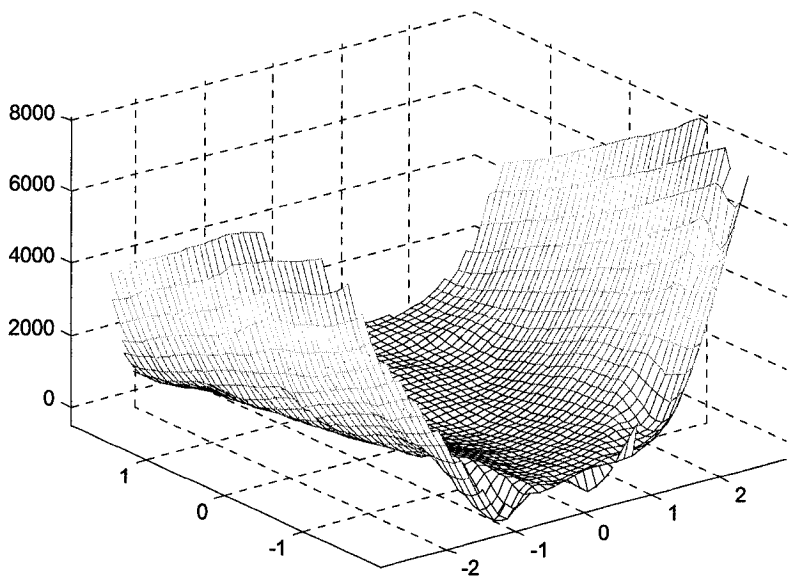

Figure B.4: Surface plotted: ANN approximation of the Rosenbrock function

Figures B.5 and B.6 comparatively present the convergence history of GA optimization search for the minimum of the original Rosenbrock function and the ANN-based GA search. As can be observed from these two figures, the ANN-based GA optimization search demonstrated the same trend as the GA search based on the original function and yielded an optimized solution with comparable accuracy (0.00980 in the ANN-GA case vs. 0.00395 in case with original function). It is worth mentioning that using the Rosenbrock function as the objective for optimization is a tough job and has been repeatedly addressed in the literature. Consequently, the optimization results obtained in this case demonstrated the validity and efficiency of the current ANN-based GA optimization scheme.

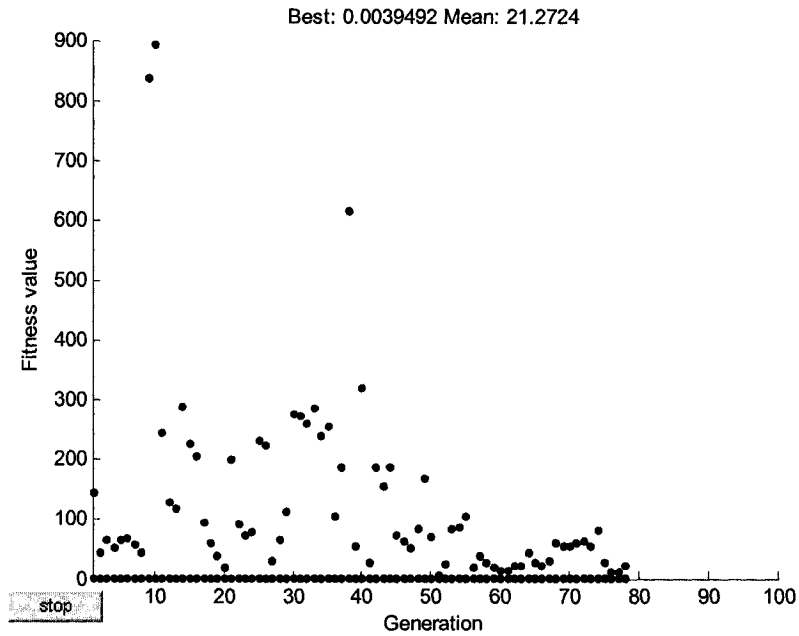

Figure B.5: Convergence of GA Optimization: the Original Rosenbrock Function

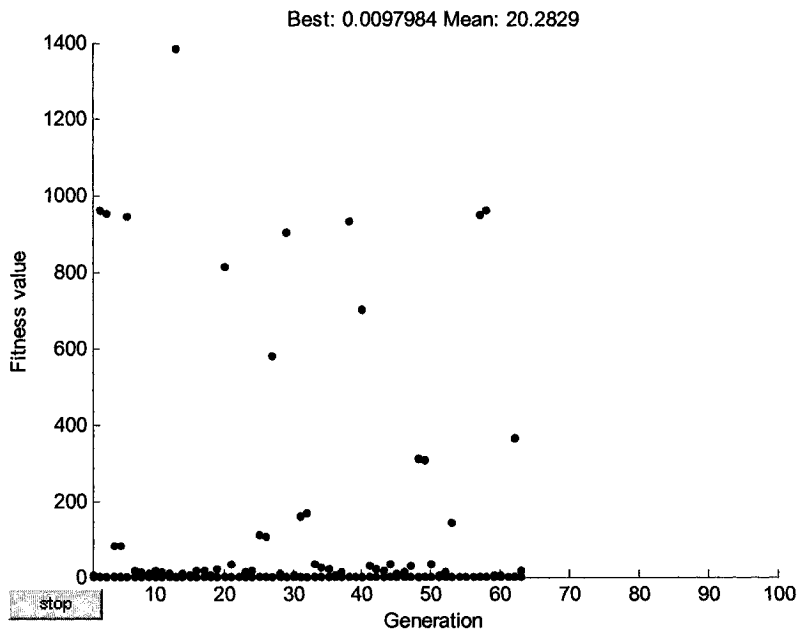

Figure B.6: Convergence of GA Optimization: ANN approximation of the Rosenbrock Function